Reduction of Pier Scour Using an Airfoil Collar

Submitted in partial fulfilment of the requirements

for the award of the degree of

Doctor of Philosophy

by

Lav Kumar Gupta

Roll No. 701902

Supervisor

Prof. P Anand Raj
&

Co-supervisor

Dr. Manish Pandey

DEPARTMENT OF CIVIL ENGINEERING

NATIONAL INSTITUTE OF TECHNOLOGY

WARANGAL - 506004 (T.S.) INDIA

DECEMBER 2023

Reduction of Pier Scour Using an Airfoil Collar

Submitted in partial fulfilment of the requirements

for the award of the degree of

Doctor of Philosophy

by

Lav Kumar Gupta

(Roll No: 701902)

Supervisor

Prof. P Anand Raj

&

Co-supervisor

Dr. Manish Pandey

DEPARTMENT OF CIVIL ENGINEERING

NATIONAL INSTITUTE OF TECHNOLOGY

WARANGAL- 506004 (T.S.) INDIA

DECEMBER 2023

NATIONAL INSTITUTE OF TECHNOLOGY WARANGAL

CERTIFICATE

This is to certify that the thesis entitled **"Reduction of Pier Scour Using an Airfoil Collar"** being submitted by **Mr. Lav Kumar Gupta** for the award of the degree of **Doctor of Philosophy** to the Faculty of Engineering and Technology of **National Institute of Technology Warangal** is a record of bonafide research work carried out by him under our supervision and it has not been submitted elsewhere for the award of any degree.

Prof. P Anand Raj & Dr. Manish Pandey

Thesis Supervisors

Department of Civil Engineering National Institute of Technology Warangal (T.S.) INDIA

Declaration

This is to certify that the work presented in the thesis entitled **"Reduction of Pier Scour Using an Airfoil Collar"** is a bonafide work done by me under the supervision of **Prof. P Anand Raj** & **Dr. Manish Pandey** and is not submitted elsewhere for the award of any degree.

I declare that this written submission represents my ideas in my own words and where others' ideas or words have been included, I have adequately cited and referenced the original sources. I also declare that I have adhered to all principles of academic honesty and integrity and have not misrepresented or fabricated or falsified any idea/data/fact/source in my submission. I understand that any violation of the above will be a cause for disciplinary action by the Institute and can also evoke penal action from the sources which have thus not been properly cited or from whom proper permission has not been taken when needed.

_____

(Name of the Student: **Lav Kumar Gupta**)

(Roll No. **701902**)

Date: _____

Abstract

Scouring around the bridge pier is a natural and complex phenomenon and it is one of the major causes of a bridge failure in the alluvial channel foundation. Failure of bridges has a potential devastating effect on public safety and economic losses, which lead to political consequences as well as environmental impacts. Therefore, it is essential to countermeasure the scour around the bridge pier. Countermeasures are used to monitor, inhibit, change, delay or minimize stream instability and bridge scour problems. It is highly beneficial because it solves the existing scour problem as well as mitigating it. There are many countermeasures used today to mitigate the scour problem. One of the major and active research areas is pier modification using collars. This thesis studies the effects of four different airfoil collars (i.e., b_{c1}=1.5b, b_{c2}=2.0b, b_{c3}=2.5b and b_{c4}=3.0b, where b_c and b are the diameter of the airfoil collar and pier respectively) as a scour countermeasure. A total of 69 experiments are conducted under two threshold velocities with two pier diameters of 0.05 and 0.06 m and four airfoil collars placed at four locations from the uniform sediment bed. All the experiments are conducted under clear water conditions with uniform sediment and a constant water depth (y) of 0.10 m. Airfoil collar is placed at four elevations, i.e., at bed level, y/4, y/2 and 3y/4 above the sediment bed level. This thesis investigates the effect of flow intensity, collar diameter on scour hole profile and computes the protection efficiencies for different locations of the collar above the sediment bed. The results show that the collar effectively reduces the scour depth. When the collar is located at bed level (i.e., y = 0, y/4, y/2 and 3y/4 above the bed level, the protection efficacies are found to be ranging between 55 to 100%, 40 to 53%, 23 to 38% and 8 to 29% for b_{c1}, b_{c2}, b_{c3}, and b_{c4} respectively. It is observed that the maximum percentages of scour reduction are 78, nearly 100 and 100% in the case of the collars b_{c2}, b_{c3} and b_{c4} respectively, when collar is located on the sediment bed. The scour hole profiles show that the length of the transverse scour hole is greater than that of the longitudinal one. This study uses nonlinear regression analysis to propose relationships for maximum scour depth and time-dependent scour development around the pier in the presence of an airfoil collar. Statistical sensitivity analyses are performed and found that the most and least sensitive parameters are the collar location and dimensionless time.

A comparative study between numerical simulation and experimental results for maximum scour depth and temporal variation of scour development with and without an airfoil collar, is carried out with two collars b_{c2} and b_{c4} using FLOW-3D. A total of six simulations are carried out: pier without AirFoil Collar (AFC), pier with collar b_{c2}, b_{c4} and b_{c2} in reverse to the flow direction (denoted by b_{c2R}) on the sediment bed and pier with collars b_{c2} and b_{c4} at $y/2$ above the sediment bed. The turbulence model used in the study is Large Eddy Simulation (LES) and the bed-load transport model utilized is van Rijn. A nested mesh configuration is used with 12.234 million mesh cells. The percentage error between the experimental and simulated results is around 7%, indicating a good correlation between the experimental and simulation results. Temporal variation of scour depth and the percentage reduction of scour depth using the AFC are explored when placed at various locations. The percentage reduction of scour depth for various cases and different orientations of the collar ranges between 11% and 100%. The increasing order of percentages of scour reduction for collars are b_{c2} at $y/2$ above the sediment bed, b_{c4} at $y/2$ above the sediment bed, b_{c2R}, b_{c2} and b_{c4} on the sediment bed respectively. The collar b_{c2} is 31.78% efficient than b_{c2R} in reducing the scour around the pier. When the collar b_{c2} and b_{c4} are placed on the sediment bed, it is observed that no scouring occurred at the upstream face of the pier and around the pier. In addition, with collar b_{c2R} no scouring occurred in the downstream face of the pier. Scour depth contours, morphological changes in sediment bed, flow patterns, longitudinal scour hole profiles, transverse scour hole profiles and streamlines are developed for the pier with and without the AFC and analyzed for salient features.

Contents

List of figures

List of tables

Nomenclature

The following list gives the notations used in chapters of the thesis.

Notation	Description	Dimension
a^*	Effective diameter	L
a_n	Net area of the collar	L^2
a_t	Total area of the collar	L^2
B	Width of the channel	L
B'	Width of the working section	L
b	Pier diameter	L
b_c	Diameter of the airfoil-shaped collar	L
c_p	Percentage clay fraction	--
D	Depth of the flume	L
D_*	Dimensionless particle size	--
D'	Depth of the working section	L
d_g	Size of riprap stone	L
d_{se}	Equilibrium scour depth around pier without collar	L
d_{sec}	Equilibrium scour depth around pier with collar	L
d_{st}	Temporal scour depth around pier without collar	L
d_{stc}	Temporal scour depth around pier with airfoil collar	L
d_{15}	Particle size at 15% finer	L
d_{16}	Particle size at 16% finer	L
d_{50}	Median grain size of the sediment	L
d_{84}	Particle size at 84% finer	L
d_{85}	Particle size at 85% finer	L
E	Efficiency of airfoil collar	--
F_d	Densiometric Froude number	--
F_{di}	Inception of sediment Froude number.	--
$F_{d\beta}$	Inception of scour Froude number	--
F_r	Froude number	--

Notation	Description	Dimension
g	Acceleration due to gravity	LT^{-2}
h_b	Height of the cable-tied block mat	L
h_h	Collar hook height	L
k_{by}	Flow depth-pier diameter parameter	--
$k_{d_{50}}$	Sediment size factor	--
k_I	Flow intensity factor	--
k_s	Pier shape factor	--
k_σ	Sediment non-uniformity factor	--
k_θ	Pier alignment factor	--
L	Length of the flume	L
l_{tb}	Top length of the cable-tied block mat	L
l_{bb}	Bottom length of the cable-tied block mat	L
L_s	Slot length	L
p	Hydrostatic pressure	$M^1 L^{-1} T^{-2}$
$\bar{p}$	Filtered pressure	$M^1 L^{-1} T^{-2}$
Q	Approach flow	L^3T^{-1}
R_e	Reynolds number	--
R_h	Hydraulic radius	L
R_L	Reference length	L
r	Distance from the pier center	L
S	Specific gravity of the sediment bed	--
$\bar{S}_{ij}$	Rate of strain tensor	--
T	Dimensionless time for pier without collar	--
T_*	Non-dimensional time scale of scour	--
T_c	Dimensionless time for pier with collar	--
T_e	Time scale of scour	T
T_R	Thickness of riprap	L
t	Elapsed time	T
t_e	Equilibrium time	T
u_i	Instantaneous velocities in i^{th} the direction	LT^{-1}

Notation	Description	Dimension
u_r	Radial velocity	LT^{-1}
u_Φ	Tangential velocity	LT^{-1}
$\bar{u}_i$	Filtered velocities in i^{th} the direction	LT^{-1}
u'_i	Sub-filtered velocities in i^{th} the direction	LT^{-1}
V	Approach flow velocity	LT^{-1}
V_a	Armor velocity	LT^{-1}
V_c	Critical flow velocity	LT^{-1}
V_{ca}	Critical armor velocity	LT^{-1}
V_{*c}	Critical shear velocity	LT^{-1}
W_s	Slot width	L
y	Flow depth measured from the sediment bed	L
z	Collar elevation above the sediment bed	L
Z_s	Sinking depth of slot	L
α	Anti-scour collar with protection angle	--
α_t	Threading angle	--
δ	Boundary layer thickness	L
δ_{ij}	filtered scale length	L
θ_{cr}	Critical Shields parameter	--
θ_s	Shields parameter due to skin friction	--
μ_t	SGS turbulent viscosity	$ML^{-1}T^{-1}$
υ	Kinematic viscosity of water	L^2T
ρ_s	Density of the sediment bed	ML^{-3}
ρ_w	Density of the water	ML^{-3}
σ_g	Geometric standard deviation	--
τ_o	Bed shear stress	$ML^{-1}T^{-2}$
τ_{*c}	Critical shear stress	$ML^{-1}T^{-2}$
τ_{ij}	SGS stress turbulent kinetic energy	ML^2T^{-2}
Φ	Radial angle	--
Φ_β	Entrainment coefficient	--

Abbreviations

Abbreviation	Definition
3-D	Three Dimensional
ADV	Acoustic Doppler Velocimeter
AFC	AirFoil Collar
CFD	Computational Fluid Dynamics
CPN 3	Collar Prototype Number 3
DNS	Direct Numerical Simulation
EPS	Extracellular Polymeric Substance
FHWA	Federal Highway Administration (U.S.)
LES	Large Eddy Simulation
MAE	Mean Absolute Error
MAPE	Mean Absolute Percentage Error
NSE	Nash-Sutcliffe Efficiency
RANS	Reynolds-Averaged Navier-Stokes
RMSE	Root Mean Square Error
SGS	Sub Grid-Scale

Chapter 1

Introduction

1.1 Background

In the transportation system, bridges constitute an essential part. Bridges are required where roads, railways, etc., cross waterways. Piers, on which the superstructure of these bridges rest, play a vital role in their stability and safety. Bridges piers often resist loads coming on them with the help of the friction between themselves and the soil around them. The frictional force depends on the contact area between the pier and the soil. For a given pier, the contact area depends on the grip length of the pier below the river bed. In the case of alluvial rivers, the grip length is to be reckoned not from the original bed of the river but the scoured bed around the pier. In the alluvial bed foundation of bridge pier, scouring is one of the primary causes of

failure (Kothyari and Kumar, 2012; Melville and Chiew, 1999a). The construction of bridges has always been a complex and challenging process, especially when spanning over water bodies (Lagasse et al. , 2007). In some instances, it becomes necessary to place piers within the water to span long distances, which can be problematic since the foundations can be undermined, jeopardizing the structural safety of the bridge. As a result, scouring poses a significant concern for public safety and infrastructure. Scouring is the removal of bed materials due to the erosive action of the flowing water. Failures of bridges threaten public safety and economic loss leading to political consequences and environmental impacts (Khaple et al., 2017; Pandey et al., 2022).

Between 1961 and 1974, it is observed that 46 out of 86 bridges were failed due to scour in US (Wang et al., 2019). In 1973, US Federal Highway Administration (FHWA) surveyed 383 bridges, out of which 20% and 70% of bridges failed due to scour around pier and abutment, respectively (Lagasse et al. , 2007; Lagasse et al., 2009). From 1980 to 1990, in Northeastern and Midwestern USA, more than 2,500 bridges were affected by flood and scour (Hunt, 2009; Shahriar et al., 2021). In US, between 1989 and 2000, more than 50% of bridges failed due to flood and scour in 500 instances of bridge damage (Wardhana and Hadipriono, 2003). In 1993, damage of $20 million is caused in coastal regions resulting in the failure of 20 bridges due to waves and scour around the pier (Prendergast and Gavin, 2014). In 1993, during a single flood event in the upstream and downstream of the Missouri River Basin, at least 22 out of 28 bridges on the waterway experienced some form of distress due to scour. The associated repair costs are more than $8 million. About 60% of bridges failed due to scour reported by National Cooperative Highway Research Program (NCHRP). For instance, in 1994, tropical storm Alberto made landfall in Georgia, USA and caused damage to over 500 bridges due to scour. Out of these, 31 are considered unsafe and needed reconstruction because scouring reached depths between 4 and 6 meters (Lagasse et al., 2009). Between 2000 and 2014, around 30% of bridge failures in China are due to scouring around bridge piers (Wang et al., 2019). In US, till 2009, more than 20,904 bridges are critically scoured and 80,000 bridges are scoured susceptible (Hunt, 2009). In 2010, The AASHTO LRFD Bridge Design Specification stated that "*A majority of bridge failure in the United States and elsewhere is the result of scour*". It is very well known that a bridge construction cost is gigantic and the failure of bridge causes more irretrievable losses. Scour around the pier is the main reason for the washing away of the bridge near Belgaon in Odisha, India and the collapse of Chadoora bridge in Budgum district, India (Pandey et al., 2022). In recent years,

several bridges in India have collapsed due to scour. In 2016, a bridge over the Savitri River in Maharashtra collapsed due to heavy rains and subsequent scouring leading to the loss of many lives (Tiffany Ap & Sugam Pokharel, 2016). In 2016, a bridge collapsed in the state of Himachal Pradesh after heavy rains caused the riverbed to erode, undermining the bridge's foundations (Express Web Desk, 2016). In 2017, a bridge in the state of Uttar Pradesh (India) collapsed after a train derailed and struck the bridge, causing the bridge's support to be undermined (Our Foreign Staff, 2017). In 2022, a bridge in the state of Bihar (India) collapsed after heavy rains caused the riverbed to erode, undermining the bridge's foundations (Manish Kumar, 2022). The Chakki railway bridge in the Kangra district of India collapsed during flash floods on August 20, 2022 (Anand, 2022). The widespread nature of scouring is evident and it has caused significant damage through various incidents (Hong et al., 2012).

Scour is classified into three categories, i.e., general, contraction and local scour (Deng et al., 2016; Lagasse et al. , 2007; Melville & Chiew, 1999; Negm et al., 2009). Scour characteristics mainly depend upon the erosion and deposition occurring due to the river flow influenced by geological and climate changes (Gupta et al., 2023). Local scour around the bridge pier is a result of a complex phenomenon from the interaction of water and sediment in a three-dimensional flow field (Dey et al., 1995; Kothyari & Kumar, 2012; Zarrati et al., 2006; Zhang et al., 2012), which results in the failure of bridges and it is not always foreseeable at the design stage but emerges later (Ahmad et al., 2015; Christopher et al., 2018; Gazi et al., 2020; Valela et al., 2021). The challenging problem for design engineers is to reduce the scour around the bridge pier due to changes in flow patterns to ensure stability and cost-effectiveness. Therefore, it is necessary to mitigate or delay scour using countermeasures. Countermeasure is defined as something used to reduce, monitor, inhibit, change, delay or minimize stream instability and bridge scour problems. Countermeasures for scouring around the bridge pier mostly depend on the selection of the protection method and on the flow characteristics, river morphology, site geometry and cost of construction and maintenance (Ghodsi et al., 2021; Moghanloo et al., 2022; Ghodsi et al., 2021; Najafzadeh & Barani, 2014). According to Lagasse et al., (2008), countermeasures can be classified into three categories: hydraulic, structural and biotechnical. It is highly beneficial because it solves the existing scour problem or mitigates future scour problems. One of the major and active research areas is structural countermeasures in which pier modifications using collars that aim to protect bridge piers by mitigating scour. The installation of a collar is also known as a flow-altering countermeasure, which reduces the amount of water flowing over the top of the pier

and directs it around the sides. Collar is simply a flat horizontal disk made of sturdy material, such as concrete or steel, which is mounted around the bridge pier. Collar impedes the downflow and horseshoe vortex along the face of pier (Chen et al., 2018; Chiew, 1992; Khodashenas et al., 2018; Valela et al., 2021; Kumar et al., 1999; Zarrati et al., 2004). The shape of the collar is usually rectangular, circular and lenticular. The performance of the collar is evaluated on the basis of collar diameter (width) and position of it from the sediment bed. The collar should be as small as possible so that it is less intrusive to the surrounding environment, easier to fabricate, requires less material and is less expensive. The idea of utilizing collars is first proposed in the 1960s. In 1967, Tanaka and Yano, and Ettema in 1980, investigated the effects of collar diameter and installation height (Garg and Verma, 2012). The impact of the collar on scour depth around the bridge pier is also studied by several investigators (Bestawy et al., 2020; Chiew, 1992; Farooq et al., 2020; Farooq & Ghumman, 2019; Garg & Verma, 2012; Khaple et al., 2017; Kumar et al., 1999; Moncada-M et al., 2009; Pandey et al., 2020, 2022; Valela et al., 2022; Valela et al., 2021b; Valela et al., 2021; Wang et al., 2019; Zarrati et al., 2004, 2006).

With the advancement in computer science, Computational Fluid Dynamics (CFD) became an essential tool for analyzing and visualizing the scour process (Qi et al., 2021). CFD is an important tool for implementing numerical simulations for studying the natural currents in water bodies with fine materials. It gives significant and reliable results compared to experimental results. Nowadays, CFD is more accessible than experimental work because of problems like data collection, scale issues, time restriction, human error and the requirement of human resources in experimental work (Pourshahbaz et al., 2020). Experimental results are obtained only where the gauges and sensors are fixed. Also, during the pandemic and health emergency, it is almost inaccessible to conduct experiments, whereas CFD becomes useful (Valela et al., 2021c). Also, data extraction can be done only from the locations where gauges and sensors are installed. On the other hand, a wide range of hydrodynamic fluid flows and robust numerical simulation modelling can be done using CFD and it allows to examine any location in the region of interest (Choufu et al., 2019; Gautam et al., 2021; Gazi et al., 2020; Giglou et al., 2018; Pourshahbaz et al., 2020). It can theoretically simulate any physical condition and allow the study of a specific isolated phenomenon. Enhancement in computational capabilities made the application of numerical methods easier in sediment transport for computations of scour around hydraulic structures (Acharya & Duan, 2011; Choufu et al., 2019; Gupta et al., 2023). Some available softwares are FLOW-3D, Ansys

FLUENT, SSIIM 2.0, OpenFOAM, Delft 3D and Telemac-Mascaret etc.

The three main turbulence models used in CFD are Reynolds-Averaged Navier-Stokes (RANS), Large Eddy Simulation (LES) and Direct Numerical Simulation (DNS) (Bhide and Abdallah, 2022). RANS solves steady-state Navier-Stokes equations, which include time-averaged velocity. It does not consider the fluctuating components, unsteadiness and anisotropic turbulence on sediment transport (Kirkil et al., 2009). In turbulent flow, energy is transferred from larger scales of motion to smaller scales of motion through a process called energy cascade. The large-scale flow structures, which are characterized by their long time and length scales, dominate the momentum and energy transport. However, at smaller scales, the flow becomes more chaotic and turbulent, with small-scale eddies and vortices appearing and dissipating rapidly. In Large Eddy Simulation (LES), the goal is to simulate the large-scale flow structures accurately while modelling the smaller-scale eddies (Chamani et al., 2011; Kirkil et al., 2009; Koken & Constantinescu, 2008). This is achieved by filtering out the small-scale turbulent fluctuations using a filter function and then applying a turbulence model to the remaining large-scale flow structures. The subgrid-scale turbulent fluctuations are modelled using various approaches, such as eddy viscosity models or dynamic models. DNS is a technique used in CFD to simulate fluid flows by solving the Navier-Stokes equations directly, without any turbulence models (Armenio, 2017). DNS provides a detailed description of all the flow scales, from the largest to the smallest and it is considered the most accurate way to simulate fluid flows (Armenio, 2017). In DNS, the flow is discretized in both space and time and the Navier-Stokes equations are solved numerically at each time step (Armenio, 2017)

1.2 Objectives

This study aims to devise a more effective method for mitigating scouring around bridge pier by using an airfoil collar. Additionally, the study aims to enhance the understanding of the impact of airfoil collar around bridge piers on scouring. Consequently, this main objective is further subdivided as follows:

i. To identify the parameters influencing the maximum scour depth and to develop a relationship between scour depth and time around the bridge pier in the presence of an airfoil collar.

ii. To study the temporal variation of scour depth around the bridge pier in the presence of an airfoil collar and develop a relationship for it.

iii. To make a comparative study between numerical simulation and experimental results for maximum scour depth and temporal variation of scour depth with and without an airfoil collar.

1.3 Scope

The primary objective of this study is to investigate bridge pier scour by developing a solution to mitigate scour and to analyze the influence of airfoil collars on scour. To accomplish these objectives, a combination of experimental and numerical methods are employed. However, it is crucial to acknowledge that this study has inherent limitations due to time and resource constraints associated with both approaches. To achieve the aforementioned objectives, experimental and numerical methods are conducted under the following constraints:

i. This study focused on circular bridge piers with a constant diameter. However, it is important to note that in practice, bridge piers come in various shapes and sizes, including elongated ones. Although the final scour countermeasure design developed in this study can be potentially adapted to accommodate different pier shapes, this aspect is not explored or completed within the scope of this research.

ii. This study focused on clear-water and transition-flow conditions while excluding live-bed experiments, but live-bed conditions may prevail in the field.

iii. Although bridge piers are often designed and constructed in groups and the behavior of scour can vary when multiple piers are located in close proximity, which falls outside the intended scope of this study. As a result, the examination of scour in the context of multiple piers is not addressed in this research. Studies are conducted with a single pier. But, in reality bridge piers are constructed in tandem, side by side and staggered, which includes the effect of interference.

iv. Numerical simulations in this study are conducted using a rigid bed rather than a more realistic mobile sediment bed. This choice is made due to the unavailability of sediment transport capabilities in the FLOW-3D toolbox at the time of the tests. As a result, the simulations focused on studying scour behavior without considering the dynamic interaction between flowing water and mobile sediment, which would have been more

representative of real-world conditions.

v. The present study is carried out with steady and uniform flow under constant depth.

vi. The study doesn't consider scour around the bridge pier due to the contraction effect in the channel.

The conditions under which bridge pier scour can be studied is extensive. Consequently, this study adopted a specific scope that focused on scour countermeasure, as well as generating information regarding scour around pier using airfoil collar for relevant worst-case scenarios. The intention is to provide insights and data for these specific conditions. However, there is large scope for future research to expand on the findings and explore additional scenarios beyond the benchmark data provided in this study.

1.4 Organization of Thesis

The thesis is organized into five chapters and an overview of each chapter is given below:

Chapter 1 gives a brief background about scour and its effects. This chapter also includes the problem statement, objectives and the scope.

Chapter 2 reviews the relevant literature on scour mechanism, scour countermeasures and their classification. Further, this chapter includes a detailed discussion of scour mechanism and the advantages and disadvantages of each countermeasure in scour mitigation. This chapter also presents a summary of the literature and the research gaps identified.

Chapter 3 discusses the experimental and numerical simulation facilities used and the conditions under which the experiments are conducted to achieve the earlier stated objectives.

Chapter 4 discusses the results of the experiments and numerical simulations for scour mitigation using airfoil collars. The results are presented in the form of graphs with appropriate interpretations.

Chapter 5 outlines the conclusions of the study and recommendations for further work. Finally, references are enumerated.

Chapter 2

Literature Review

Scour is a natural phenomenon involving sediment bed erosion when the stream flow exceeds a threshold or critical velocity (Liang et al., 2020; Pizarro et al., 2020; Tang et al., 2022). This phenomenon of bed erosion continues until the equilibrium condition, which is the balance between the rate of deposition and erosion (Chang et al., 2004; Prendergast and Gavin, 2014). Scour is a function of channel geometry, flow characteristics, fluid properties and sediment characteristics of the bed (Izadinia and Heidarpour, 2012; Kothyari et al., 2007). Due to flooding and scour, bridge collapses can potentially cause injuries, death and property damage on a magnitude similar to air disasters, terrorist incidents and natural calamities (Deng et al., 2016; Wardhana & Hadipriono, 2003). Therefore, understanding what causes bridges to collapse is the most effective approach for engineers to prevent catastrophic accidents. The endeavors related to bridge scour can be broadly classified into two groups: those rooted in science and those based on engineering. The former primarily focuses on comprehending the scour process academically, whereas the latter is vital for providing practical guidance

(Barbhuiya et al., 2020; Prendergast & Gavin, 2014). The complex nature of local scour around bridge piers has become a subject of great interest. Extensive research is being conducted to address its destructive consequences, including the potential for bridge failures. Therefore, it is very important to understand its mechanism to mitigate its impacts and the type of countermeasures needed to protect the pier from the local scour. A detailed literature review is done on the aspects mentioned above and is presented below.

2.1 Classification of scour

The scour in the vicinity of a bridge pier may be classified under the following two categories. The classification of scour based on flow characteristics, vis-à-vis structure, includes general or natural, contraction and local scour and based on sediment transport, i.e., clear-water and live-bed scour (Dey, 1995; Tang et al., 2022).

2.1.1. Classification based on characteristics of flow

2.1.1.1 General or natural scour

Scour occurs due to the change in the river's characteristics, such as the meandering river (at its outer bends), regardless of the obstruction (Barbhuiya et al., 2020; Pizarro et al., 2020). This type of scour involves removing sediment from the bed and banks of the channel, which can affect the entire width or a significant portion of it. Based on the duration of scour development, the general scour can be short- or long-term (Liang et al., 2020; Tang et al., 2022). It is short-term if scour is caused by any of the following reasons: single flood, floods of shorter duration in succession, bedform migration, flow convergence and a shift in meandering stream thalweg or braids. It is long-term if scour is caused by any of the following reasons: land use changes, volcanic activities, climate changes, dam or reservoir construction, channel straightening and streambed mining (Liang et al., 2020).

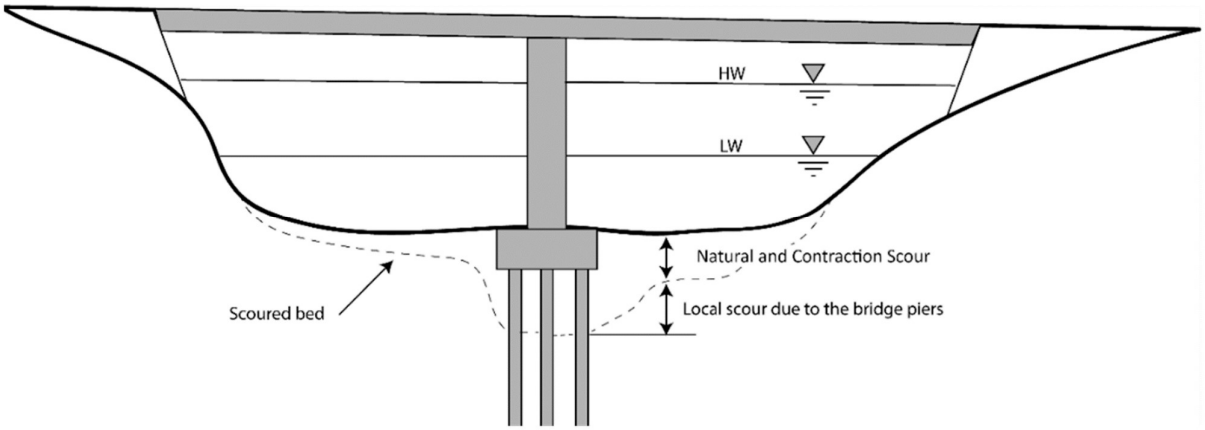

Figure 2.1 Types of scours (natural, contraction and local scour) caused by bridge (Pizarro et al., 2020).

2.1.1.2 Contraction scour

It occurs if a structure causes the narrowing (reduction of width of the channel) of the river waterway, necessitating the provision of guide banks, by the accelerated flow (Ghazvinei et al., 2014; Pizarro et al., 2020). As a result, channel contractions are created at the bridge pier and in cross-drainage works (Dey, 1995; Prendergast and Gavin, 2014; Shahriar et al., 2021). It depends on the divergence of the bridge waterways into that of the river width. Accumulation of debris and ice-jamming can also add to the contraction scour. Based on the quantity of sediment transport, contraction scour occurs in two cases: a live-bed and clear-water. In the live-bed condition, the bed material is transported from upstream, while it is negligible in the clear-water condition (Pizarro et al., 2020).

Figure 2.2 Accumulation of debris around bridge piers (Source: Jenny Knight)

2.1.1.3 Local scour

It results from alterations imposed on the flow field due to structural obstruction along the flow path, creating a scouring hole surrounding that structure (Gazi and Afzal, 2020a). In hydraulic engineering, local scour around the bridge pier is a global phenomenon affecting structures' safety. Local scour causes the failure of bridges threatening public safety and resulting in economic losses (Deng et al., 2016a; Dey, 1995; Lai et al., 2022).

(a) (b)

Figure 2.3: Local scour around the bridge pier: sources (a): https://www.usgs.gov/centers/oki-water) and source (b) (Pizarro et al., 2020).

2.1.2 Classification based on sediment transport

2.1.2.1 Live-bed scour

This is referred to as scour with sediment transport. Here, the shear stress on the bed is greater than the critical shear stress (Brandimarte et al., 2012; Pizarro et al., 2020; Wang et al., 2019). Compared to the clear-water scour, this type of scour occurs more rapidly and oscillates non-periodically in nature. In general, equilibrium scour depth in live-bed conditions is slightly smaller than those in clear-water conditions. Under identical conditions, scour depth in the latter case is about 10% more than the former (Barbhuiya & Mazumder, 2014; Hong et al., 2017). Experimenting with clear-water flow is easier to perform than with sediment-transporting flows. Many investigators prefer to perform experiments in clear-water flow condition, although streams often tends to carry sediment (Chiew, 1992; Rahman & Muramoto, 1999; Vahdati et al., 2020).

2.1.2.2 Clear-water scour

If the bed materials in the natural flow upstream of the structure are at rest and the stream is free of suspended sediment, it is known as clear-water scour (Barbhuiya et al., 2020; Brandimarte et al., 2012). In other words, the shear stress on the bed of the structure is less than the shear stress required for the initiation of particle movement. In this case, the final equilibrium is reached when sediment transport out of scour hole is zero (Dey, 1995).

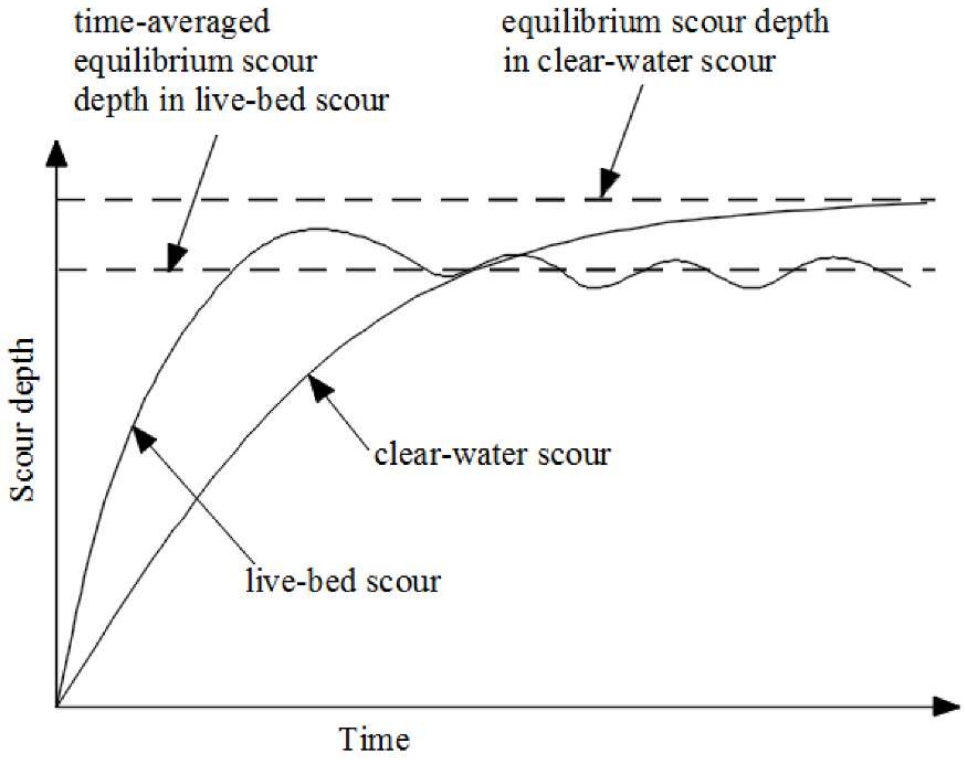

Figure 2.4: Clear-water and live-bed scour (Melville & Chiew, 1999).

2.2 Scour mechanism

Understanding the mechanism of scour is very important before its mitigation. The scour mechanism includes three stages: (i) flow upstream of the pier, (ii) separation of the flow and (iii) flow downstream. The sudden obstruction of a pier in the stream makes the flow velocity zero at the stagnation point, resulting in a vertical pressure gradient. A division of upflow and downflow at the stagnation point on the leading face of the pier are created due to this gradient (Chiew, 1995; Deng et al., 2016; Dey, 1995; Shahriar et al., 2021). As shown in Figure 2.5, the downflow component is guided towards the bed and creates a scour hole by

eroding the sediment bed. The formation of a helical flow pattern in the scour hole caused by the horseshoe vortex results in higher velocities near the bed, leading to an enlargement of the scour hole (Afaridegan et al., 2022; Kumar, 2017). With the increasing depth of the scour hole, the strength of the horseshoe vortex weakens, resulting in a lower sediment transport rate. The horseshoe vortex continues downstream beside the pier before dissipating into the surrounding turbulence (Tafarojnoruz et al., 2010; Vijayasree et al., 2020). As a result of the flow component, a bow wave forms near the free surface next to the obstruction. However, this bow wave does not participate in the scour process; instead rotates in the opposite direction of the horseshoe vortex (Barkdoll et al., 2007; Gazi and Afzal, 2020b; Liang et al., 2020).

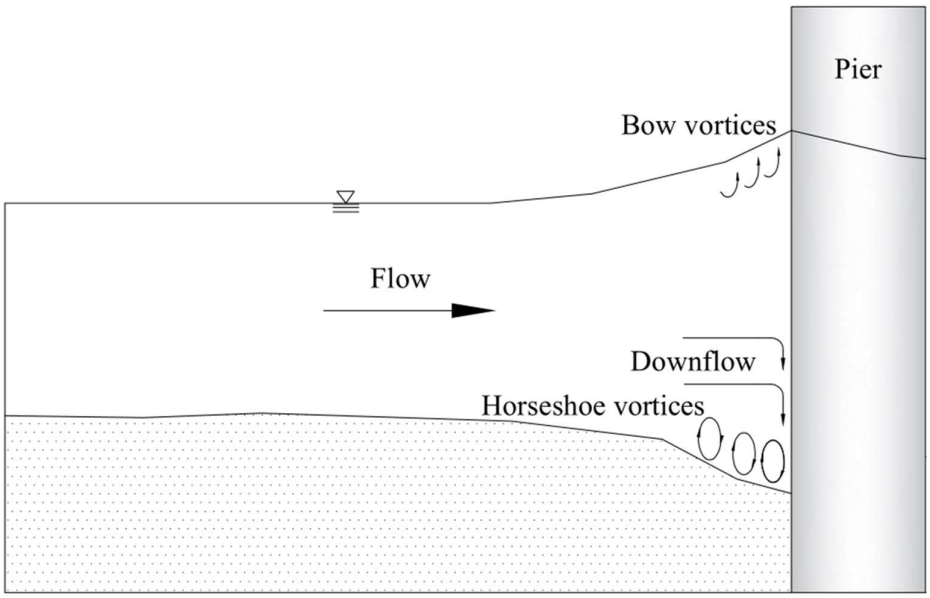

Figure 2.5: Mechanism of local scour at the upstream side of the pier (Guo et al., 2012)

The maximum energy in the approach flow occurs at the upstream face of the pier, which is the sum of hydrostatic and kinetic components at any given depth of the approach flow. When the flow field interacts with the pier, as shown in Figure. 2.6, a boundary layer is created along the pier's perimeter, leading to the flow separation (Narayana et al., 2022). Assuming fully developed flow conditions, pressure can be approximated by Bernoulli's equation as follows:

$$p + \rho_w g y + \frac{1}{2}\rho_w ({u_r}^2 + {u_\Phi}^2) = \text{constant} \quad (2.1)$$

where p is hydrostatic pressure, ρ_w is the density of water, g is the acceleration due to gravity, y is water depth; radial (u_r) and tangential (u_Φ) velocities are given by Equations (2.2) and (2.3).

$$u_r = -V\left(1 - \frac{b^2}{4r^2}\right)cos\,\phi \tag{2.2}$$

$$u_\phi = V\left(1 + \frac{b^2}{4r^2}\right)sin\,\phi \tag{2.3}$$

where V is the approach velocity, b is the pier diameter, r is the distance from the pier center ($r \geq b/2$) and ϕ is the radial angle. By substituting radial and tangential velocities in Equation (2.1), we get:

$$p + \rho_w g y + \frac{1}{2}\rho_w V^2\left(\frac{b^2}{4r^2} - \frac{b^2}{2r^2}cos2\phi + 1\right) = \text{constant} \tag{2.4}$$

To obtain pressure gradient in the radial direction, differentiate Equation (2.4) with respect to the radial angle as shown below:

$$\frac{\partial p}{\partial \phi} = -\frac{1}{2}\rho_w V^2\left(\frac{b^2}{r^2}\right)sin2\phi \tag{2.5}$$

From Equation (2.5), the pressure gradient is zero at the stagnation point where ϕ = 0° and $r = b/2$, indicating that no sediment moves downstream at the pier's leading edge during scour initiation. On the other hand, the maximum negative pressure gradient is at ϕ = ± 45° and $r = b/2$, indicating scour initiation and flow separation.

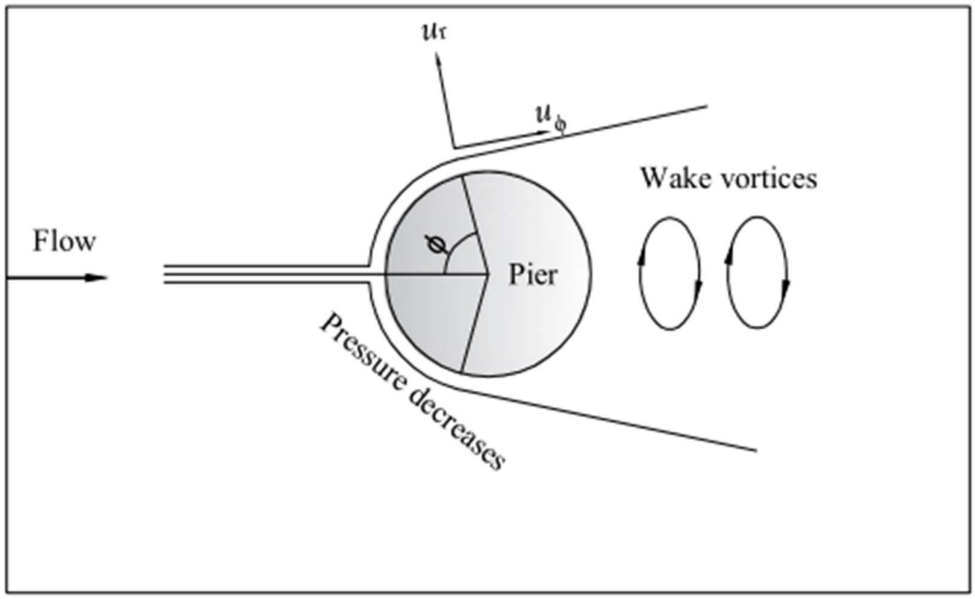

Figure 2.6: Flow interaction with pier at scour initiation (Guo et al., 2012).

Vortex shedding occurs from the flow separation points, forming wake vortices (Chaudhuri et al., 2018; Kumar, 2017). These vortices create a vertical velocity gradient, with the maximum velocity occurring at the bed and decreasing towards the free surface, as shown in Figure 2.7. The wake vortices cause sediment to be suspended in the stream, leading to scouring. As the flow moves downstream, the strength of the wake vortices decreases, but the scour process continues until the equilibrium condition is reached (Shahriar et al., 2021).

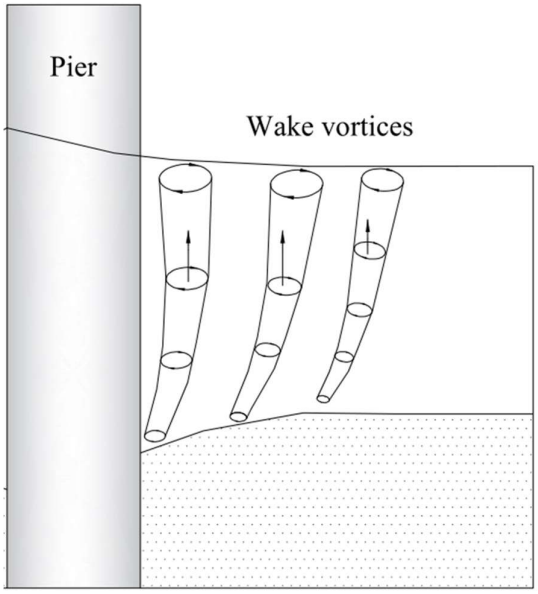

Figure 2.7 Formation of wake vortices on the downstream side of the pier (Guo et al., 2012).

2.3 Empirical equations for scour depth estimation

This section provides the estimation of temporal (d_{st}) and equilibrium scour depth (d_{se}) around circular bridge pier. Several equations have been suggested to estimate the depth of local scour at bridge piers. These equations estimate the scour depth at any time interval or equilibrium conditions. These depths are affected by the following parameters.

i. Flow properties: approach flow depth (y), approach velocity (V), critical velocity (V_c) and acceleration due to gravity (g);
ii. Flow geometry: bed width (B) and pier diameter (b);
iii. Fluid properties: water density (ρ_w), the kinematic viscosity (υ) of water;
iv. Sediment properties: relative density of sediment (S), mean sediment size (d_{50}) and geometric standard deviation (σ_g);
v. Time: elapsed time (t) and equilibrium time (t_e);

vi. Non-dimensional parameters: particle size, $D_* = d_{50}\left(\frac{(S-1)g}{\upsilon^2}\right)^{1/3}$, Froude number $\left(F_r = \frac{V}{\sqrt{gy}}\right)$, densimetric Froude number $\left(F_d = \frac{V}{\sqrt{(S-1)gd_{50}}}\right)$, reference length $\left(R_L = (b^2y)^{1/3}\right)$ and time $\left(T = t\frac{\sqrt{(S-1)gd_{50}}}{R_L}\right)$.

2.3.1 Temporal scour depth

Expressions for temporal scour depth around the bridge pier are presented in Table 2.1.

Table 2.1: Expressions for temporal scour depth around bridge pier.

Authors	Expression	Remarks
Sumer & Fredsøe (1992)	$d_{st} = d_{se}(1 - e^{\frac{-t}{T_e}})$	Time scale of scour, $T_e = \frac{T_* b^2}{\sqrt{(S-1)g{d_{50}}^3}}$, Non-dimensional time scale of scour, $T_* = \frac{\delta {\theta_s}^{-2.2}}{2000b}$ where $\delta =$ boundary layer thickness Shields parameter due to skin friction, $\theta_s = \frac{C_D \mathrm{V}^2}{(S-1)gd_{50}}$, where logarithmic relationship, $C_D = \frac{0.4}{\ln(\frac{z_s}{y}+1)}$ and roughness height due to skin friction, $z_s = \frac{d_{50}}{12}$
Melville and Chiew (1999)	$\frac{d_{st}}{d_{se}} = e^{-0.03\left\|\frac{V_c}{V} ln\left(\frac{t}{t_e}\right)\right\|^{1.6}}$	$t_e = \begin{cases} 48.26\frac{b}{V}\left(\frac{V}{V_c} - 0.4\right) & \text{for } \frac{y}{b} > 6 \\ 30.89\frac{b}{V}\left(\frac{V}{V_c} - 0.4\right)\frac{y}{b} & \text{for } \frac{y}{b} \leq 6 \end{cases}$ Used for the cylindrical pier in uniform sediment
Oliveto and Hager (2002)	$\frac{d_{st}}{R_L} = 0.068N{\sigma_g}^{-0.5}{F_d}^{1.5}logT$	Shape number, $N = 1$ for the circular pier and 1.25 for the rectangular pier. Used when $F_d > F_{di}$, where $F_{di} =$ Inception of sediment Froude number.

Kothyari et al. (2007)	$\frac{d_{st}}{R_L} = 0.272{\sigma_g}^{-0.5}(F_{di} - F_{d\beta})^{2/3} logT$	$F_{di} = \begin{cases} 2.33{D_*}^{-1/4}\left(\frac{R_h}{d_{50}}\right)^{1/6} \\ \text{for } D_* \leq 10 \text{ viscous regime} \\ 1.08{D_*}^{-1/12}\left(\frac{R_h}{d_{50}}\right)^{1/6} \\ \text{for } 10 < D_* < 150 \text{ transition regime} \\ 1.65\left(\frac{R_h}{d_{50}}\right)^{1/6} \\ \text{for } D_* \geq 150 \text{ rough regime} \end{cases}$ Where R_h is the hydraulic radius, inception of scour Froude number, $F_{d\beta} = \Phi_\beta F_{di}$ where entrainment effect, $\Phi_\beta = 1 - \frac{2}{3}\left(\frac{b}{B}\right)^{1/4}$
Lança et al (2013)	$\frac{d_{st}}{d_{se}} = 1 - e^{-a_1\left(\frac{Vt}{b}\right)^{a_2}}$	Where a_1 and a_2 are constants given below: $a_1 = 1.22\left(\frac{b}{d_{50}}\right)^{-0.764}$ $a_2 = 0.09\left(\frac{b}{d_{50}}\right)^{0.244}$

2.3.2 Equilibrium scour depth

Expressions for equilibrium scour depth around the bridge pier are presented in Table 2.2.

Table 2.2: Expressions for equilibrium scour depth around bridge pier.

Authors	Expression	Remarks
Molinas and Hosni (1999)	$\frac{d_{se}}{b} = 18.92\left[\frac{F_r^{0.8}}{(1+c_p)^{1.88}}\right]$	c_p = Percentage clay fraction used for cohesive sediment bed.
Melville, (2000)	$d_{se} = k_{by}k_I k_{d_{50}} k_s k_\theta k_\sigma$	k_{by} = Flow depth-pier diameter parameter $k_{by}\left(\frac{b}{y} < 0.7\right) = 2.4b$ $k_{by}\left(0.7 \le \frac{b}{y} < 5\right) = 2(by)^{0.5}$ $k_{by}\left(\frac{b}{y} \ge 5\right) = 4.5y$ k_I = Flow intensity factor $k_I = \begin{cases} \frac{V-(V_a-V_c)}{V_c} \text{ for } \frac{V-(V_a-V_c)}{V_c} < 1 \\ 1 \text{ for } \frac{V-(V_a-V_c)}{V_c} \ge 1 \end{cases}$ Armor velocity, $V_a = 0.8V_{ca}$ $\frac{V_{ca}}{V_{*c}} = 5.75log\left(\frac{5.53y}{d_{50}}\right)$ where V_{ca} is critical armor velocity and V_{*c} is critical shear velocity calculated by Shield's approach.

		$k_{d_{50}}$ = Sediment size factor $k_{d_{50}}\left(\frac{b}{d_{50}} \leq 25\right) = 0.57log\left(\frac{2.24b}{d_{50}}\right)$ $k_{d_{50}}\left(\frac{b}{d_{50}} > 25\right) = 1$ Pier shape factor, $k_s = 1$ for circular piers Pier alignment factor, $k_\theta = 1$ for circular piers Sediment non-uniformity factor, $k_\sigma = \frac{d_{se(non\ uniform\ sediment)}}{d_{se(uniform\ sediment)}}$
Richardson and Davis (2001)	$\frac{d_{se}}{b} = 2k_1k_2k_3k_4\left(\frac{y}{b}\right)^{0.35}{F_r}^{0.43}$	Correction factor for pier shape, $k_1 = 1$ for circular pier. Correction factor for attach angle, $k_2 = 1$ for direct flow. Correction factor for bed form, $k_3 = 1.1$ for clear-water scour. Correction factor for armoring, $k_4 = 1$ for sand bed material
Sheppard and Demir (2011)	$\frac{d_{se}}{a^*} = 2.5\tanh\left[\left[\frac{y}{a^*}\right]^{0.4}\right]$	a^*= effective diameter = projected width * shape factor Used for transitional ($0.2 \leq y/a^* < 1.4$) and wide piers ($y/a^* < 0.2$).
Guo et al. (2012)	$\frac{d_{se}}{\sqrt{by}} = \tanh\left[\frac{[(S-1)g]^2}{3.75{\sigma_g}^{1.5}}\right]$	Used for clear-water scour in the case of singular circular piers in non-cohesive sediment mixtures.
Kim et al. (2014)	$\frac{d_{se}}{y} = 0.69\left(\frac{b}{y}\right)^{0.35}\left(\frac{d_{50}}{y}\right)^{-0.10}{\sigma_g}^{0.39}{F_r}^{0.56}$	Used for d_{50}= 0.12-11mm and σ_g = 1.2-20.34.

Choi and Choi 2016)	$\frac{d_t}{d_{se}} = e^{0.065\left(\frac{V}{V_{cr}}\right)^{0.35}\left(\frac{y}{b}\right)^{0.19} ln\left(\frac{t}{t_e}\right)}$	t_e $= \begin{cases} 18.94\left(\frac{V^2}{V_{cr}b}\right)^{-1}\left(\frac{y}{b}\right)\left(\frac{b}{d}\right)^{2.6} & \text{for } \frac{y}{b} > 6 \\ 0.36\left(\frac{V^2}{V_{cr}b}\right)^{-1}\left(\frac{y}{b}\right)^{0.52}\left(\frac{b}{d}\right)^{2.6} & \text{for } \frac{y}{b} \leq 6 \end{cases}$ used for the cylindrical pier in uniform sediment
Pandey et al. (2020)	$d_{se} = 0.5k_{by}k_Ik_{d_{50}}k_sk_\theta k_\sigma$	k_{by} = Flow depth-pier diameter parameter $k_{by}\left(\frac{y}{b} < 2.5\right) = 0.45y + b$ $k_{by}\left(\frac{y}{b} \geq 2.5\right) = 2.1b$ k_I = Flow intensity factor $k_I = \frac{0.4V}{V_c} + 0.1$ for $0.4 < \frac{V}{V_c} < 1$ $k_{d_{50}}$ = Sediment size factor $k_{d_{50}}\left(\frac{b}{d_{50}} \leq 35\right) = 0.57log\left(\frac{2.24b}{d_{50}}\right)$ $k_{d_{50}}\left(\frac{b}{d_{50}} > 35\right) = 1$ Pier shape factor, $k_s = 1$ for circular piers Pier alignment factor, $k_\theta = 1$ for circular piers Sediment non-uniformity factor, $k_\sigma = \frac{d_{se(non\ uniform\ sediment)}}{d_{se(uniform\ sediment)}}$

Franzetti et al., (2022)	$\frac{d_t}{b} = 0.257F_1\left(\frac{y}{b}\right)F_2\left(\frac{b}{d_{50}}\right)F_3(\sigma_g)$ $F_4\left(\frac{V}{V_{cr}}\right)F_5\left(\frac{tV}{\sqrt{(S-1)b}}\right)$	$F_1\left(\frac{y}{b}\right) = 1 - 0.675e^{-1.451\left(\frac{y}{b}\right)}$ $F_2\left(\frac{b}{d_{50}}\right) = 0.849\left(\left(\frac{b}{d_{50}}\right)^{1.815} e^{-2.99\left(\frac{b}{d_{50}}\right)^{0.235}} + 0.511\right)$ $F_3(\sigma_g) = 0.74\left(e^{-0.066\sigma_g^{3.923}} + 0.416\right)$ $F_4\left(\frac{V}{V_{cr}}\right) = \begin{cases} 1 - 0.217(1-V)^3 & \text{for } V \le 1 \\ 1 & \text{for } V > 1 \end{cases}$ $F_5\left(\frac{tV}{\sqrt{(S-1)b}}\right) = 1 - e^{-0.083\left(\frac{tV}{\sqrt{(S-1)b}}\right)^{0.231}}$ used for the cylindrical pier in clear water conditions
Nandi and Das (2023)	$\frac{d_t}{b} = 2.86F_1\left(\frac{V}{V_{cr}}\right)F_2\left(\frac{y}{b}\right)F_3(\sigma_g)$ $F_4\left(\frac{b}{d_{50}}\right)F_5\left(\frac{tV}{\sqrt{(S-1)b}}\right)F_6(\beta)$	$F_1\left(\frac{V}{V_{cr}}\right) = \begin{cases} 1.1791\left(1 - \frac{V}{V_{cr}}\right) & \text{for } \frac{V}{V_{cr}} \le 1 \\ 1 & \text{for } \frac{V}{V_{cr}} > 1 \end{cases}$ $F_2\left(\frac{y}{b}\right) = \begin{cases} 0.7786\left(\frac{y}{b}\right)^{0.1759} & \text{for } \frac{y}{b} \le 4 \\ 1 & \text{for } \frac{y}{b} > 4 \end{cases}$ $F_3(\sigma_g) = 0.3538 + \frac{0.6854}{1 + e^{6.9924ln\left(\frac{\sigma_g}{1.7196}\right)}}$ $F_4\left(\frac{b}{d_{50}}\right) = 0.8491\left(\left(\frac{b}{d_{50}}\right)^{1.8158} e^{-2.9905\left(\frac{b}{d_{50}}\right)^{0.235}} + 0.5112\right)$ $F_5\left(\frac{tV}{\sqrt{(S-1)b}}\right) = 1 - e^{-0.1\left(\frac{tV}{\sqrt{(S-1)b}}\right)^{0.2}}$

		used for the cylindrical pier in clear water conditions

2.4 Scour countermeasures

The challenges posed by scouring may not always be predictable during the design phase, but they can potentially arise later. Scour countermeasures monitor, control, inhibit, change, delay, or minimize bridge scour problems and address existing and future scour issues (Lagasse et al., 2008). It can be difficult for an engineer to choose the most suitable countermeasure for a given situation, as each has its own advantages and disadvantages. According to Lagasse et al., (2008), countermeasures can be classified into three categories: (i) hydraulic, (ii) structural and (iii) biotechnical, as shown in Figure 2.8. A detailed discussion of scour countermeasures is presented in the following sections.

2.4.1 Hydraulic countermeasures

Hydraulic countermeasures aim to modify the flow path of water by utilizing the river training structure or armoring the riverbed (Lagasse et al., 2008). These are easier to install, less disruptive to the bridge and cost-effective. These are further categorized as river training structures, including spur dikes, guide banks, sacrificial piles, submerged vanes and bed armoring devices, including riprap, partially grouted riprap, cable-tied bocks and gabions.

2.4.1.1 River training structures

River training structures alter the flow characteristics in the vicinity of the upstream of the bridge pier to reduce the risk of scour resulting from the passage of the flow (Lagasse et al., 2008). These structures can be made from various materials, such as metal, wood, or concrete and are generally perpendicular and parallel to the flow direction and area covering. Spur dikes and guide banks are the countermeasures that are perpendicular and parallel to the flow, respectively. The area covering countermeasures includes sacrificial piles and submerged vanes.

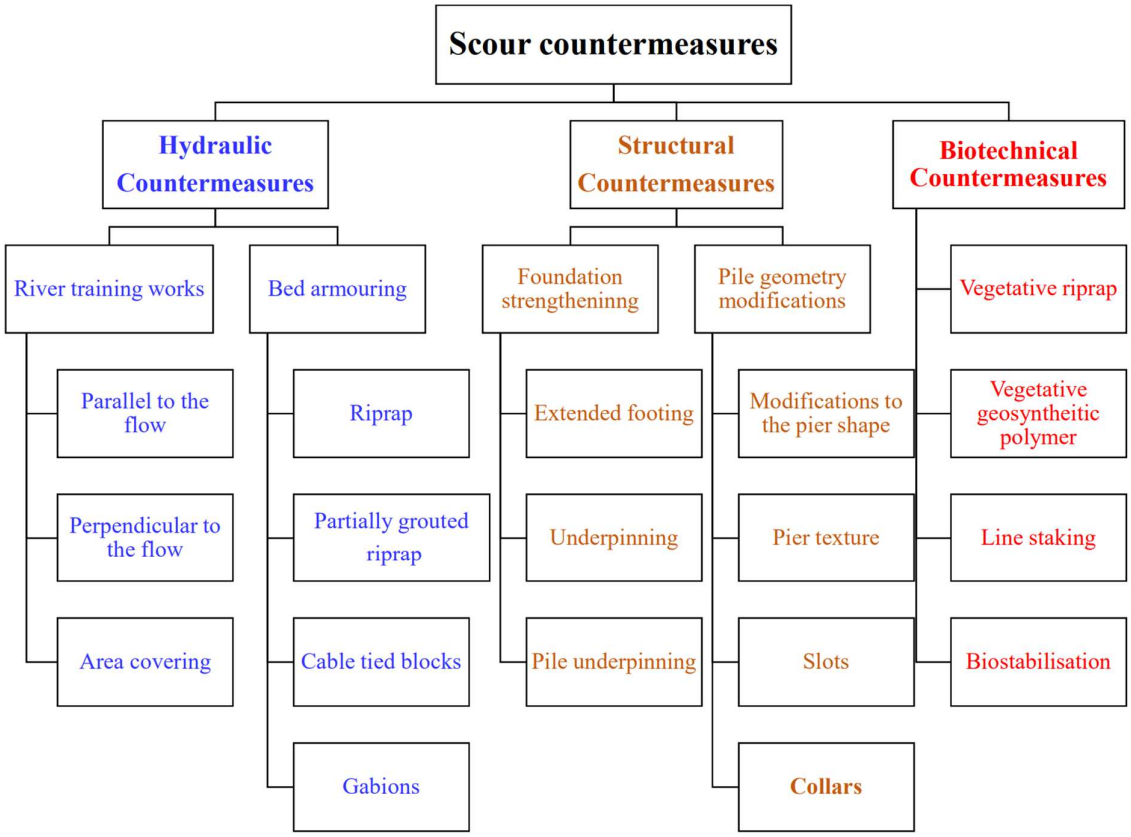

Figure 2.8: Classification of scour countermeasures.

Spur dikes are one of the most common river training structures made of rock, concrete or other materials (Lagasse et al., 2008). These are long and narrow, extending from the river bank into the river and are usually built perpendicular to the flow, as shown in Figure 2.9. If spur dikes point downstream, bed shear stress reduces as the movement of the water is guided away from the bank resulting in less scour (Lagasse et al., 2008). By reducing the shear stress, spur dikes can help to protect the bank from erosion and prevent the loss of land. To promote stability along a riverbank, several spur dikes may be installed at relatively close intervals from each other. These dikes decrease the mean flow velocity, allowing sediment to settle and accumulate between them. Accumulation of debris is the main area of concern which restricts the usage of spur dikes (Kothyari et al., 2007).

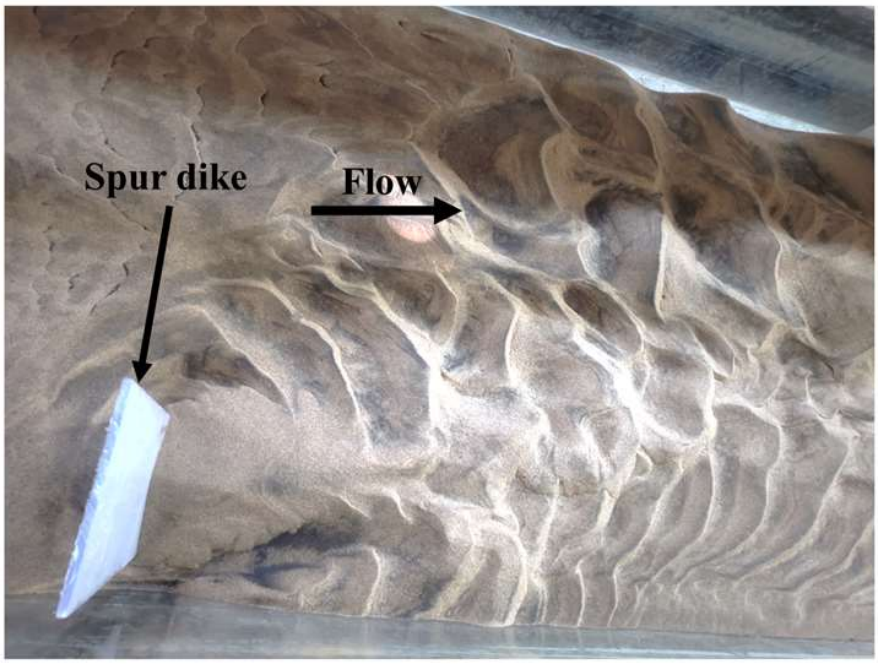

Figure 2.9: Spur dike placed perpendicular to the flow in an experimental setup at NIT Warangal.

Guide banks are similar to bunds and embankments, mainly constructed almost parallel to the flow direction. Guide banks built near the bank helps in decreasing the boundary shear stress since water gets channelized by flowing through the guide banks resulting in lesser flow velocities along the bank. As a result, scour gets reduced (Melville & Hadfield, 1999). If guide banks are constructed along two bridge abutments with wider openings, i.e., bell-shaped towards the upstream mitigating local scour around the bridge piers. However, higher flow velocities and flood discharges may induce instability in the guide banks. By installing guide banks either parallel to one another or angled outwards in the downstream direction, the flow of water can be redirected and the velocity can be reduced, which can help to prevent erosion and other issues (Melville et al., 2006).

Unlike the previously mentioned river training structures, which are situated alongside the river banks, these are spread out across the upstream flow. "Area covering" is a general term that could refer to any structure or technique that aims to cover a specific river area or its surroundings. It includes sacrificial piles, submerged vanes or sills (Gaudio et al., 2012; Ghorbani and Kells, 2008; Melville1 and Hadfield, 1999). Sacrificial piles, typically constructed from steel or wood, are anchored into the riverbed upstream of a bridge pier to redirect the forceful flow of water. This redirection creates a slower velocity wake region

behind the piles, effectively reducing the erosion or scour that may occur around the pier. The effectiveness of the sacrificial piles depends on several factors, including the number of piles, their diameter, height and orientation. Figure 2.10 shows the experimental setup of sacrificial piles around the pier. Studies have revealed that the optimal configuration for sacrificial piles is triangular, pointing upstream which reduces scour by 56% (Melville1 and Hadfield, 1999).

Submerged vanes are typically made of durable materials such as concrete, stones or other erosion-resistant materials. They are designed to be partially or fully submerged in water. Installing a vane near a pier alters the streamlines, diverting them away from the pier and diminishing the intensity of the horseshoe vortex. Ghorbani and Kells (2008) concluded that when vane heights other than 0 cm are used, cylindrical piers experience an increased scour depth. While river training structures have the potential to mitigate scour under certain circumstances, there is no single structure that can provide an effective solution for all scenarios. Due to this limitation, river training structures may not be the most suitable option for addressing scour-related issues.

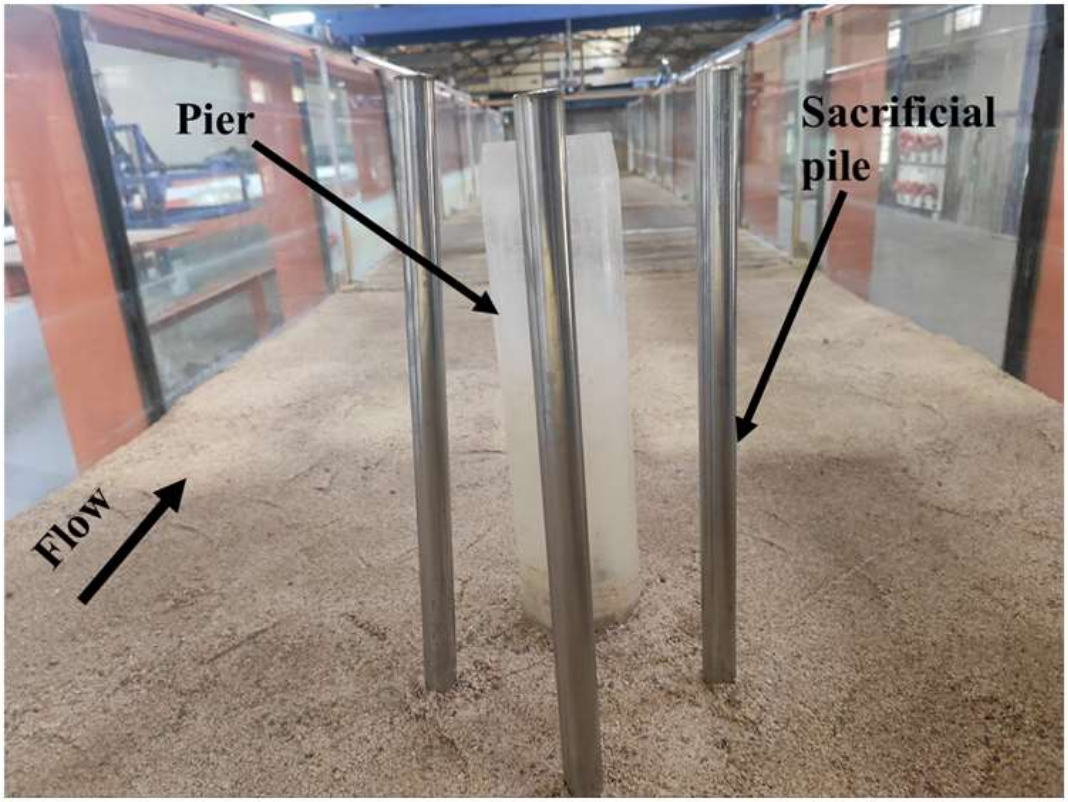

Figure 2.10: Sacrificial piles around the pier in an experimental setup at NIT Warangal.

2.4.1.2 Bed armoring countermeasures

Bed armoring countermeasures enhance the resistance of streambeds and function as a physical barrier. According to Lagasse et al., (2008), armoring involves placing a protective layer over the riverbed to enhance the resistance of the underlying erodible material against the powerful forces generated by the passing flow. Riprap, partially grouted riprap, cable-tied blocks and gabions are some of the bed armoring countermeasures discussed below.

Riprap is a widely used countermeasure to prevent scour due to its demonstrated effectiveness and widespread acceptance (Chiew, 1992; Chiew, 1995; Park, 2008). It involves placing larger stones on top of the riverbed, as shown in Figure 2.11. It is typically done at locations where the riverbed experiences accelerated flow.

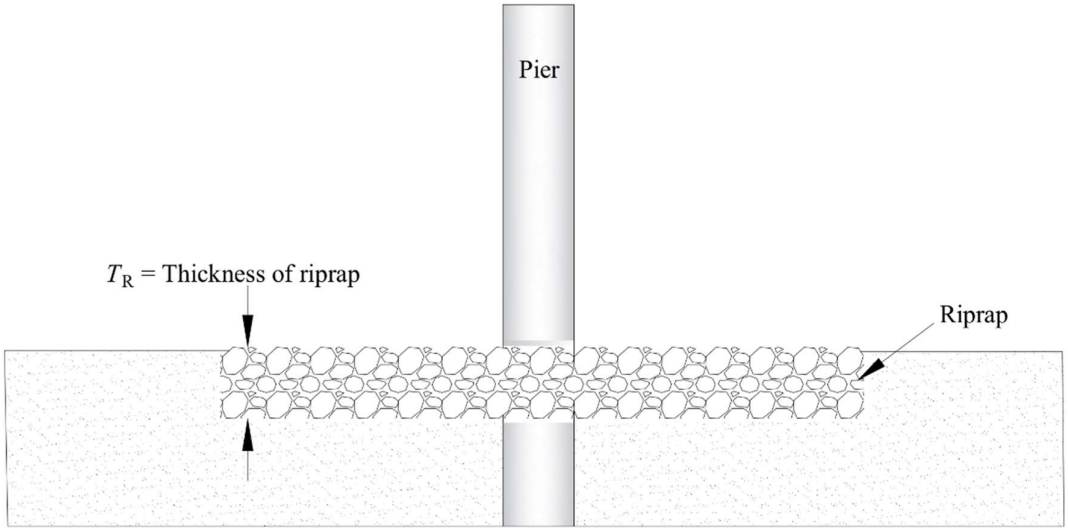

Figure 2.11: Riprap configuration around the pier (Chiew, 1995).

Riprap is often used in areas where water flow is particularly strong, such as river channels and is also used in coastal areas to protect against wave action and coastal erosion (Barkdoll et al., 2007). Stones used for riprap are larger than the riverbed material and their greater mass requires higher shear stresses from the flowing water to dislodge them. As a result, the use of riprap reduces scour (Lauchlan & Melville, 2001). The size of immovable riprap stones is determined from two approaches, i.e., critical shear stress and critical flow velocity of approach. It is observed that scour around the pier starts at 50% of critical flow velocity and it doesn't depend on the diameter of the sediment particle (Bhalerao and Garde, 2010). The size

of riprap stone (d_g) recommended by Patel and Raju (2010) is given by the following Equation (2.6);

$$d_g = \frac{12\tau_o}{(S-1)\tau_{*c}\sigma_g} \tag{2.6}$$

where τ_o is bed shear stress, S is specific gravity, τ_{*c} is critical shear stress and σ_g geometrical standard deviation. Bhalerao and Garde (2010) have recommended the following Equation (2.7) for the thickness of riprap (T_R);

$$T_R = \frac{V^2}{2g(S-1)} \tag{2.7}$$

Worman (1990) gave the Equation (2.8) for the thickness of riprap (T_R), in which d_{85} and d_{15} are particle size at 85% and 15% finer, respectively.

$$\frac{V}{gT_R} = 6\left(\frac{d_{85}}{d_{15}}\right) \tag{2.8}$$

Riprap can fail in three ways under clear-water conditions. The initial failure mode arises when the stones used are too small and lack sufficient mass to withstand the flow-induced stress. The second type of failure is caused by winnowing, which refers to gradually removing smaller riverbed particles from beneath the layer of larger riprap stones. If the winnowing persists, the pier gets surrounded by scour hole as the riprap fails to offer adequate protection (Chiew, 1995). The final cause of failure is edge failure, whereby erosion occurs around the outermost stones of the riprap layer. This can result in the displacement of some of the edge stones, which are carried away by the flowing water (Yoon and Kim, 2004).

Consequently, the underlying finer material becomes exposed and eventually erodes, leading to the potential detachment of the riprap layer. Finally, in live-bed conditions, riprap is susceptible to an additional type of embedment failure (Ballegooy, 2004; Lagasse et al., 2008; Melville et al., 2006). Partially Grouted Riprap is a type of riprap in which 50% of voids are filled with grout. It is a standard riprap with 50% of the void filled with grout (Lagasse et al., 2008). Grout acts like glue and holds the stones together. However, specific issues are associated with installing partially grouted riprap, particularly regarding filling the voids accurately on the worksite. Also, it is not always possible to grout specific locations due to factors such as site conditions, equipment availability and the availability of grout, thereby

restricting the application of this method to specific areas (Bhalerao & Garde, 2010; Kreyenschulte et al., 2020; Lagasse et al., 2007; Lagasse et al., 2008).

Cable-tied blocks known as Articulating Concrete Blocks (ACB) are the system of interlocking concrete blocks designed to absorb and dissipate the energy of flowing water, thereby reducing erosion and scour (Ballegooy, 2004; Barkdoll et al., 2007). The concrete blocks are precast and interconnected with cables to form a mat-like structure. The cables can be made of steel or any synthetic material that is strong enough to hold the blocks against the water flow. Due to this interconnections these blocks act as a system rather than independently (Ettema et al., 2006). The geometric parameters top length (l_{tb}), bottom length (l_{bb}) and height (h_b) of the cable-tied block mat are shown in Figure 2.12. As the blocks' size increases, the block mat's shear stress capacity increases (Melville et al., 2006). The mat and the blocks can be lifted off due to the high-pressure gradients forming. To avoid this problem, the mat should be firmly anchored into the riverbed. The pier should be firmly tied to the mat to avoid scouring between the pier and the mat.

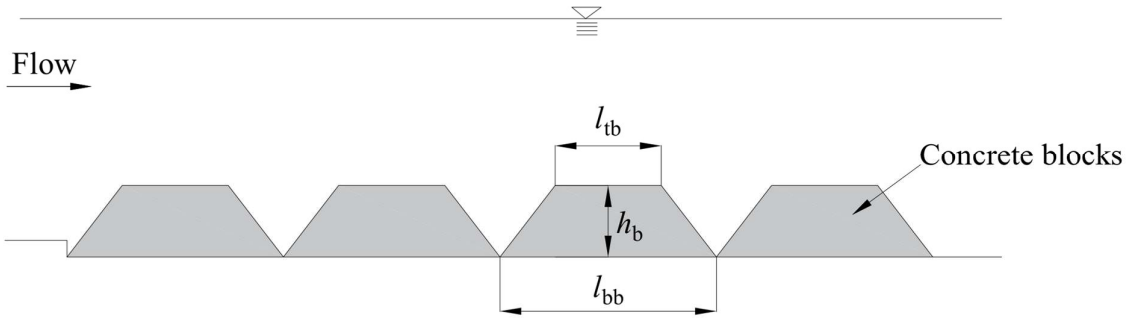

Figure 2.12: Geometric parameters of cable-tied blocks (Melville et al., 2006).

Gabions are wired mesh baskets filled with stones placed around the pier on the riverbed, providing a protective layer that helps prevent scour, as shown in Figure 2.13 (Melville et al., 2006). One of the benefits of gabions is that they can be filled on-site with any stone, making them a flexible and adaptable solution. In addition, the wired mesh used in gabion allows the containers to deform and adapt to moderate changes in the riverbed, providing additional protection against scour (Yoon and Kim, 2004). Gabions are a cost-effective solution widely used in bridge construction and other infrastructure projects. However, due to the relative lack of rigidity of the wired mesh, it may gradually be damaged, leading to eventual breakage and the release of contained stones. When this happens, the gabion mesh loses its purpose and the stones, which are smaller in size, are washed downstream without providing any benefits.

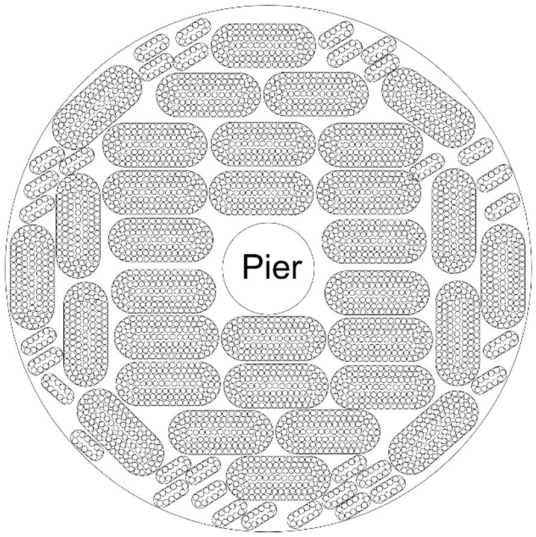

Figure 2.13: Gabion placed around the pier (Yoon and Kim, 2004).

2.4.2 Structural countermeasures

The objective of the structural countermeasures is to strengthen the bridge pier to reduce the effect of scour. It can be achieved by strengthening the foundation below the pier or modifying its geometry.

2.4.2.1 Foundation strengthening

Foundation strengthening is performed by extending the footings, underpinning and pile underpinning. Footing is extended by increasing its horizontal dimensions by concreting below the ground level. Due to the increment in bearing area, stress induced on the footing is reduced and this extension around the footing behaves as an apron protecting the bed. The location of the top of the footing is vital for protecting the river bed against the vortices. Scour depth is more if the location of the top of the footing is above the river bed when compared to the uniform pier (Melville & Raudkivi, 1996). So, the amount of scour reduction depends on how far away the footing extends above the river bed (Jones et al., 1995). Undermining refers to erosion below the footing during floods, which brings up the challenge of extending the existing footing to prevent it from occurring.

Underpinning involves increasing the depth of the footing into the river bed, i.e., vertical extension of the footing. Concrete is filled by excavating the soil beneath the footing. This strengthens and prevents the footing from becoming unstable due to scour. However,

excavation below the existing footing may not be suitable for old masonry bridges and closure of the traffic during its construction process creates a disturbance (Agrawal et al., 2005). Underpinning is expensive and labour-intensive and therefore it is generally used for repairing purposes rather than scour protection. Pile underpinning provides stability to the pier by installing piles below the footing and beyond the predicted scour depth, as shown in Figure 2.14 (Ettema et al., 2006). If a large number of piles are to be placed below the footing, expansion of footing and arrangement of pile cap is necessary, which enhances the cost of construction and labour requirement. All the methods of foundation strengthening alter the natural state of the pier. So, these methods should be adopted only during extreme scour conditions.

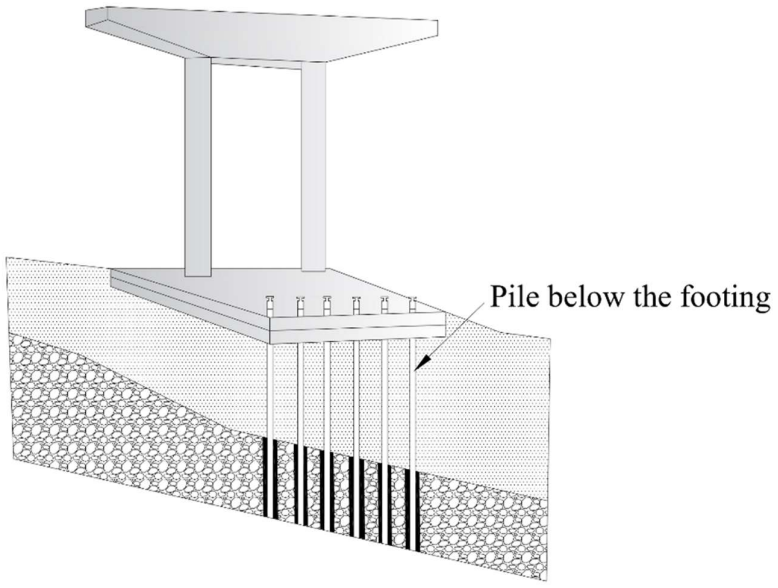

Figure 2.14: Pile underpinning below the pile cap (Agrawal et al., 2005).

2.4.2.2 Pier geometry modifications

Pier geometry can be modified by altering the pier shape, pier texture, providing slots to the pier and installing a collar around the pier. These modifications alter the flow field around the pier so that intensity of vortices becomes less effective.

2.4.2.2.1 Pier shape modifications

Pier shape modifications reduce the impact of the downflow and intensity of the horseshoe vortices. Vortex formation is attributed to the curvature of flow, which results in scouring around the upstream nose of the pier (Al-Shukur & Obeid 2016; Tison, 1961). Pier shapes can

favour scour reduction if they are designed to streamline with the flow (Melville & Sutherland, 1988). This is because a streamlined pier has a sharper leading edge, reducing the intensity of downflow and horseshoe vortices. Al-Shukur and Obeid (2016), conducted experiments with ten different shapes of piers and concluded that the maximum scour reduction is by a streamlined pier, which reduced the scour depth by 60% when compared to the rectangular pier. Even though sharp-nosed and hexagonal piers look streamlined, less scour reduction is observed due to the presence of corners. The lenticular pier, which is a type of streamlined pier, showed scour reduction as high as 68% when compared to the rectangular pier (Vijayasree et al., 2020, 2019). This can also be verified with CFD modelling by Jalal and Hassan (2020) wherein a lenticular pier reduced 40% more scour than a rectangular pier. The scour depths of rectangular, square and circular piers are greater than those of streamlined piers because of the larger surface area that is exposed to the water flow. Omara et al., (2022) concluded that circular piers are more efficient in scour reduction than square and rectangular piers with a lesser length-to-width ratio. The shape of the pier also affects the location of the scour hole. Tison (1961) observed that a rectangular pier experienced its maximum scour depth at the upstream nose, whereas for the streamlined shapes, the maximum scour depth occurred at the sides. For the diamond-shaped pier, maximum scour was observed near the corners and minimum scours near the nose (Khosronejad et al., 2012).

2.4.2.2.2 Pier texture

The texture of a pier can be modified through the techniques such as threading or covering the pier with a sheath. These techniques create a surface with friction on the pier face and redirect some horseshoe vortices, resulting in less scour. Threading is wrapping the cable around the pier helically, as shown in Figure 2.15. Threading can be effective even in oblique flows with circular piers. The number of threads, threading angle (α_t) and cable diameter influence scour reduction. Decreasing the threading angle and increasing the number of threads may yield higher scour reduction. Dey and Sumer (2008) suggested triple threading with α_t = 15°, which can reduce scour by 46.3%. By increasing the cable-to-pier diameter ratio, scour reduction around the pier can be as high as 52% (Muhawenimana et al., 2022). The addition of sheath around a pier is the least disruptive and potentially requires minimal maintenance. Gris (2010) used a specially designed sheath around a pier, as shown in Figure 2.16, which reduced the scour by 30%. It has inclined protrusions in front of the collar upstream, creating

inclined vortices, thereby diminishing the intensity of downflow. The rest of the surface with projections creates turbulence, thereby decreasing the intensity of wake vortices downstream.

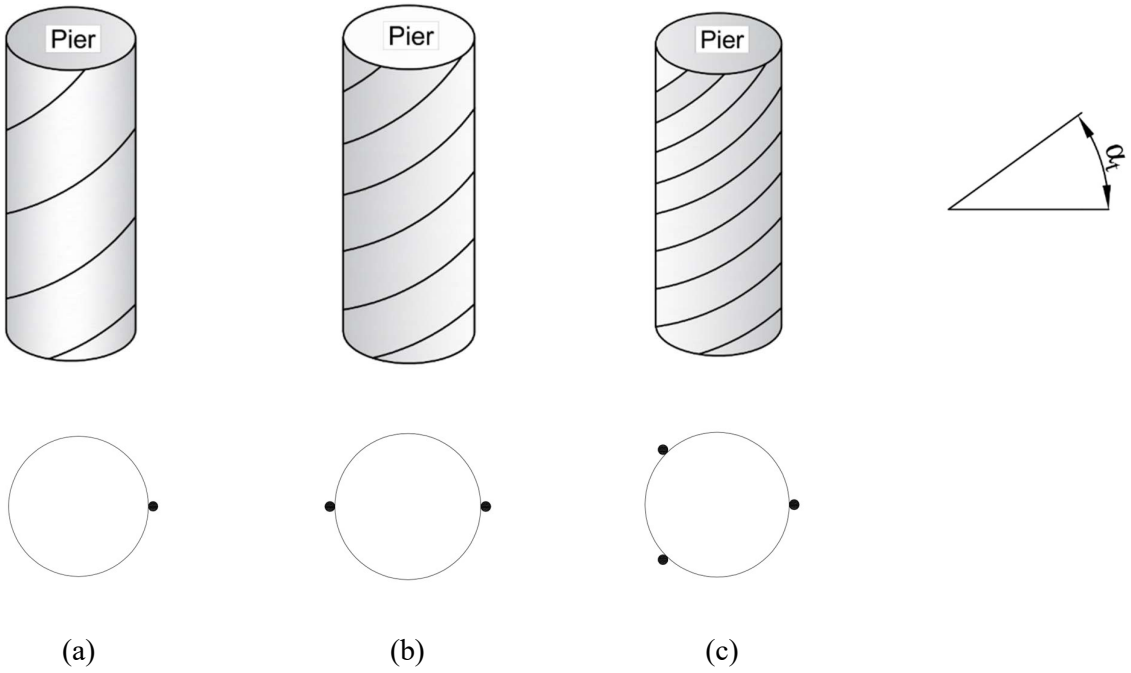

Figure 2.15: (a) Single, (b) Double and (c) Triple threading around the pier (Gaudio et al., 2012).

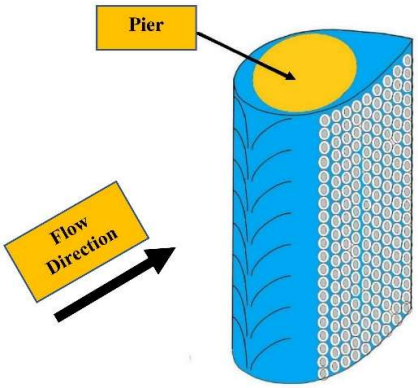

Figure 2.16: Artificial sheath around the pier (Gris, 2010).

2.4.2.2.3 Pier slot

A slot typically refers to a vertical cut made on the downstream face of the pier. It directs the downflow away from the bed, reducing its scour potential and decreasing the intensity of the

horseshoe vortex if the slot is made near the bed. The slot can be near the bed or the free water surface. Slots made near the free surface have a minimal scour reduction effect (Bestawy et al., 2020; Chiew, 1992). Factors affecting the slot's efficiency in scour reduction are slot width (W_s), length (L_s) and sinking depth (Z_s) which are shown in Figure 2.17(a) (Chiew, 1992; Grimaldi et al., 2009). Maximum scour reduction of 30% is observed when W_s/b = 1/4, Z_s/y =1/3 and length of the slot $L_s = y$ (Grimaldi et al., 2009). The scour depth decreases as the slot length increases (Moncada et al., 2009). It is observed by the results of Gaudio et al., (2012), the efficiency of scour reduction increased to 35% when slot length increased from $L_s = y$ to $L_s = y + d_{se}$. Different-shaped slots, as shown in Figure 2.17(b), can increase the flow rate through them and decrease the intensity of the downflow. Bestawy et al., (2020) experimented with parallel slots, Y-slot, T-slots and sigma slots and obtained scour reduction efficiencies of 22%, 47.5%, 50.8% and 59.3% respectively. Obstructing debris in the slot during the floods can prevent flow from passing through, making the countermeasure ineffective. Also, the presence of debris affects the scour reduction efficiency of the slot. If debris are situated close to the water surface, the maximum scour depth may be decreased by as much as 32% or increased by up to 11%, depending on the shape of the debris (Hamidifar et al., 2022). The primary drawback of the slots is that it is almost impossible to create slots for existing piers as they can jeopardize their structural stability (Kumar et al., 1999).

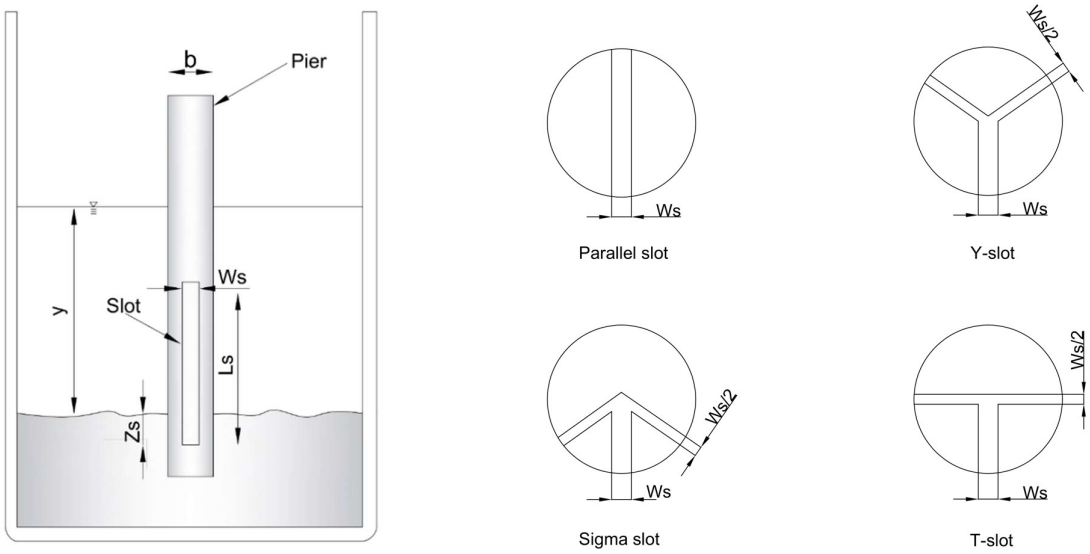

Figure 2.17: (a) Arrangement of slot and (b) Types of slots (Gaudio et al., 2012).

2.4.2.2.4 Collars

Collars are an area of active research in the field of scour countermeasures that aim to protect bridge piers by mitigating scour. It is typically a flat horizontal disk made of sturdy material, such as concrete or steel of different shapes which is attached to the pier. Collars can be located above, below or on the sediment bed. The collar hinders the downflow impact reducing the intensity of the horseshoe vortex. The collar installation is also known as a flow-altering countermeasure, which reduces the amount of water flowing over the top of the pier and directs it to the sides. The efficiency of the collar in scour reduction is influenced by shape, width (b_c), elevation of the collar from the sediment bed (z) and hook height (h_h) The idea of utilizing collars was first proposed in the 1960s. The diameter and location of the collar on the pier are the two primary factors that determine the collar's performance. Several researchers have studied the impact of collars on the scour depth around bridge piers. Tanaka and Yano (1967) and Ettema (1980) have investigated the effects of collar diameter and installation height (Garg and Verma, 2012).

Chiew (1992) studied the influence of circular collars on scour reduction and its location with respect to the sediment bed level. Maximum scour reduction of up to 50% can be obtained when a collar of $2b$ is placed $0.2y$ below the bed level. Scour reduction decreases as the collar moves above the bed level. Kumar et al., (1999) conducted experiments using collar and slot methods and concluded that the slotting approach is not effective when applied over a broad area. However, their findings were based on using only one slot width and they recommended that additional research be conducted using various slot widths to obtain more precise results. They observed that using a collar is a more effective method than a slot for reducing the local scour.

Zarrati et al., (2004) conducted experiments under different conditions including pier alignment, skewness, collar width and elevation. The results showed that wider collars at lower levels were more effective in reducing scouring and that the effectiveness decreased as the pier became more skewed. The maximum reduction of scouring was achieved with a collar that had a width equal to the pier width at streambed elevation. This collar achieved a reduction of 74% when the pier was aligned, 56% when it was skewed at 5° and 35% when it was skewed at 10° to the flow.

Zarrati et al., (2006) investigated the effectiveness of utilizing independent and continuous pier collars in combination with riprap to reduce the local scour around bridge pier groups. It is concluded that two piers aligned in a line, employing a combination of continuous collars and riprap yields the most substantial reduction in scour, resulting in a reduction of about 50 and 60% for the front and rear piers, respectively. The study also concluded that the efficiency of collars is more evident when dealing with a rectangular pier aligned with the flow than with two piers in a line. Moncada-M et al., (2009) conducted study on the impact of collars and slots on the maximum equilibrium scour depth. They used a single pier with a diameter of b and employed two different collar sizes, $2b$ and $3b$ and incorporated a slot of 1.8 cm width in combination with the collars. They concluded that the collar was the most effective in reducing scour depth when placed at the bed level. For the slot, the optimal results are observed when the slot is positioned near the bed. Also, observed that an increase in collar diameter and slot width resulted in a decrease in maximum scour depth.

Heidarpour et al., (2010) examined the effectiveness of using cable, collar, or combination of both as countermeasures against local scouring at a smooth circular bridge pier, near the threshold flow conditions for uniform sediment motion. The findings suggest that using a combination of cable and collar is the most efficient way to reduce scour depth. The optimal configuration for this combination was found to be a cable-pier diameter ratio of 0.15 and thread angle of 15°, which reduced scour depth upstream of the pier by approximately 53%. Furthermore, the study found that using both cable and collar delayed the scouring compared to using only a collar and reduced the rate of scouring compared to using only a cable.

Gaudio et al., (2012) conducted laboratory experiments with five different techniques for reducing pier scour. These techniques included using a collar with sacrificial piles, bed sill with collar, slot with sacrificial piles, collar in combination with slot and bed sill with submerged vanes. It was observed that the most effective method for reducing scour around piers is the use of a pier collar in combination with a slot.

Garg & Verma, (2012) conducted a study to examine the effects of using three different collars with a diameter of 1.5 times the pier diameter (b) on the maximum scour depth and concluded that approximately 80% reduction in maximum scour depth when compared to an unprotected pier.

Jahangirzadeh et al., (2014) conducting laboratory experiments and numerical modelling. A comparison between circular and rectangular collars is made and, in both cases, scour reduction by the rectangular collar is more than the circular collar.

Chen et al., (2018) conducted laboratory experiments with a single hook and numerical simulation by FLOW-3D with double hook using collar widths of $1.25b$ and hook height of $0.25b$. Pier with a single hooked collar placed on the bed reduced scouring by 42% and a pier with a double hooked collar placed on the bed reduced scouring by 50%. Chen et al., (2018) concluded that a double-hooked collar is more efficient in reducing scour than a single-hooked collar. The hook can be provided for different cross-sections of the pier.

Wang et al., (2019) introduced a new parameter called protection angle (α), which is the angular extent of the circular collar, as shown in Figure 2.18. A series of experiments with a circular collar of different protection angles in live bed conditions are conducted. Maximum efficiency of 56.6% is observed with the circular collar of $2.5b$ width, with a protection angle of 360°.

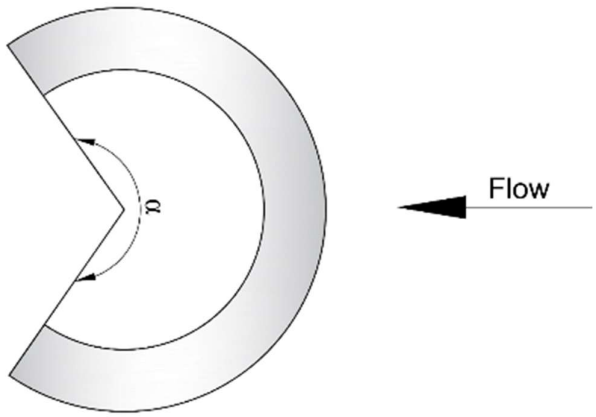

Figure 2.18: Anti-scour collar with protection angle (α) (Wang et al., 2019).

Bestawy et al., (2020) tested flat, 90° and 45°-winged collars around a circular pier and proposed the conical-shaped collar. Its efficiency in scour reduction is as high as 61%, followed by a 45°-winged collar with 50% efficiency. A projection called hook is sometimes provided along the collar's circumference. The collar with a hook deflects the downflow on the front face of the pier, resulting in a reduction in horseshoe vortex strength, as shown in Figure 2.19.

Farooq et al., (2020) investigated the impact of a newly proposed octagonal hooked collar modification on the scour around a vertical pier of octagonal cross-section. The results show that increasing the width of the hooked collar up to 2.5 times the pier width significantly reduced the maximum scour depth. The best combination is found to be a hooked collar width of 2.5 times the pier width and a sidewall height of 0.45 times the pier width, which minimized around 73.3% of the scour hole depth compared to the scenario without any modification.

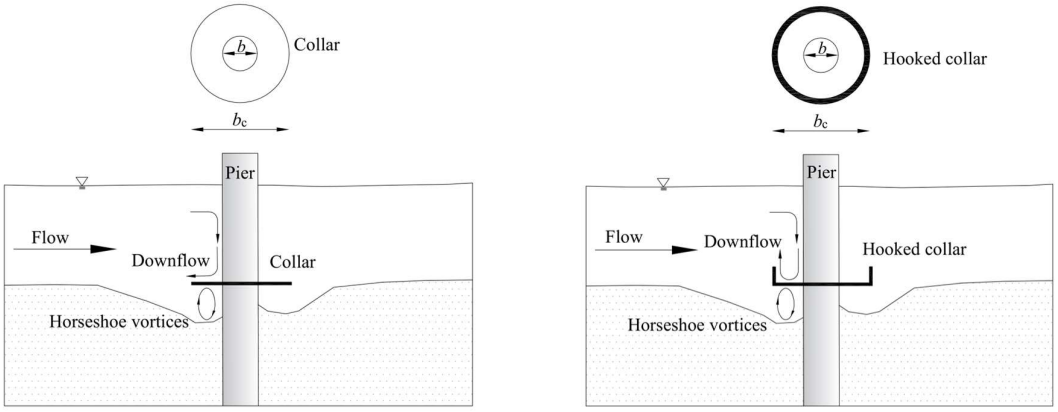

(a) (b)

Figure 2.19: Mechanism of scour with (a) collar and (b) hooked collar (Chen et al., 2018).

Pandey et al., (2022) experimented with circular collars of varying widths to determine the efficient width of the collars. After the statistical analysis, it is found that collar widths of $1.5b$ to $2.5b$ are preferable, followed by collar widths of $2.5b$ to $6b$. Pandey et al., (2020) performed a sensitivity analysis to identify the most sensitive parameters when a circular collar is used. It is found that b_c/b, h/y and T are sensitive parameters affecting the temporal scour depth. Pandey et al., (2020, 2022) obtained a maximum scour depth reduction of 26.4% for collar width b_c = $1.5b$ for d_{50}= 0.4 mm and 41.3% for collar width b_c= $2.3b$ for d_{50}= 0.27 mm and collar placed on bed in both the cases. The maximum scour depth reduction occurred for collar widths of $1.5b \leq b_c \leq 2.5b$. They proposed relationship for estimation of temporal and maximum scour depth.

Hamidifar et al., (2022) addressed the problem of debris accumulation with the collars, where cylindrical, rectangular and triangular-shaped debris are used to find their effect on the

circular collar. On average, the efficiency of the collar is reduced by 25% in the presence of debris and a maximum reduction of 43% is seen when rectangular debris is above the collar.

Izadinia & Heidarpour (2022) used a new controllable and non-permanent technique, i.e., air bubble injection, to reduce scour around the bridge pier. A collar with radial holes is fixed around a pier and is connected to the pressurized air system. The bubble is released at three radial distances. As a result, it is observed that complete air bubble injection around the pier reduced the scour by 44%.

Valela et al., (2022) designed a new collar, Collar Prototype Number 3 (CPN3), which is a viable solution for reducing scour around bridge piers. By utilizing numerical modelling and physical prototype testing, the study shows that Collar Prototype Number 3 significantly reduces scour in terms of maximum depth downstream of the pier and overall scour hole volume by 69.7% and 75.7%, respectively.

Farooq et al., (2023) used a plain lenticular collar for a pier with a lenticular cross-section having a collar width of $3b$ and this resulted in a maximum scour depth reduction of 37%. The use of a hooked lenticular collar, with hook height $0.3b$ and collar width $2b$ located at the bed level, attained a scour reduction efficiency of 60.2%.

Qi et al., (2023) proposed a permeable collar and observed that with the increase in collar porosity, the efficiency of the collar increased initially and after reaching the optimal efficiency of 78.1% at 50% of porosity, it started to reduce. The scour reduction efficiency decreased rapidly as the collar thickness is increased, with a reduction up to 89.6% when the collar thickness was $0.15b$.

2.4.2.3 Scour estimation equations using collar

Scour estimation equations using collars as a scour countermeasure is presented in Table 2.3. The parameters of the collar which influence the temporal scour depth with the collar (d_{stc}) and equilibrium scour depth with collar (d_{sec}) are collar diameter or width (b_c), hook height of the collar (h_h), the elevation of the collar above the bed level (z), the elevation of the collar from the water surface (h), the net area of the collar (a_n) and the total area of the collar (a_t).

Table 2.3: Scour prediction equations using collars as a scour countermeasure.

Authors	Expression	Remarks
Kumar et al. (1999)	$\frac{d_{se}-d_{sec}}{d_{se}}=0.057\left(\frac{b_c}{b}\right)^{1.612}\left(\frac{h}{y}\right)^{0.837}$	Applicable for the circular collar around the circular pier and $z \geq d_{se}$
Jahangirzadeh et al. (2014)	$\frac{d_{se}-d_{sec}}{d_{se}}=0.0057e^{4.71(\frac{a_n}{a_t})}e^{-0.96(\frac{z}{b})}$	Applicable for the circular collar around the circular pier.
	$\frac{d_{se}-d_{sec}}{d_{se}}=0.009e^{4.22(\frac{a_n}{a_t})}e^{-(\frac{b_c}{b})}$	Applicable for the rectangular collar around the circular pier.
Farooq et al. (2020)	$\frac{d_{se}-d_{sec}}{d_{se}}=0.68e^{2.56(\frac{a_n}{a_t})}e^{0.98(\frac{b_c}{b})}e^{-1.42(\frac{h_h}{b})}$	Applicable for the octagonal hooked collar around the octagonal pier.
Pandey et al. (2020)	$\frac{d_{stc}}{d_{st}}=0.23\left(\frac{b_c}{b}\right)^{-0.82}\left(\frac{h}{y}\right)^{-0.58}logT_c$ $\left(T_c=t\frac{\sqrt{(S-1)gd_{50}}}{({b_c}^2y)^{1/3}}\right)$	Applicable when the collar is fixed around the pier or $z \geq 0$.
Pandey et al. (2022)	$\frac{d_{se}-d_{sec}}{d_{se}}=0.2\left(\frac{b_c}{b}\right)^{0.17}\left(\frac{h}{y}\right)^{0.48}$	Equation showed good results for $1.5b \leq b_c \leq 2.5b$ and when the circular

		collar is fixed at and above the bed.
Valela et al. (2022)	$d_{se} = 2268{F_r}^2 - 1534\ F_r + 305$	Applicable for the collar with an outward slope and $F_r \leq 0.34$
Farooq et al. (2023)	$\frac{d_{se} - d_{sec}}{d_{se}} = -56\left(\frac{z}{b}\right)^2 + \left(0.24\left(\frac{b_c}{z}\right) - 7\right)\left(\frac{z}{b}\right) + 1.13\left(\frac{b_c}{z}\right) + 52$	Applicable for lenticular hooked collar around the lenticular pier above the bed level.

2.4.3 Biotechnical countermeasures

Biotechnical countermeasures use vegetation to mitigate the scour around the pier. Vegetation can hold the sediment around it firmly and reduce the flow velocity, thereby reducing scour (Clopper et al., 2007; Lagasse et al., 2008). The presence of aesthetics, cost-effectiveness and environmental sustainability in these countermeasures motivates their adoption. However, their effectiveness is compromised by the absence of on-site growth conditions and the accumulation of debris. Nevertheless, these can be effective if used in combination with the other countermeasures.

Vegetative riprap is a scour countermeasure that utilizes vegetation to reinforce traditional riprap structures. It includes live plants or other vegetation in the riprap layer, providing additional stability and protection against scour (Clopper et al., 2007; Lagasse et al., 2009). Grasse and other low-growing plants are often used to stabilize slopes and reduce erosion, as shown in Figure 2.20, while deeper-rooted shrubs and trees can reinforce the riprap layer. The use of vegetative riprap can offer several advantages over traditional riprap structures. First, vegetation dissipates the energy of flowing water, reducing the likelihood of scour and erosion. Additionally, vegetation can improve water quality and enhance aesthetic appeal. However, the effectiveness of vegetative riprap depends on several factors, including the site conditions, the type of vegetation used and the maintenance of the site. Therefore, proper design, installation and maintenance are critical to the success of vegetative riprap as a scour countermeasure (Pizarro et al., 2020).

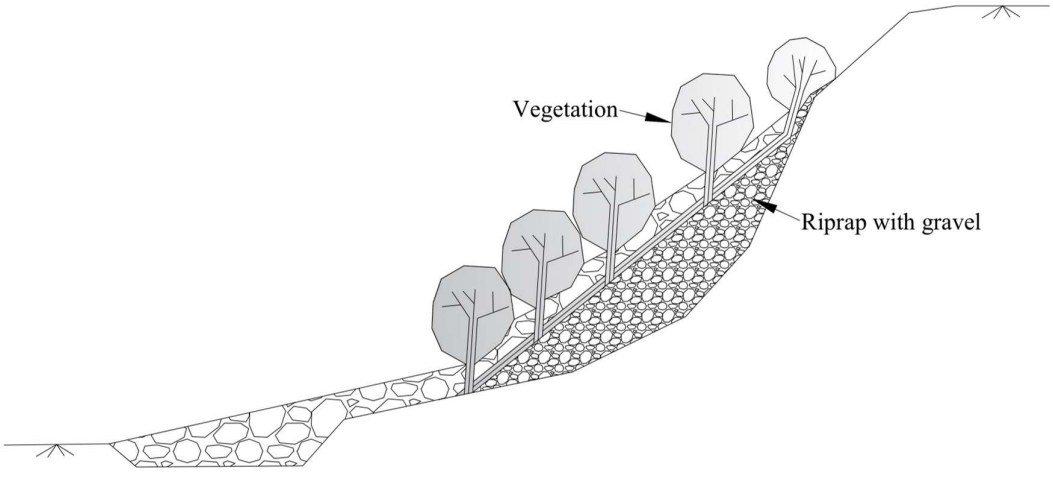

Figure 2.20: Vegetative riprap for slope protection (Lagasse et al., 2009).

Vegetative geosynthetic polymers are materials used in erosion control and scour prevention that combines the benefits of vegetation and geosynthetics. These materials typically comprise a geosynthetic polymer layer with openings that allow vegetation to grow (Zhang & Nakagawa, 2008). The layer is designed to provide structural support and prevent erosion, while the vegetation roots help to anchor the soil in place and absorb water, preventing scour. A geocell is a three-dimensional honeycomb structure made from geosynthetic materials that can be filled with soil, aggregate or vegetation (Bathurst and Knight, 1998). When installed on a slope or bank, the geocell provides stability and support while the vegetation grows through the openings in the geocell walls. This system can help prevent scour by anchoring the soil in place and reducing the water flow velocity. These are particularly effective in areas where traditional erosion control methods may not be feasible or desirable due to environmental concerns or aesthetic considerations.

Line staking is a technique used in scour prevention that involves driving stakes or pilings into the bed of a body of water along a particular alignment or line (Gupta et al., 2023; Lagasse et al., 2009). The stakes or pilings are usually made of wood, steel, or concrete and are driven into the bed at regular intervals, typically perpendicular to the flow direction. This technique aims to create an artificial barrier that deflects or slows down the water flow, reducing the potential for scour (Jones et al., 1995). The effectiveness of line staking depends on several factors, including site conditions, stake spacing, orientation, proper installation and maintenance. It should be used in conjunction with other techniques to ensure maximum protection against scour. Sometimes, driving stakes into the soil is complicated based on-site conditions. Biostabilisation is a method that involves the addition of polymeric substances to the sediment to develop resistance against scour (Schindler et al., 2022). In an attempt to reduce scour around a circular pier, Schindler et al., (2022) conducted experiments with a mixture of dry sand and various percentages of Extracellular Polymeric Substance (EPS) ranging from 0.0125% to 0.5%. Reduction in scour depth, the volume of scour, and time to equilibrium are linearly related to the increase in the percentage of EPS content. Almost 96% of scour reduction efficiency is observed at 0.5% of EPS content (Schindler et al., 2022). The shortcomings of conventional scour countermeasures that can be avoided using stabilization include the cost of material, logistic expenses, on-site assembly and disturbance to the local ecology.

2.5 Summary and research gaps identified

Literature review shows that the downflow and horseshoe vortices are responsible for the scour. To reduce their intensity, scour countermeasures are used. Scour countermeasures can be classified into hydraulic, structural and biotechnical. Hydraulic countermeasures mitigate the scour by modifying the flow behavior and armoring the riverbeds. However, there are situations where hydraulic countermeasures are not feasible due to limited resources or environmental restrictions. Structural countermeasures reduce scour by modifying the structural components above or below the bridge. Above the bed level, the pier can be modified with respect to its shape, texture and slot installation. In addition to this, installing a collar round the pier is widely used due to its higher efficiency in scour reduction. Biotechnical countermeasures use vegetation to mitigate the scour around the pier. Vegetation can hold the sediment around it firmly and reduce the flow velocity, thereby reducing scour (Clopper et al., 2007; Lagasse et al., 2008). The presence of aesthetics, cost-effectiveness and environmental sustainability in these countermeasures motivates their adoption. Following points are observed:

i. A conventional method, such as a rectangular collar, is found to be not so effective in reducing the scour
ii. The circular collar is effective in reducing scour for collar diameters of $2.5b$ and $3b$, where b is the pier diameter.
iii. With an octagonal hooked collar around an octagonal pier placed on the bed reduced the scour by 73.3%.
iv. The Collar Prototype Number3 (CPN3) proposed by Valela et al. (2021), reduced the scour by 69% and effectively contained the undermining below the collar.
v. Complete air bubble injection around the pier reduced the scour by 44%.
vi. Lenticular hooked is the best suited for reducing scour around the bridge pier.
vii. Different types of countermeasures can be combined to mitigate the scour effectively.
viii. A combination of collar and other countermeasures is best suited to reduce the scour around the pier.

A literature review of scour mechanism and countermeasures reveals that there are very limited studies were available and can be considered to be the gaps for further investigation:

i. The flow and scour pattern around the bridge pier in the presence of an airfoil-shape collar.

ii. Numerical simulation of scour around bridge pier with and without airfoil shape collar with different locations.

iii. The scour and flow pattern around the bridge pier in the presence of a streamlined tapered sheath.

iv. Reduction of pier scour using circular and octagonal collars in non-uniform sand.

v. Reduction of pier scour using sacrificial piles, vanes and collars.

vi. Performance of different collars in non-uniform sediment.

vii. Scour around the bridge pier using solid and permeable collars.

viii. Most of the experimental work on the scour mitigation is carried out with uniform sand, which lacks armoring effect on the formation of the scour hole. Therefore, more experimental work on scour mitigation should carry out with non-uniform sediment.

ix. The lack of corners or abrupt changes in the curvature of the circular collar limits the interaction between the flowing water and the collar, resulting in reduced energy dissipation. This could lead to higher flow velocities near the structure and escalate the likelihood of scour occurrence. Therefore, hexagonal, octagonal and lenticular collars should test as protection devices in uniform and non-uniform sand.

x. Many investigators prefer to perform experiments in the case of clear-water flow. However, the flow in nature often tends to carry sediment, so more studies should carry out in live-bed conditions.

xi. A minimal amount of work is being done with the combination of countermeasures.

xii. More studies should be undertaken on eco-friendly scour countermeasures.

Chapter 3

Experimental method and numerical simulation

The available literature on scour depth around circular uniform piers with scour countermeasures shows limited information on scouring around the pier with different types of collars. However, these collars are insufficient to protect the pier from scouring. Furthermore, few studies have been conducted on the effectiveness of collars using Computational Fluid Dynamics (CFD). Therefore, it is intended to study the flow pattern and temporal variation of the scour depth around a pier with an airfoil-shaped collar. The present chapter discusses in details the experimental runs conducted for the analysis. This chapter describes the methodology adopted for conducting the experiments. The experiments are conducted at the Fluid Mechanics and Water Resources Laboratory of National Institute of Technology, Warangal, Telangana, India. The details of the experimental setup, numerical

setup, materials used, experimental conditions, hydraulic conditions and data collection procedure are discussed.

3.1 Experimental setup and materials

3.1.1 Flume

The experiments are conducted in the Fluid Mechanics Laboratory of the Civil Engineering Department at NIT Warangal, Telangana, India. The rectangular flume is 10.3 m in length, 0.8 m in width and 0.4 m in depth. The flume receives water supply from the water tank of constant head. The water supply in the flume is regulated using the pump's delivery valve, which is fixed at the inlet of the flume pipe. A concrete wall made of brick is provided in the rectangular tank to minimize the turbulence in the flow entering the flume. Gravels and boulders are filled 0.50m from the flume's inlet towards the downstream, to absorb turbulence and to get a steady-uniform flow. Adjustable rails are mounted on the wall of the flume to carry the point gauge, Acoustic Doppler Velocimeter (ADV) and other equipment used to measure water surface elevation, flow pattern and sediment bed level. An adjustable wooden gate is provided at the downstream end of the flume to get constant water depth of the flow. The flume has a working section of 2.3 x 0.8 x 0.4 m located at 4 m from the upstream and downstream sides of the channel, as shown in Figure 3.1. The working section has a side wall of glass to visualize the flow and scour processes around the pier. The maximum flow rate through this channel is 0.055 m^3/s with a pump capacity of 11.19 kW. The line diagram of the experimental setup in side and plan view is shown in Figure 3.2.

3.1.2 Pier

Two circular pier models, made of acrylic materials of 0.05 and 0.06 m diameters, are fixed (one at a time) at the center of the working section, normal to the flume bed. The length and thickness of the pier models are 0.60 m and 0.004 m, respectively. The pier is placed at the center of the working section along the flow direction, as shown in Figures 3.1 and 3.2.

Figure 3.1: Photographic view of the working section of the flume used in experiments.

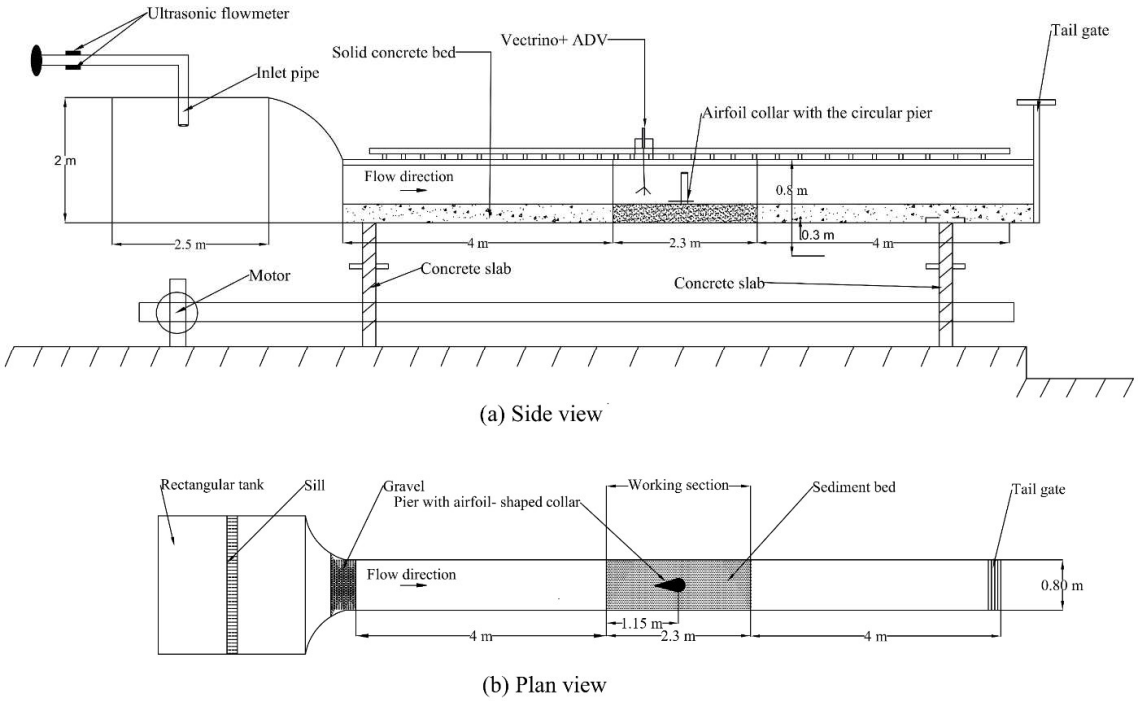

Figure 3.2: Line diagram of the experimental setup; (a) side and (b) plan view.

3.1.3 Sediment Bed

The sediment used in all experiments is retained and passed through two successive sieves. River sediment is passed through two sieve sizes of 425 and 150-micron sieve to obtain uniform sediment. The median grain size of the sediment bed (d_{50}) is 0.32 mm and the specific gravity of the sand (S) is 2.65. Geometric standard deviation ($\sigma_g = \sqrt{d_{84}/d_{16}}$) is 1.31, where d_{84} and d_{16} are the particle size at 84% and 16% finer, respectively. As $\sigma_g < 1.4$, the sediment is uniform (Dey & Sarkar, 2006). The particle size distribution plot is shown in Figure 3.3.

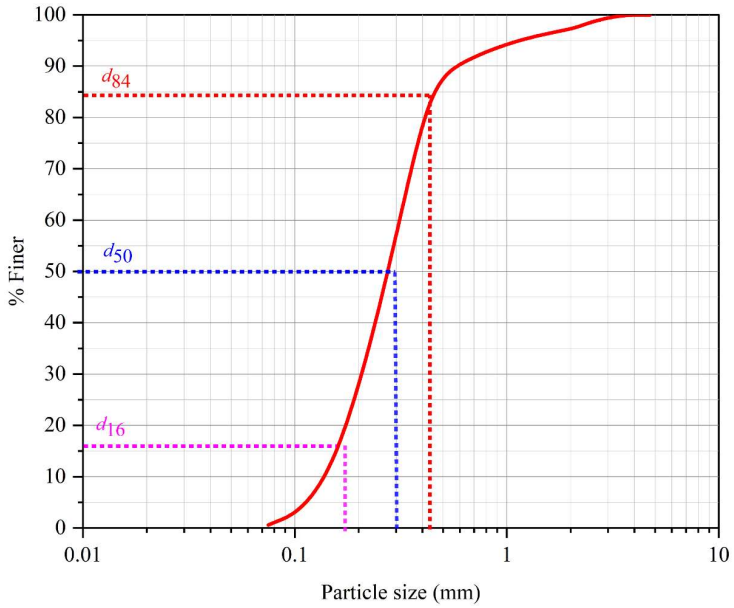

Figure 3.3: Particle size distribution of uniform sediment bed.

3.1.4 Air Foil Collar (AFC)

An airfoil-shaped collar is a device that can be used to reduce the scouring around bridge piers caused by the flowing water. In this study an AFC as a scour countermeasure is used for several reasons.

i. The collar design is based on the principle of fluid dynamics and is intended to minimize turbulence, reducing the energy of water flow around the pier.

ii. AFC generates a lift force that helps to keep the collar in place and prevents it from being washed away.

iii. AFC is effective in reducing the horseshoe vortex due to its upstream triangular nose

shape structure in longitudinal direction. On the transverse side, circular parts are provided to counter the wake vortices.

iv. It is typically fabricated by joining a triangle and half-circle of different diameters, creating a shape resembling an airfoil. Collar is mounted around the pier to impede the downward flow along the front face of the pier.

v. The collar is improved to resemble a streamlined body so that the separation of boundary layers occurs only at the body's extreme rear resulting in a small wake and consequently small pressure drag.

vi. The drag coefficient of a streamlined body is less than for other body shapes.

vii. Most of the researchers found that scour hole profile is similar to elliptical and airfoil-shape. Therefore, it is decided to provide airfoil shapes as scour countermeasures.

Figure 3.4 shows description of an airfoil-shaped collar b_{c2} and Figure 3.5 shows different types of collars in the experimental setup. It is joined with a half circle to a triangle in an airfoil shape, making it easy to construct on the field. The study uses four different airfoil-shaped collars made of acrylic material. The airfoil-shaped collar has four different diameters, i.e., b_{c1}= 1.5b, b_{c2} = 2b, b_{c3} = 2.5b and b_{c4} = 3b, where b is the diameter of the pier. The chord length of the collar (L_c) is two times of collar diameter (b_c). To avoid the contraction effect, the ratio of collar diameter to the channel width is kept around 0.20 (Kothyari et al., 2007; Singh et al., 2020). The thickness of collar possesses the most negligible possible thickness and, in this case, it is kept at 4 mm. The airfoil-shaped collars are placed at four locations, i.e., on bed level, y/4, y/2 and 3y/4 above the sediment bed level, where y is the depth of flow which is kept constant (10 cm) throughout the experimental runs. A pier with an airfoil collar is placed at the center of the working section, i.e., 5.15 m from the inlet of the channel.

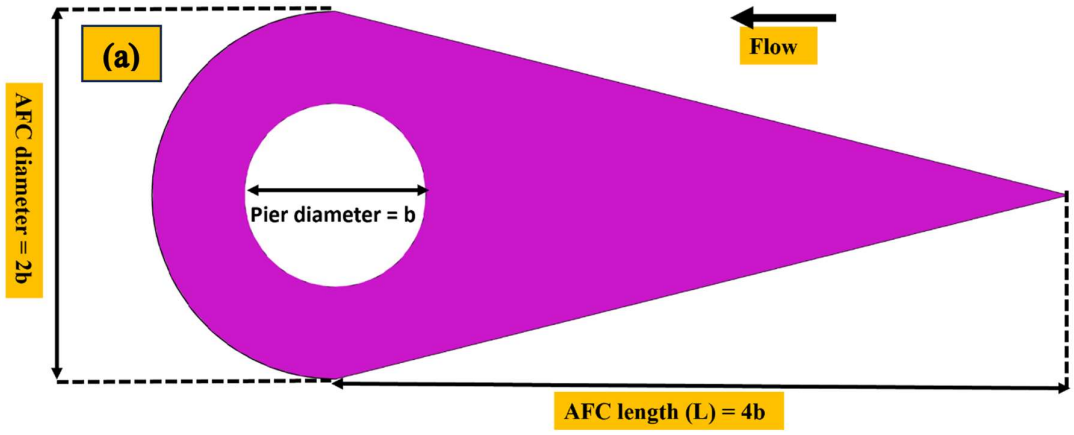

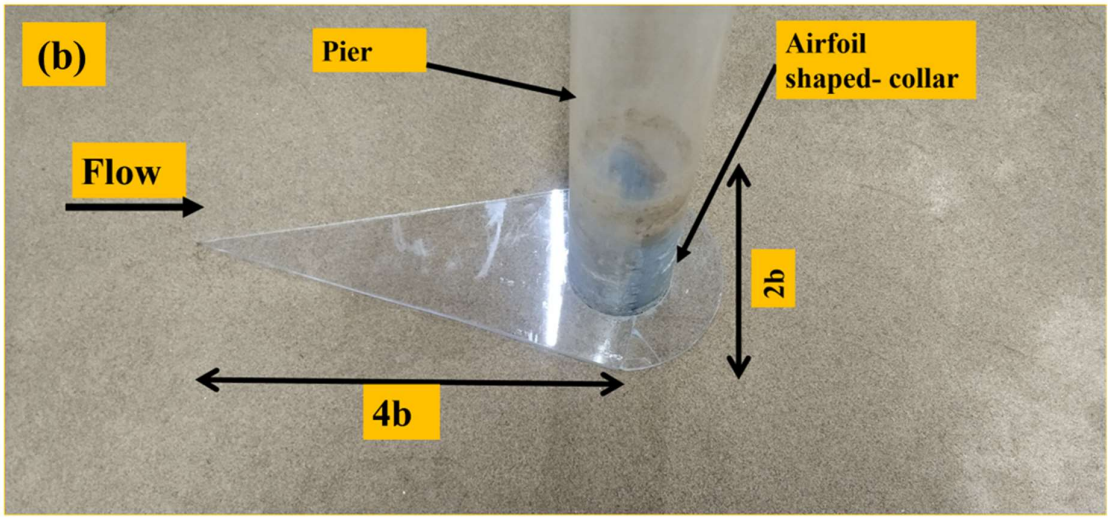

Figure 3.4: Description of airfoil-shaped collar b_{c2}: (a) sketch of b_{c2}; (b) collar b_{c2}.

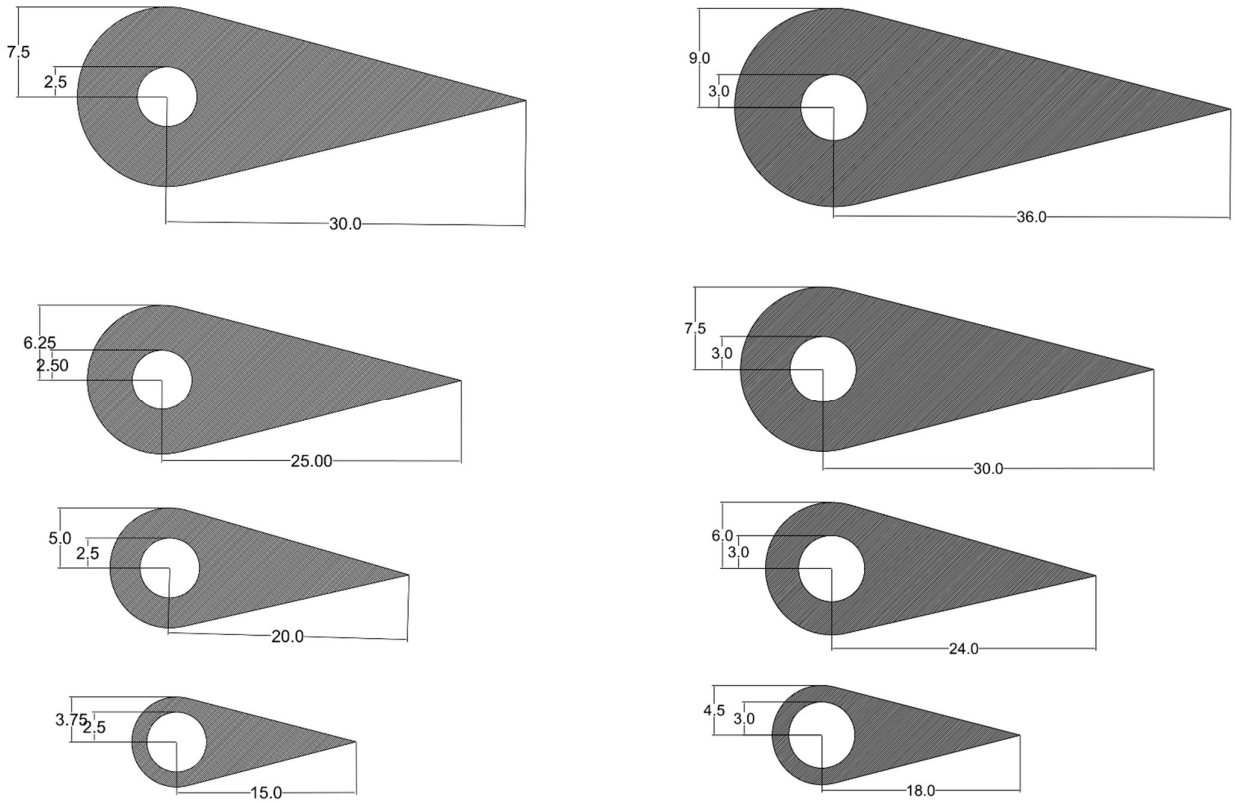

(a) (b)

Figure 3.5: Description of all airfoil-shaped collars with their dimensions. (a) for a pier of diameter 0.05 m and (b) for a pier of diameter 0.06 m (All dimensions are in centimeters).

3.2 Dimensional analysis

Factors affecting the time-dependent scour depth (d_{stc}) around the bridge pier with collar:

i. Geometry properties: width of channel (B), diameter of pier (b), diameter of airfoil-shaped collar (b_c), thickness of collar (t_c), length of the airfoil-shaped collar (L_c), elevation of collar from the sediment bed (z).
ii. Flow properties: water elevation (y) is measured from sediment bed, approach flow velocity (V), acceleration due to gravity (g).
iii. Fluid properties: density of fluid (ρ), kinematic viscosity (ν).
iv. Bed properties: median particle size of sediment bed (d_{50}), density of sediment bed (ρ_s), standard deviation (σ).
v. Time: elapsed time (t) and equilibrium time (t_e).

d_{stc} is represented by a functional relationship:

$$f_1\,(d_{stc},\ B,\ b,\ b_c,\ t_c,\ L_c,\ z,\ \ g, y,\ V,\ \rho,\ \nu, d_{50},\ \rho_s,\ \sigma, t,\ \ t_e) = 0 \tag{3.1}$$

Using the Buckingham π theorem, the dimensionless form is obtained as follows:

$$f_2 = \left(\frac{d_{stc}}{b},\ \frac{B}{b}, \frac{y}{b},\ \frac{b_c}{b},\ \frac{t_c}{b},\ \frac{L_c}{b}, \frac{Vt_e}{b}, \frac{Vt}{b}, \frac{Vb}{\nu},\ \frac{\rho_s}{\rho},\ \frac{gy}{V^2}\right) \tag{3.2}$$

Constants in experimental runs are B, b, t_c, ρ, ν, d_{50}, ρ_s, σ_g, $\frac{gy}{V^2}(1/Fr^2$, Fr: Froude number) and $\frac{Vb}{\nu}$ (Reynolds number). The local scour is not influenced by the kinematic viscosity if the $R_e \geq 7{,}000$. Since R_e in the present experiment is 14,820, it can be disregarded (Daneshfaraz et al., 2021; Khaple et al., 2017). The effects of constant terms in experimental runs could be neglected and Equation (3.2) may be simplified as Equation (3.3).

$$f_3 = \left(\frac{d_{stc}}{b},\ \frac{b_c}{b},\ \frac{L_c}{b}, \frac{z}{b}, \frac{Vt}{b}\right) \tag{3.3}$$

where $\frac{d_{stc}}{b}$ is dimensionless scour depth, $\frac{b_c}{b}$ is the proportion of collar diameter to pier diameter, $\frac{L_c}{b}$ is length proportion to pier diameter and $\frac{Vt}{b}$ dimensionless time.

3.3 Experimental conditions

Many factors, such as the contraction effect, side wall effect, sediment size effect, viscosity effect and scour conditions influence the desirable experimental conditions. Due to the contraction of channel width, the flow accelerates, which may result in contraction scouring. To avoid contraction effect, the ratio of pier diameter or collar diameter to the channel width is maintained well below 0.2 (Melville & Sutherland, 1988). The side wall effect is due to the narrowness of the channel which generates secondary currents. These currents redistribute the boundary shear stress between the bed and side walls which make maximum velocity fall short of the free water surface, which is called the dip phenomenon. To avoid this effect, channel width should be at least ten times the pier diameter. To avoid scaling effect of sediment size (d_{50}), pier of diameter as high as fifty times the median grain size is used, i.e., $b/d_{50} \geq 50$. Otherwise scaling d_{50} according to the geometric scale results in very small model sediment sizes exhibiting interparticle forces that are not present in sand-bed rivers. The study is conducted with two different piers and two different flow intensities under clear-water conditions, which means that the sediment particles are not allowed to move with water. In clear-water condition, maximum scouring depth around the pier without any scour protection varies from 1.1 to 2.3 times pier diameter. Experimental conditions are followed to avoid the effects discussed above are presented in Table 3.1.

Table 3.1: Experimental conditions.

SN	Effect	Standard practice	Present study	References
1	Contraction effect	$b\ or\ b_c/B$ ≤0.2	0.20	Melville & Sutherland, (1988)
2	Uniform sand	σ_g < 1.4	1.31	Dey, (1995)
3	Negligible flow viscosity	$R_e > 7000$	14,820	Daneshfaraz et al. (2021)
4	Sidewall effect	$B/b \geq 10$	13.33	Khaple et al. (2017)
5	Clear-water scouring	V/Vc <1	0.98	Memar et al. (2020)
6	Sediment size effect	$b/d_{50} \geq 50$	187.5	Tafarojnoruz et al. (2012)
7	Equilibrium condition	Variation of d_{st} < 0.05b in 24 hours	Achieved	Melville & Chiew (1999)
8	Ripples formation	d_{50} > 0.7mm, V_c< 0.6 V_{*c} (R_{*e} < 11.6) & F_r < 1	Ripples are formed	Raudkivi & Ettema, (1983)

3.4 Hydraulic conditions

Hydraulic conditions refer to the flow characteristics of a fluid (usually water) within a system or a specific experiment. The hydraulic conditions can vary depending on the objectives of the experiment and the specific parameters being studied. Here are some common hydraulic conditions that are relevant for various experiments are: flow rate, velocity, pressure, Reynolds number, Froude number, water depth, water temperature and sediment characteristics.

3.4.1 Ultrasonic flowmeter

An ultrasonic flowmeter measures the discharge/flow-rate (Q) in the flume with an accuracy of ± 1%, which is kept at the exit of the inlet pipe. The measured discharge is used to calibrate the weir. The ultrasonic flow meter is from NAGMAN CALIBRATION SERVICES LLP, of model SONICNAG 6000 having an accuracy of ±1%, as shown in Figure 3.6. It has two components; two transducers and signal processing unit. The transducer placed at upstream of pipe flow is for transmitting ultrasonic wave signals whiles the other one is for receiving the same. Both are connected to the supply line according to flow direction. The difference in the transit time of reflected sound wave due to flow is converted into flow velocity data in the transmitter cum signal processing unit and discharge can be directly read. Advantages of ultrasonic flowmeters include: (a) non-intrusive measurement (b) wide application range (c) bi-directional measurement and (d) accuracy.

3.4.2 Acoustic Doppler Velocimeter (ADV)

A high-resolution Acoustic Doppler Velocimeter (ADV) measures the instantaneous velocity components u, v and w in X-, Y- and Z-directions, respectively, at the vicinity of the collared-pier system. ADV is a reliable instrument for measuring the turbulent quantities with better accuracy in 3-D open channel flows (Dixit and Patel, 2015). ADV used for the present study is manufactured by Nortek Inc. branded as Vectrino^{+}. This ADV had a sampling volume height of 5 mm with a maximum sampling rate up to 200 Hz. The main parts in this instrument are an acoustic wave transmitter and three receiver probes. Instrument is placed around the vicinity of pier-collared system to obtain data from a grid of observation points as shown in Figure 3.7. These data are transferred to a computer and stored. Later with the help of two software named Vectron Plus and Explorer V, this data is converted into 3-D velocity

data. The ADV used in the present study has an accuracy of ±0.5% of measured value ± 1 mm/s. The approach flow velocity (V) from a single observation point is obtained for a time period of 3 minutes with a frequency of 100 Hz which give better results with minimum noise interventions (Gordon and Cox, 2000). The data from ADV is used to plot the velocity vector field. This is mainly used to validate the results from CFD simulations.

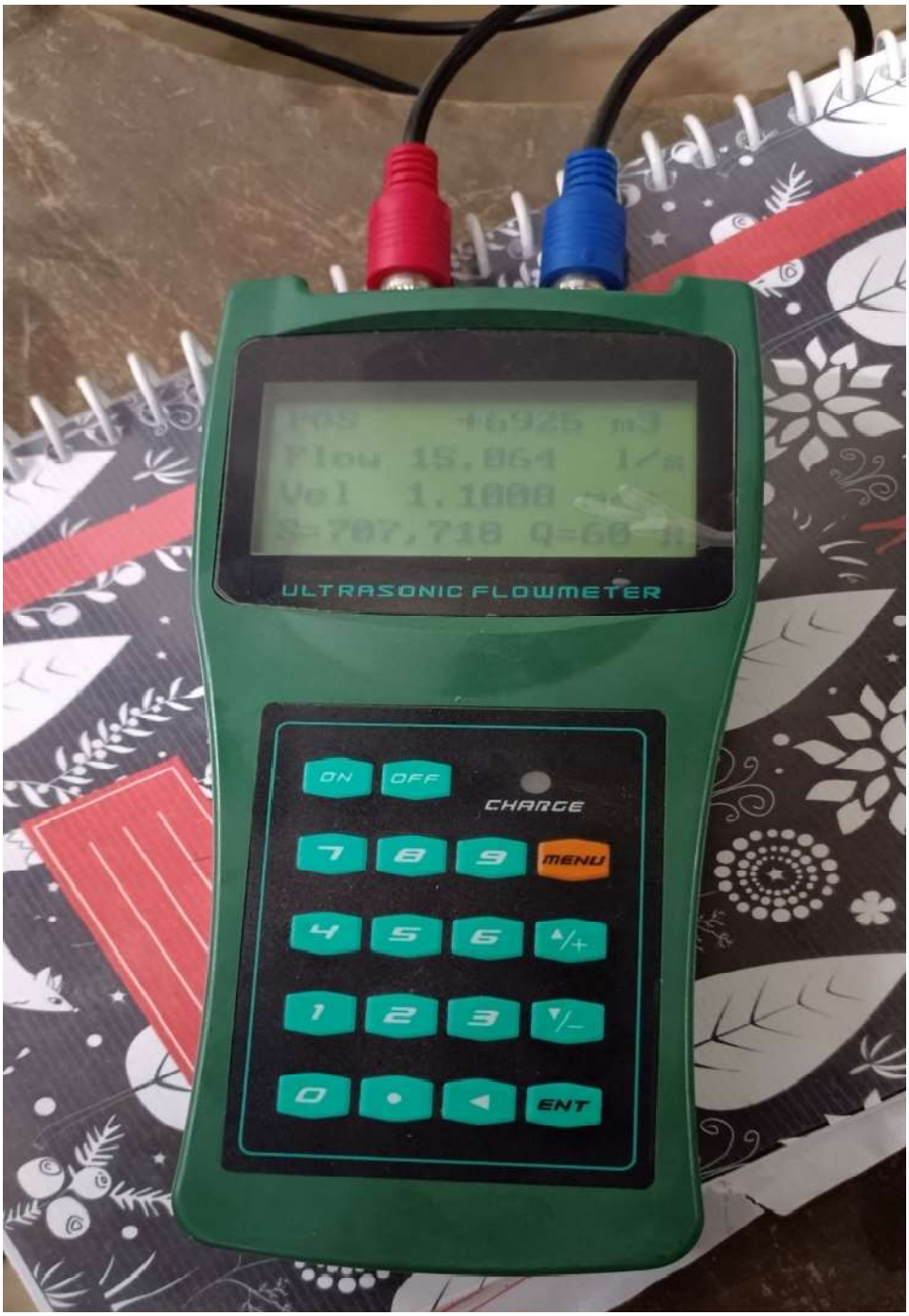

Figure 3.6: Photographic view of ultrasonic flowmeter.

Figure 3.7: Photographic view of an ADV instrument setup.

3.4.3 Digital point gauge

Planning and design of a hydraulic system with safe operation is possible my means of exact knowledge on the water surface elevation (Reddy and Bhallamudi, 2004). Point gauge measures the flow depth in the main channel, temporal scour depth and contours of scour depth. Digital point gauges are of accuracy ±0.1 mm is used during experimentations as shown in Figure 3.8 (Pagliara and Kurdistani, 2017). Digital point gauge is particularly useful when precision measurements are required and digital readout simplifies the measuring process, reducing the potential for human errors.

Figure 3.8: Photographic view of digital point gauge.

3.4.4 Critical flow velocity

Critical flow velocity for sediment particles refers to the minimum velocity required to initiate sediment movement or erosion of the bed material in a fluid (typically water) flow. When the flow velocity is below the critical value, sediment particles tend to settle and remain relatively

stable on the bed. However, once the flow velocity exceeds the critical value, it becomes capable of transporting sediment particles. The critical flow velocity is influenced by various factors, including the size, shape and density of the sediment particles, as well as the characteristics of the fluid. Larger, heavier particles generally require higher flow velocities to initiate movement, while smaller, lighter particles can be entrained at lower velocities. The critical flow velocity is an important parameter in understanding sediment transport and erosion processes in rivers, streams and coastal areas. It is used in sediment transport equations and models to predict the movement and deposition of sediment particles under various flow conditions. Researchers and engineers study critical flow velocity to design and manage hydraulic structures, such as dams, bridges and culverts, to ensure that sediment movement does not cause excessive erosion or blockages that could lead to undesirable consequences in the watercourse. The critical flow velocity of the sediment particles is calculated using Equation (3.4), where V_c and V_{*c} are critical flow and critical shear velocity, respectively (Melville, 1997; Melville & Chiew, 1999) and V_{*c} is calculated using the Shields curve.

$$\frac{V_c}{V_{*c}} = 5.75\ log\left(\frac{5.53\ y}{d_{50}}\right) \tag{3.4}$$

3.4.5 Details of experimental runs

All experimental runs are conducted under clear-water conditions (V/V_c) <1, constant flow intensity (V/V_c), Reynolds number (R_e) and Froude number (F_r) as presented in Table 3.2. Time-dependent and maximum equilibrium scour depths are measured using the digital point gauge meter with an accuracy of ± 0.1 mm. All the experiments are conducted for 8-10 hours. Experiments are conducted in two cases: Case I is a baseline experiment, i.e., experimental runs without AFC and Case II represents the experimental run with AFC.

Table 3.2: Flow and sediment bed parameters.

d_{50} (mm)	y (m)	V_{*c} (m/s)	V_c (m/s)	V (m/s)	V/V_c	R_e	F_r
0.32	0.10	0.0138	0.252	0.247	0.98	14,820	0.249
0.32	0.10	0.0138	0.252	0.195	0.75	11,700	0197

This study used two different piers of 0.05 and 0.06 m diameters. Four different airfoil collars (b_{c1}, b_{c2}, b_{c3} *and* b_{c4}) are used at four various elevations (at bed level (i.e., y = 0, where y is the water elevation from the bed), y/4, y/2 and 3y/4 above the bed level). Study uses two different flow intensities, V/V_c of 0.75 and 0.98. The number of experiments conducted are:

i. Without collar = 2x2= 4;
ii. With collar = 2x4x4x2= 64; and
iii. With collar (b_{c2R}) on bed level installing reverse to the flow direction = 1;

Therefore, the total number of experiments conducted without and with collar = 4+64+1= 69

3.5 Experimental procedure and data collection

This section details the step-by-step process of conducting the experiment. The first step is to perform the sieve analysis of river sediment and measure the sediment particles' median size and geometrical standard deviation. To check whether the sediment particle is uniform or non-uniform, calculate the value of σ_g. To get the uniform sand, obtained river sediment retained (425- micron sieve) and passed through (150-micron sieve) two successive sieves which is used in the experiments. In the working section, sediment bed preparations are carried out with a surface roller and the sediment bed level is equal to the flume bed level. Each experimental run is started after the sediment bed is properly levelled using the surface rollers. The level of the bed is checked using the spirit level. Pier without and with airfoil shaped collar is placed at the center of the working section as shown in Figure 3.9.

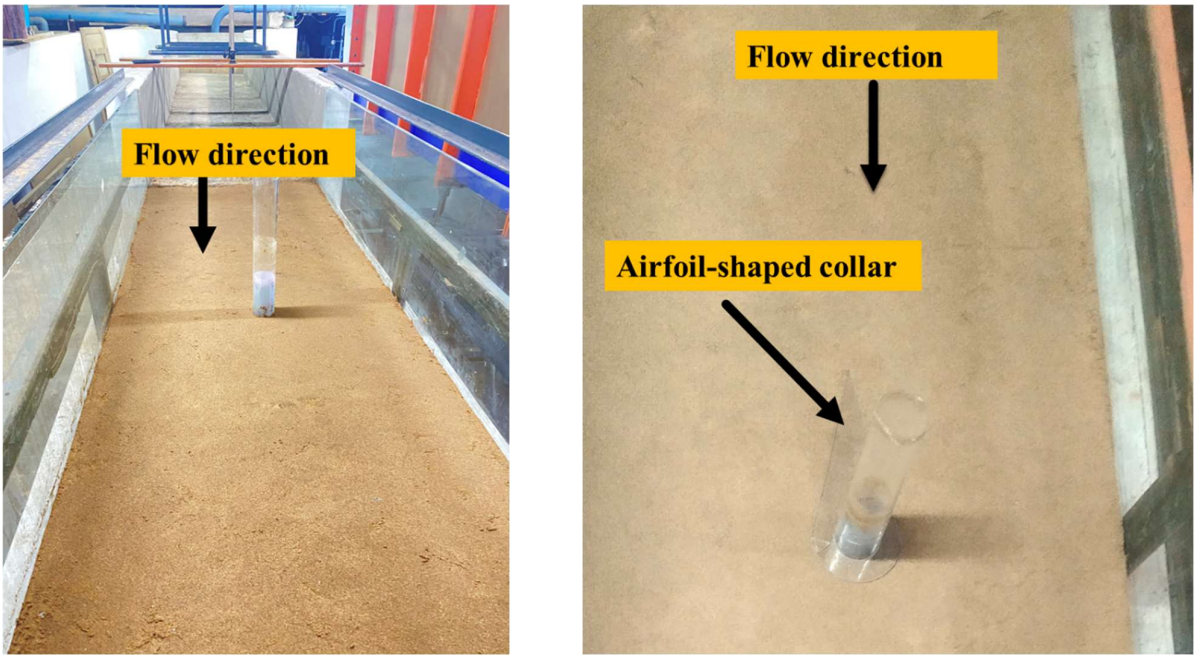

(a) (b)

Figure 3.9: The sediment bed with: (a) Pier without collar and (b) Pier with collar

The working section is leveled with flume level and covered with tarpaulin sheet, plywood and some weights are placed on it, so that flowing water doesn't erode the sediment bed before reaching the desirable hydraulic conditions as shown in Figure 3.10.

Figure 3.10: Covering sediment bed with PVC sheet and plywood.

When the desired water depth and average velocity are established, plywood and tarpaulin sheets are removed delicately so that there is almost no change in the sediment bed surface. After that, scour depths are measured at distinct times 2, 3, 5, 7, 10, 15, 30, 45, 60, 90, 120, 240, 300, 360,420, 480 and 540 minutes. The temporal scour depth is measured till the equilibrium or end condition is reached. Temporal and equilibrium scour depth are measured using digital point gauge. Figure 3.11 shows scour around the pier without collar at any elapsed time during the experiment. Summary of experimental setup, procedure and analysis is presented in the form of flowchart as shown in Figure 3.12.

Figure 3.11: Scour around the pier without collar after four hours of elapsed time

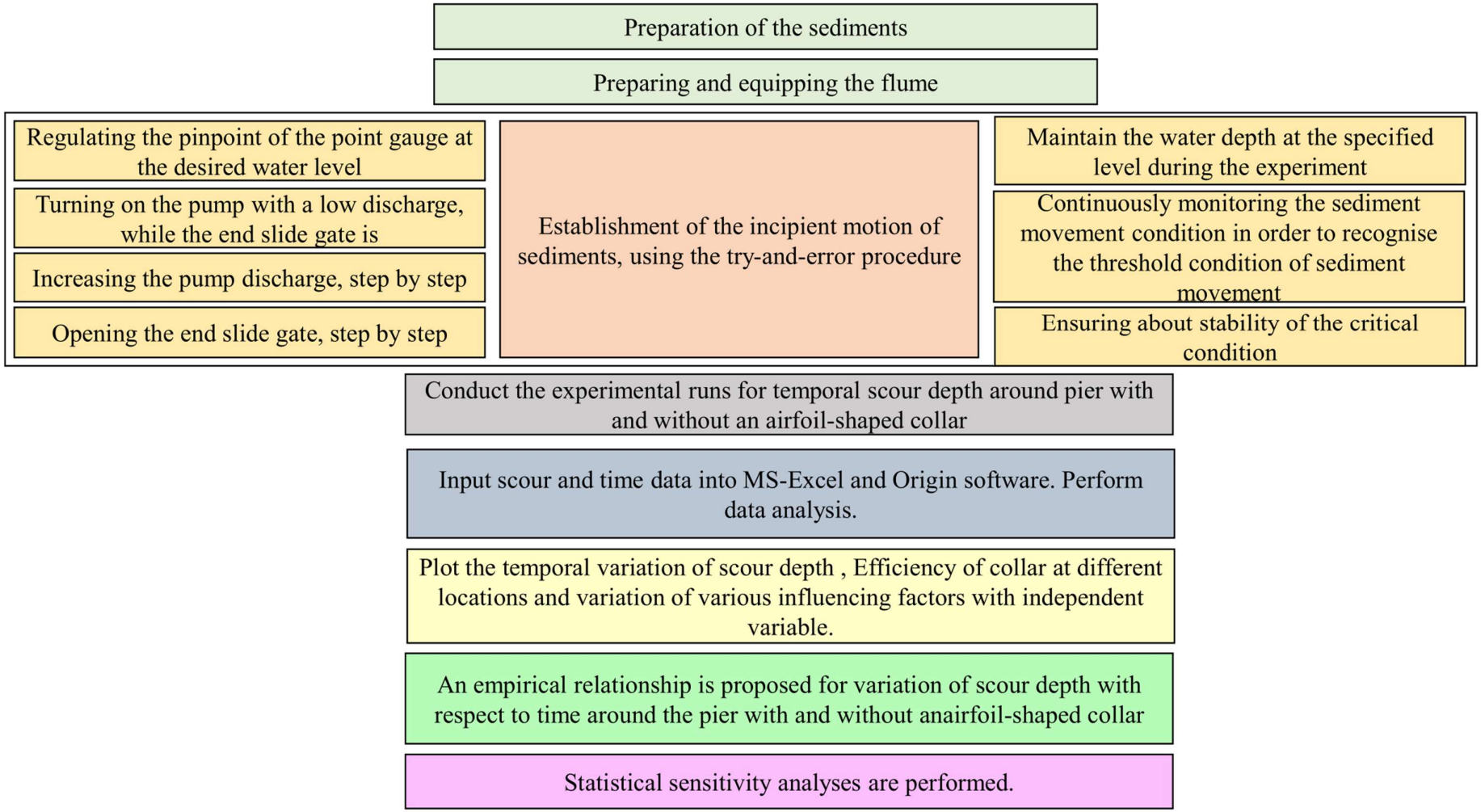

Figure 3.12: Flowchart of the procedure and analysis.

3.6 Governing equations in CFD

Computational Fluid Dynamics (CFD) is an important tool for implementing numerical simulations for studying the natural currents in water bodies with fine materials (Choufu et al., 2019). Experimental studies incur more cost, time, human resources, restrictions and data collection problems and only permits data to be extracted from limited locations (Armenio, 2017; Choufu et al., 2019; Daneshfaraz et al., 2021; Ghaderi et al., 2021; Gupta et al., 2023a; Pourshahbaz et al., 2020). Additionally, data extraction can be performed only from the locations where gauges and sensors are installed (Ghaderi et al., 2021; Vasquez and Walsh, 2009). On the other hand, a wide range of hydrodynamic fluid flows and robust numerical simulation modelling can be performed using CFD and it allows for examination of any location in the region of interest (Muhawenimana et al., 2023; Pourshahbaz et al., 2020). It can theoretically simulate any physical condition and allow the study of a specific isolated phenomenon (Farooq et al., 2023a; Farooq and Ghumman, 2019; Valela et al., 2022a). Enhancement in computational capabilities made the application of numerical methods easier in sediment transport for computations of scour around hydraulic structures (Barbhuiya et al., 2020; Vasquez and Walsh, 2009; Wei et al., 2014). The simulation study is carried out with the help of the CFD software FLOW-3D. FLOW-3D offers several advantages and capabilities that distinguish it from other available software packages (Gupta et al., 2023a; Wei et al., 2014). Here are some key advantages of FLOW-3D, such as:

i. User-Friendly Interface
ii. FLOW-3D excels in modeling free surface flows, multiphase flows and fluid-structure interaction problems. It has robust capabilities for simulating complex fluid behaviors, such as wave interactions, free surface deformation, air entrainment and solid-fluid interaction.
iii. FLOW-3D employs the Volume of Fluid method for accurate and efficient tracking of fluid interfaces in multiphase flow simulations. The Volume of Fluid (VoF) method allows for precise representation of fluid-fluid interfaces, capturing complex interfacial dynamics and enabling the analysis of phenomena such as sloshing, splashing and wave breaking.
iv. FLOW-3D offers a range of turbulence models, including Reynolds-Averaged Navier-Stokes (RANS) models and Large Eddy Simulation (LES). These models allow users to accurately capture and analyze turbulent flow phenomena, such as vortex shedding, turbulent mixing and flow separation, providing insights into complex flow behavior.
v. FLOW-3D includes a wide range of physics models and solvers, such as heat transfer,

mass transfer, solidification/melting and cavitation.

vi. FLOW-3D has a strong track record of validation through comparison with experimental data and benchmark studies.

The equations presented in FLOW-3D are derived from the fundamental principles of conservation of mass and momentum, which are embedded in FLOW-3D to simulate fluid flow and related phenomena (Vasquez and Walsh, 2009). It solves the non-linear Navier–Stokes equations for three-dimensional flow while tracking the water surface using the Volume of Fluid (VoF) model.

3.6.1 Volume of Fluid (VoF) model

FLOW-3D uses the finite difference method to solve Navier-Stokes equations under non-hydrostatic conditions (Jalal and Hassan, 2020b). Under different conditions, it solves the turbulent flow transport bed-load and the suspended bed-load equation (Lai et al., 2022). The model evaluates the scour and sediment transport (i.e., suspended load, bed-load and sediment entrainment) by advection-diffusion mechanism. It uses the Volume of Fluid (VoF) method and solves fluid-fluid and fluid-air interface problems. This study involves a two-phase system, i.e., sediment and fluid moving together. Equation (3.5) simulates the experimental data as FLOW-3D utilizes VoF approach (Flow Science, Inc. 2016). The VoF method is a numerical technique used to track the interface between two immiscible fluids or phases in CFD simulations. It is a popular approach for modeling multiphase flows in FLOW-3D and other CFD software. The VoF method in FLOW-3D offers a robust and efficient approach for simulating complex multiphase flows. It is particularly well-suited for applications such as free surface flows, bubble dynamics, droplet impact and wave-structure interactions. By accurately tracking the fluid interface, FLOW-3D can provide valuable insights into multiphase flow behavior and its impact on various engineering and scientific problems (Man et al., 2019).

$$\frac{\partial F}{\partial t}+\frac{1}{V_F}\left(\frac{\partial(FuA_x)}{\partial x}+\frac{\partial\left(FvA_y\right)}{\partial y}+\frac{\partial(FwA_z)}{\partial z}\right)=0 \qquad (3.5)$$

where F is fluid fractional function, F = 0 when mesh cell is empty and F = 1 when the cell is full. V_F is the fluid volume fraction for the intermediate value, F = 0.5 can be assigned. The velocity components u, v, w are in in X-, Y- and Z-directions, respectively and A_x, A_y, A_z are area fractions in X-, Y- and Z-directions, respectively.

3.6.2 Fractional Area Volume Obstacle Representation (FAVOR) model

The model evaluates the flow around rigid objects by Fractional Area Volume Obstacle Representation (FAVOR). The FAVOR method is a numerical technique used in CFD simulations to handle complex geometries and obstacles within the computational domain. It is a key feature of the FLOW-3D software. The key aspects and advantages of the FAVOR method are:

i. The FAVOR method represents the complex geometry or obstacles as fractional areas or volumes within the computational domain. This representation simplifies the computational mesh and reduces the computational effort compared to traditional mesh-based approaches.
ii. This simplifies the meshing process, reduces computational resources and improves computational efficiency.
iii. FAVOR allows for the efficient simulation of flow around multiple and intricate obstacles with varying shapes, sizes and orientations.
iv. It enables the simulation of complex geometries encountered in real-world applications, such as flow around spur dikes, flow through porous media, industrial equipment and natural environments.
v. FAVOR captures the flow obstruction and its influence on the fluid flow field.
vi. FAVOR reduces the dependence on computational mesh resolution. This makes FAVOR particularly advantageous when dealing with large-scale simulations or situations with varying obstacle sizes.

3.6.3 Navier-Stokes equations

The Navier-Stokes equations include the equation for the continuity (mass conservation) and momentum (momentum conservation) equation. The three main turbulence models used in CFD are Reynolds-Averaged Navier-Stokes (RANS), LES and DNS (Bhide and Abdallah, 2022). A sketch of the usual levels of approximation of DNS, RANS, URANS and LES in CFD methods is shown in Figure 3.13.

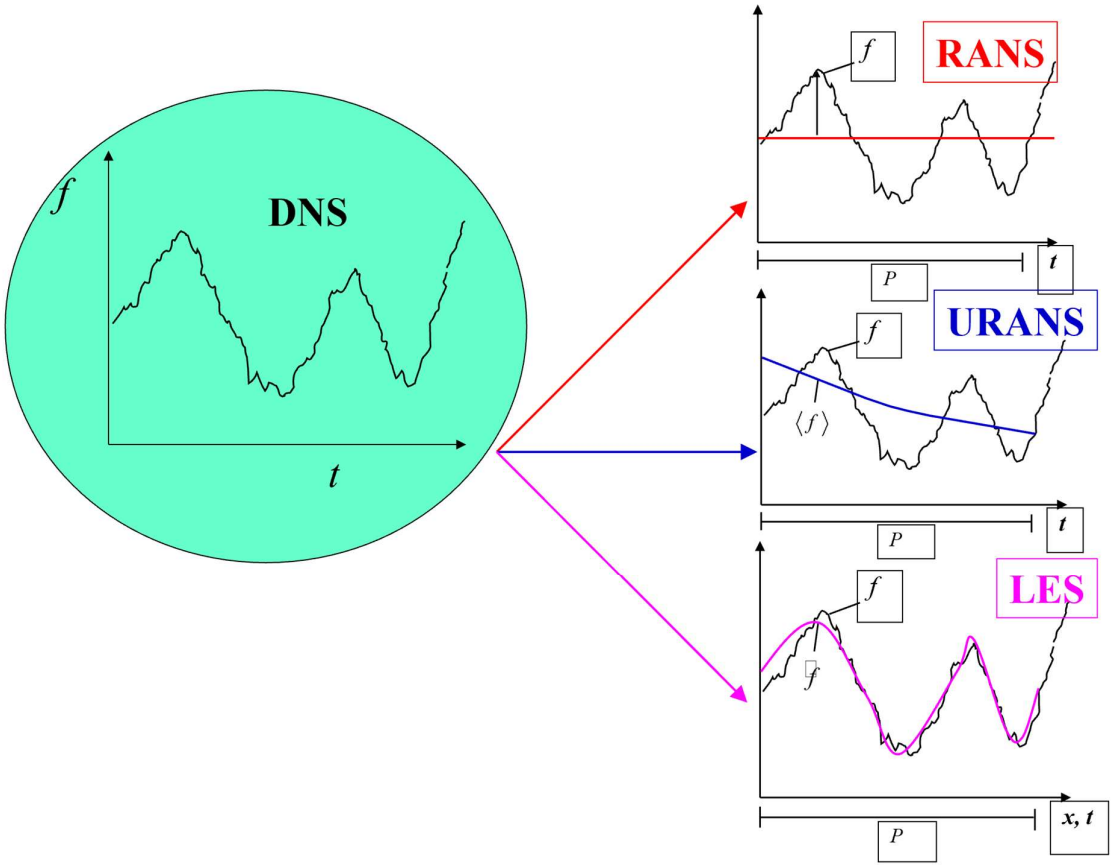

Figure 3.13: Levels of approximation of DNS, RANS, URANS and LES.

3.6.4 Direct Numerical Simulation (DNS)

The concept of DNS can be traced back to the pioneering work of Lewis Fry Richardson, a British mathematician and meteorologist who developed the first numerical weather prediction model in the early 1920s. However, as it is known today, the DNS technique was developed in the mid-1960s by the mathematician and fluid dynamicist Andreas Acrivos and his colleagues. Their work laid the foundations for using DNS in simulating fluid flows and since then, DNS has become an essential tool in computational fluid dynamics (Armenio, 2017; Koken and Constantinescu, 2008b; Pandey and Mohapatra, 2023). DNS is a technique used in CFD to simulate fluid flows by solving the Navier-Stokes equations directly, without any turbulence models (Armenio, 2017). DNS provides a detailed description of all the flow scales, from the largest to the smallest and it is considered the most reliable way to simulate fluid flows (Armenio, 2017). In DNS, the flow is discretized in both space and time and the Navier-Stokes equations are solved numerically at each time step (Armenio, 2017). The method is computationally expensive and requires a large number of grid points to resolve all

the turbulent scales. DNS provides a high-fidelity solution that can be used to validate turbulence models used in other simulation methods, such as LES and RANS (Acharya and Duan, 2011; Choufu et al., 2019; Keating et al., 2004). Due to high computational requirements for DNS, researchers often use different modeling approaches, such as LES or RANS models.

3.6.5 Reynolds-Averaged Navier–Stokes (RANS) equations

The Reynolds-Averaged Navier–Stokes (RANS) equations introduce the concept of Reynolds averaging, which separates the flow variables into mean and fluctuating components (Daneshfaraz et al., 2021; Gupta et al., 2023). The mean flow variables are time-averaged quantities, while the fluctuating variables represent the turbulent fluctuations in the flow. The RANS approach involves averaging the Navier-Stokes equations over time or space, which results in equations for the mean velocity and pressure fields. The fluctuating components of the flow are modeled using various closure models, which account for the effects of turbulence. The RANS approach is widely used in CFD to simulate a variety of flow problems, including those involving complex geometries, boundary conditions and flow regimes (Choufu et al., 2019; Pourshahbaz et al., 2022). It has found applications in many industries, including aerospace, automotive, energy and environmental engineering. One of the main advantages of the RANS approach is its computational efficiency compared to more advanced turbulence modeling techniques, such as LES and DNS. However, RANS models may not precisely capture certain aspects of the flow physics, such as unsteady or highly turbulent flows and can be sensitive to the choice of closure model and numerical scheme.

3.6.6 Large Eddy Simulation (LES) or Filtered Navier-Stokes equations

LES technique was first introduced in the mid-1960s by J. Smagorinsky, a meteorologist at the National Center for Atmospheric Research (NCAR)(Armenio, 2017; Dhamankar et al., 2018; Ningyu, 1997). Smagorinsky proposed the idea of explicitly simulating only the largest turbulent structures in the flow while modeling the effect of smaller scales on the larger ones (Hinterberger and Rodi, 2007; Keating et al., 2004). Over the years, researchers in the fields of fluid mechanics, meteorology and computational science have further developed and refined the idea of LES, making it an essential tool for simulating turbulent flows in a variety of practical applications (Armenio, 2017). It involves solving the Navier-Stokes equations for the large-scale turbulent structures while modeling the effects of smaller-scale turbulence. In

LES, the largest turbulent structures in the flow are explicitly resolved, while the smaller structures are modeled using Sub Grid-Scale (SGS) models (Churchfield et al., 2013; Daneshfaraz et al., 2021). These models approximate the effects of the smaller scales on the larger scales of motion, allowing for the simulation of turbulence without having to resolve all the scales explicitly. LES is particularly useful for simulating turbulent flows that have a large separation between the largest and smallest scales, such as those found in jet engines, atmospheric flows and combustion systems (Dhamankar et al., 2018). It can also provide detailed information about the unsteady nature of turbulence, which is important in many practical applications. One of the main challenges of LES is the computational cost, as it requires resolving the largest turbulent scales, which can be computationally expensive (Choufu et al., 2019; Pourshahbaz et al., 2022). However, advances in computational power have made LES increasingly practical for simulating complex turbulent flows.

Due to its unique capabilities, LES model is a popular turbulence model for simulating turbulent flow (Acharya and Duan, 2011; Koken and Constantinescu, 2008b). It allows for explicitly solving the large eddies in the calculation while also implicitly accounting for the smaller eddies through a SGS model (Man et al., 2019). Unlike RANS-type turbulence models, the LES model effectively captures the transient characteristics of vortices, which poses a significant challenge for other approaches (Koken and Constantinescu, 2008b). Kolmogorov (1941) suggested that large eddies of the flow are dependent on the geometry while the smaller scales are universal. LES can decrease the computational cost by neglecting the minor length scales.

The filtered Navier–Stokes equations include the filtered continuity and momentum equations. These equations compute both the mean flow and large eddies (Daneshfaraz et al., 2021; Man et al., 2019). The study uses the LES method as a turbulence model, which decomposes the instantaneous variables (velocity and pressure) into filtered (resolved) and sub-filtered (unresolved or residual) variables. Here, velocity is used as an example.

$$u_i = \bar{u}_i + u'_i \tag{3.6}$$

where u_i, $\bar{u}_i$ and u'_i are instantaneous, filtered and sub-filtered velocities, respectively. LES method as a turbulence model is shown below:

$$\frac{\partial \rho}{\partial t} + \frac{\partial (\rho \bar{u}_i)}{\partial x_i} = 0 \tag{3.7}$$

$$\frac{\partial \bar{u}_i}{\partial t} + \bar{u}_j \frac{\partial \bar{u}_i}{\partial x_j} = -\frac{1}{\rho} \frac{\partial \bar{p}}{\partial x_i} + \frac{\partial}{\partial x_j} \left(\nu \frac{\partial \bar{u}_i}{\partial x_j} \right) + \frac{1}{\rho} \frac{\partial \tau_{ij}}{\partial x_j} \tag{3.8}$$

where ρ is the fluid density, t is time, $\bar{u}_i$ are filtered velocities in i^{th} direction, x_i ($i =$

$1,2\ and\ 3$) are three axes in the cartesian coordinate system, $\bar{p}$ is filtered pressure, ν is kinematic viscosity and the term $\frac{\partial \tau_{ij}}{\partial x_j}$ brings the nonlinearity in the system because of $\overline{u_j \frac{\partial u_i}{\partial x_j}} \neq \bar{u}_j \frac{\partial \bar{u}_i}{\partial x_j}$ hence,

$$\tau_{ij} = \bar{u}_i \bar{u}_j - \overline{u_i u_j} \tag{3.9}$$

where τ_{ij} is SGS stress and similar equations can be derived for the SGS field (i.e., the residual field) and it is calculated using Boussinesq's hypothesis.

$$\tau_{ij} - \frac{1}{3} \tau_{kk} \delta_{ij} = -2\mu_t \bar{S}_{ij} \tag{3.10}$$

where, τ_{kk} is the SGS stress turbulent kinetic energy, δ_{ij} is filtered scale length, μ_t is SGS turbulent viscosity and $\bar{S}_{ij}$ is the rate of strain tensor for the resolved scale defined by

$$\bar{S}_{ij} = \frac{1}{2} \left(\frac{\partial \bar{u}_i}{\partial \bar{x}_j} + \frac{\partial \bar{u}_j}{\partial \bar{x}_i} \right) \tag{3.11}$$

Then filtered Navier-Stokes equations can be the following equation

$$\frac{\partial \bar{u}_i}{\partial t} + \bar{u}_j \frac{\partial \bar{u}_i}{\partial x_j} = -\frac{1}{\rho} \frac{\partial \bar{p}}{\partial x_i} + \frac{\partial}{\partial x_j} \left([\mu + \mu_t] \frac{\partial \bar{u}_i}{\partial x_j} \right) \tag{3.12}$$

3.6.7 Sediment transport model

A sediment transport model is a mathematical and computational framework used to simulate the movement and deposition of sediment in natural water bodies such as rivers, estuaries, coastal areas and lakes (Kirkil et al., 2009; Man et al., 2019; Pandey and Mohapatra, 2023; Qi et al., 2023). Various processes govern sediment transport, including erosion, transport and deposition. There are three sediment transport models in FLOW-3D. They are: (i) Meyer-Peter and Müller model (ii) Nielsen model and (iii) van Rijn model.

This study uses the van Rijn sediment model which is applicable to a wide range of sediment sizes, including both sand and gravel, which makes it suitable for diverse sediment transport scenarios. Its formulation takes into account factors such as sediment diameter, flow velocity and slope, providing a comprehensive representation of bedload transport. The van Rijn model offers a good balance between simplicity and accuracy. It provides a relatively simple formulation that can be easily implemented in numerical models or engineering calculations. Previous studies have utilized the van Rijn model and achieved satisfactory results. The van Rijn model is one of the most widely accepted and validated equation for estimating bedload transport in sediment transport studies. It has been extensively tested against experimental

data and field measurements in various flow conditions and sediment types, making it a reliable choice. Despite its simplicity, the model has shown good agreement with experimental data in many cases, making it a practical choice for bedload estimation. The van Rijn model is widely used in hydraulic engineering and coastal management projects to estimate sediment transport rates, assess the potential for erosion or deposition and design erosion control measures. It provides a practical and reliable tool for understanding and managing sediment transport processes in rivers, estuaries and coastal areas. The van Rijn model is used to calculate the volumetric sediment transport rate per bed width. The volumetric sediment transport rate per bed width is given by van Rijn model and is given by Equation (3.13) (van Rijn, 1984a, 1984b, 1984c; van Rijn, 1987).

$$\Phi = \beta {D_*}^{-0.3} \left(\frac{\theta}{\theta_{cr}} - 1.0\right)^{2.1} C_b \tag{3.13}$$

where ϕ is dimensionless rate of bed-load transport, β is bed load coefficient, D_* is dimensionless particle size, θ and θ_{cr} are local and critical Shields parameters, respectively. Critical Shield numbers which is a ratio between the shear stress by the submerged weight of the sediment particles at incipient condition but local Shields parameter is ratio of shear stress to submerged weight of sediment particle at any conditions (Ghaderi and Abbasi, 2019; Kuhnle et al., 2002; Li, 2016; Pourshahbaz et al., 2020). C_b is the amount of sediment in a sample, expressed as a percentage of the total volume of the sample. The critical Shields number (θ_{cr}) is calculated using the Soulsby-Whitehouse equation (Equation 3.14) and equal to 0.033.

$$\theta_{cr} = \frac{0.3}{1 + 1.2D_*} + 0.055(1 - e^{-0.2D_*}) \tag{3.14}$$

where dimensionless particle size(D_*) is calculated using the Equation (3.15)

$$D_* = d_{50} \left(\frac{(S-1)g}{\upsilon^2}\right)^{1/3} \tag{3.15}$$

3.7 Numerical setup

Experiments are conducted in a rectangular flume of length 10.3 m, width of 0.8 m and 0.5 m depth. The working section of the flume is situated at a distance of 4 m from the inlet and has dimensions of 2.3 m in length, 0.8 m in width and 0.3 m in depth. The circular pier of 5 cm diameter (b) is considered in this study and is kept at the center, both in the longitudinal and

transverse directions of the working section. The sediment bed is prepared with uniform sand with median size diameter (d_{50}) of 0.32 mm with σ_g = 1.31. The thickness of the sediment bed is 30 cm. Pier diameter (b) is selected such that effect of sidewall and contraction effect are negligible. In channel, discharge is measured by an ultrasonic flowmeter with an accuracy of ± 0.0001 m^3/s installed at the pipe inlet's exit. All the experiments are conducted with constant water depth (y = 10 cm) and under clear condition, i.e., V/V_c < 1 to ensure no transport of sediment into the scour hole from upstream. The study is carried out with the flow intensity (V/V_c) of 0.98. Figure 3.14 shows the simulation setup of the working section in FLOW-3D. The pier is placed at center of the working section with AFC attached to it. The AFC geometry is built in AUTOCAD and is imported to FLOW-3D. The two different collars of 4 mm thickness are used in the study with a diameter of b_{c2}($2b$) and b_{c4} ($3b$) and a length of $4b$ and $6b$. The input properties of sediment and hydraulic conditions are shown in Table 3.3. Simulations are carried out for six cases, as presented in Table 3.4.

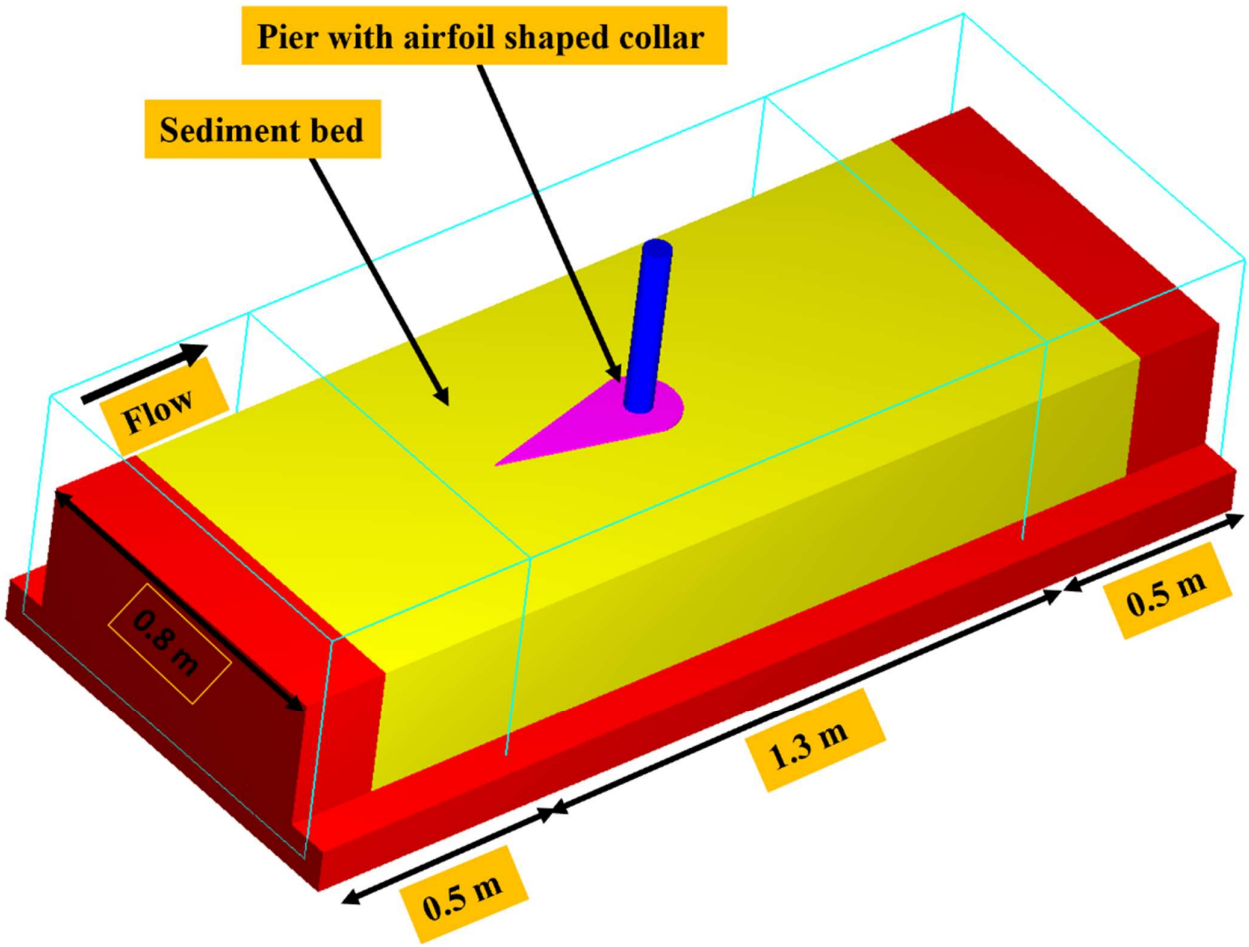

Figure 3.14: Simulation setup of working section.

Table 3.3: Sediment and hydraulic conditions in the simulation setup

Median particle size, $\boldsymbol{d_{50}}$ (m)	Specific gravity of sediment, $\boldsymbol{G_s}$	Critical Shields parameter, $\boldsymbol{\theta_{cr}}$	Angle of repose	Bed load coefficient	Flow depth, $\boldsymbol{y}$ (cm)	Critical flow velocity, $\boldsymbol{V_c}$ (m/s)	Froude number, $\boldsymbol{F_r}$
0.00032	2.65	0.033	29°	0.045	0.10	0.252	0.25

Table 3.4: Description of simulation for six cases.

Case No	Location of AFC with respect to sediment bed
1	Pier without AFC
2	Pier with AFC having diameter $2b$ on sediment bed (b_{c2})
3	Pier with AFC having diameter $2b$ on sediment bed in reverse to the flow direction (b_{c2R})
4	Pier with AFC having diameter $2b$ at $y/2$ above the sediment bed $(b_{c2})_{@\, y/2}$
5	Pier with AFC having diameter $3b$ on the sediment bed (b_{c4})
6	Pier with AFC having diameter $3b$ at $y/2$ above the sediment bed $(b_{c4})_{@\, y/2}$

3.8 Mesh sensitivity analysis

In FLOW-3D, meshing can be produced by cylindrical and cartesian coordinate system. This study uses a cartesian coordinate system. Meshing is done using the Fractional Area-Volume Obstacle Representation (FAVOR) method for complex geometry (Flow Science, 2016). Generally, finer mesh sizes are used near pier with AFC and coarser meshes are used for the remaining geometry. The study uses nested meshes and can be provided for very thin geometries as shown in Figure 3.15. Nested meshes refer to a technique in CFD where

multiple meshes with different resolutions are used to simulate a flow domain. These meshes are hierarchically structured, with finer meshes embedded within coarser meshes, creating a nested grid structure. This approach is particularly suitable for handling very thin geometries in CFD simulations. This approach balances computational efficiency with the need to resolve intricate flow features. Nested meshes are particularly useful for simulating flows in very thin geometries because the accuracy of the numerical solution is often limited by the size of the smallest features in the geometry. By using a nested mesh, the size of the smallest features in the region of interest can be significantly reduced, which can lead to a significant improvement in the accuracy of the solution. In addition to improving accuracy, nested meshes can also improve the reliability and reduces computational cost of numerical models. Some general guidelines for selecting an appropriate mesh size.

i. Use a finer mesh for problems with complex geometry or boundary conditions.
ii. Use a coarser mesh for problems with simple geometry or boundary conditions.
iii. Use a locally refined mesh for problems with high stress gradients or other areas where accuracy is critical.
iv. Run multiple simulations with different mesh sizes to assess the convergence of the results.

Sensitivity analysis of meshing in CFD is an important consideration to estimate scour depth. Four different mesh cell sizes are used to validate the numerical results with experimental results. Finer meshes give accurate results compared to coarser meshes, or more discrepancies could occur in coarser meshes. However, it is observed that finer meshes took more time for simulation results or to reach equilibrium. Moreover, finer meshes consume more computational costs. The total number of mesh cells is 12,233,789 (12.234 million), with coarse cells of 2,225,664 and fine cells of 10,008,125. Table 3.5 shows the mesh sensitivity analysis and it is observed that decreasing the mesh cell size increases the accuracy of the results. So, the study uses coarse and fine cell sizes of 0.8 and 0.4 cm, respectively. A computer with 128GB RAM and i-7 processor is used to simulate the scour process with the simulation running for eight to twelve days. Figures 3.16 and 3.17 show the sketch of coarse mesh setup for entire geometry and nested mesh setup at the vicinity of pier with an airfoil-shaped collar, respectively.

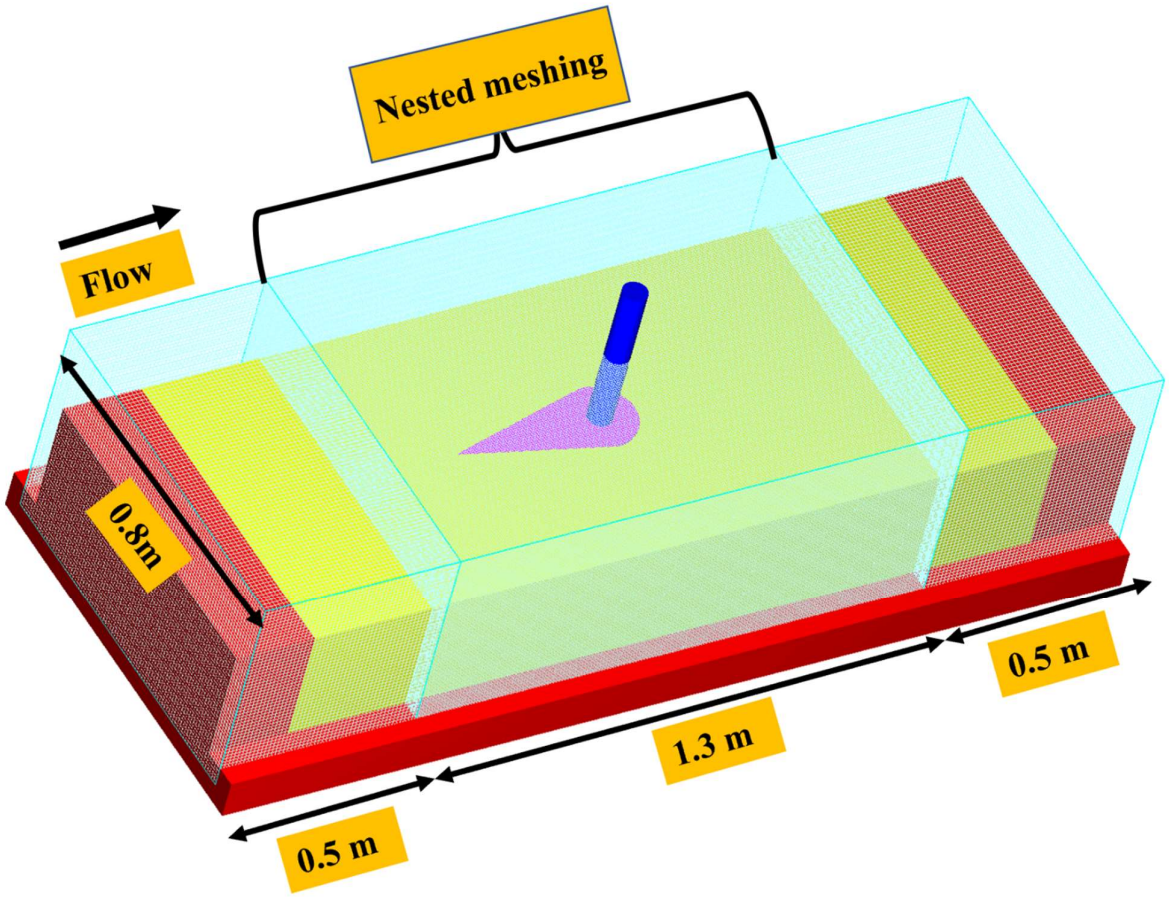

Figure 3.15: Sketch of mesh setup.

Table 3.5: Mesh sensitivity analysis.

S. N.	Meshing		Experimental results (cm)	FLOW-3D results (cm)	Error (%)	Estimated computational time (days)	Total no of mesh cells (million)
	Coarse mesh cell size (cm)	Fine mesh cell size (cm)					
1	2	1	6.8	3.3	51.47	2.5	0.783
2	1	0.5	6.8	4.7	30.88	8	6.533
3	0.8	0.5	6.8	6.3	7.35	10	7.374
4	0.8	0.4	6.8	6.33	6.91	18	12.234

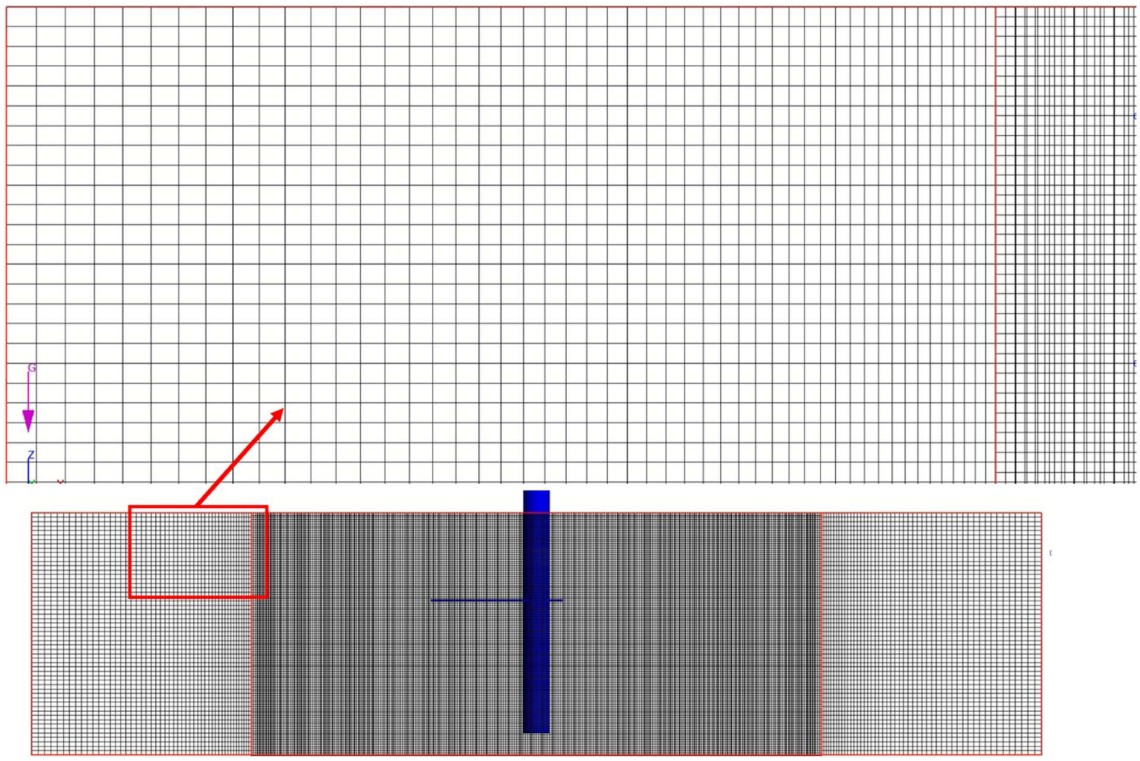

Figure 3.16: Coarse mesh setup for entire geometry.

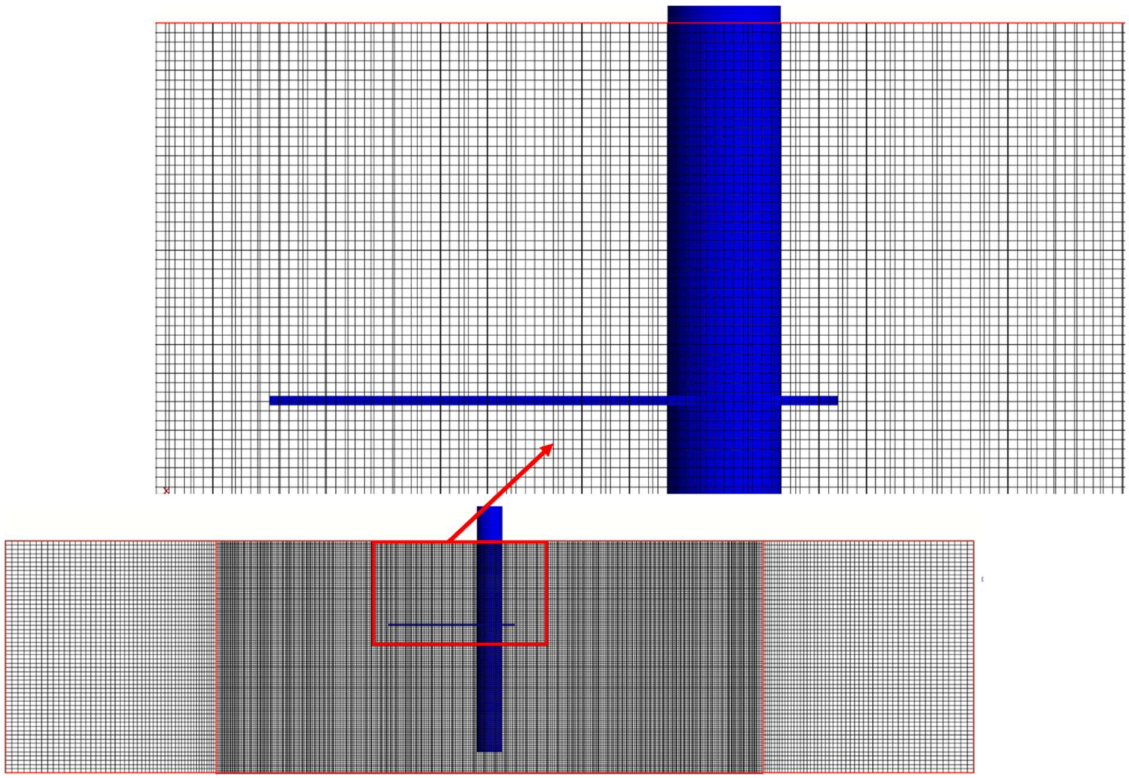

Figure 3.17: Nested mesh at the vicinity of pier with an airfoil collar.

3.9 Boundary and initial conditions

The input boundary conditions used in the simulation is shown in Figure 3.18. The upstream and downstream boundary conditions are velocity (V) and continuative (C), respectively. Floor, lateral and free surface boundary conditions are wall (W), wall (W) and symmetry (S), respectively. In FLOW-3D, the velocity is specified as the input for the flow simulation, representing the initial flow conditions. Continuity is maintained at the outflow boundary condition to ensure a smooth continuation of the flow. This boundary condition allows the flow to exit the domain without any disturbances. For the wall boundary condition, FLOW-3D assumes a virtually frictionless behavior, simulating a smooth and slippery bed and sides of the channel. This means that the effects of viscous friction between the fluid and the wall are neglected, allowing the flow to slide along the boundaries without significant resistance. On the other hand, the symmetry boundary condition in FLOW-3D represents an inviscid property of the wall. This condition assumes that there is no flow across the symmetry plane, simulating a mirror-like reflection of the flow. It effectively enforces the symmetry of the flow field, allowing the simulation to capture half of the domain and mirror the results to represent the entire flow domain. The initial pressure is hydrostatic and for saturation of sand, an initial fluid region of 0.50 m is kept.

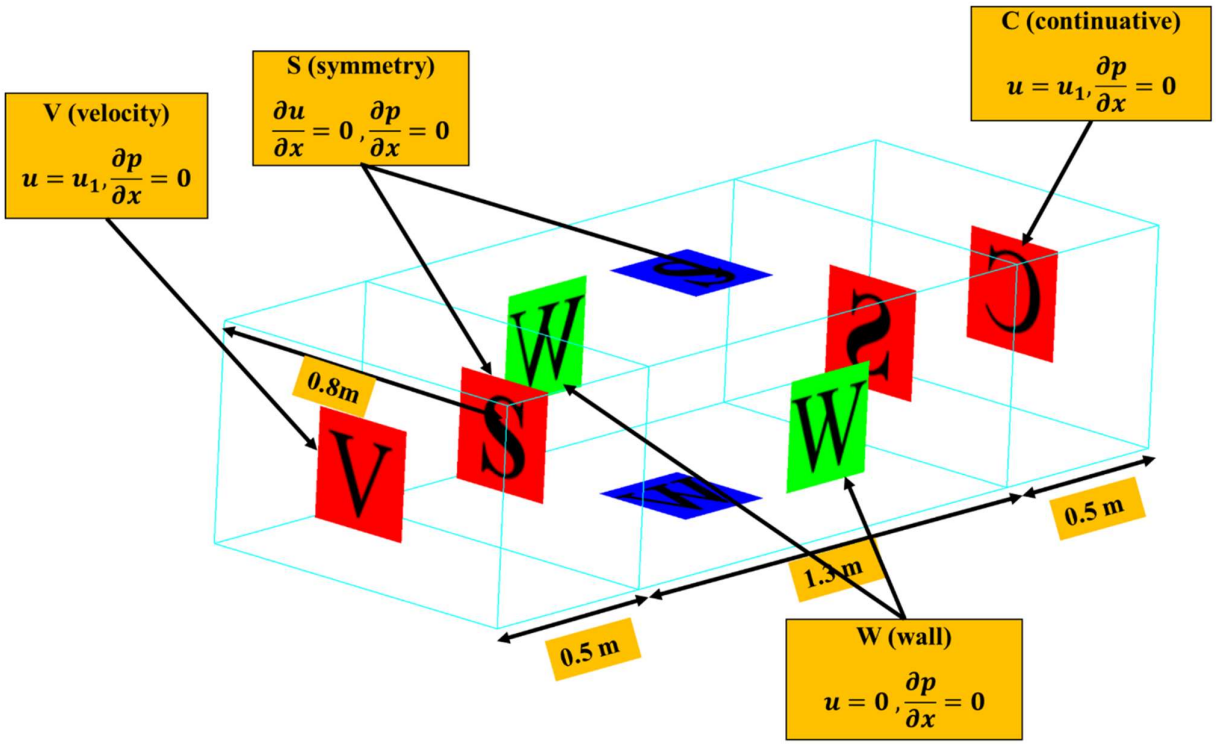

Figure 3.18: Boundary conditions annotated.

Chapter 4

Results and Discussions

This chapter presents a detailed analysis of the experimental and simulated results to meet the objectives of the study. The baseline experiments (pier without collar) are performed, their results are discussed and a relationship is proposed. Experiments are conducted with airfoil collars and their efficiency against scour reduction is computed. The effect of collar diameter and collar elevation on scour depth are presented. This study uses nonlinear regression analysis to propose an empirical relationship for the maximum scour depth and time-dependent scour development around the pier in the presence of an airfoil collar. Statistical sensitivity analyses are performed to check the accuracy and reliability of the proposed relationship to identify the most and least sensitive parameters.

Experimental results without and with airfoil collars are listed in Tables 4.1 and 4.2. In Table 4.2, experimental runs (1-64) show the outcomes for all airfoil collars at four different locations and experimental run 65 shows the results for collar b_{c2} when placed on the bed level reverse to the flow direction, denoted by b_{c2R}. If the change in scour depth is less than 0.05b in 24 hours, then it is defined as equilibrium scour depth (d_{se}), as mentioned in Tables 4.1 and 4.2 (Kothyari & Kumar, 2012; Melville & Chiew, 1999).

Table 4.1: Hydraulic conditions and experimental outcomes for pier without airfoil collar.

ER	d_{50} (m)	$b(m)$	$V(m/s)$	V/V_c	$y(m)$	F_r	R_e	d_{se}(m)
1	0.00032	0.05	0.247	0.95	0.10	0.249	12,350	0.065
2	0.00032	0.05	0.195	0.75	0.10	0.197	9,750	0.053
3	0.00032	0.06	0.247	0.95	0.10	0.249	14820	0.080
4	0.00032	0.06	0.195	0.75	0.10	0.197	11,700	0.067

where ER= experimental runs, d_{50} = median size of sediment particles, b = pier diameter, V = flow velocity, V/V_c= flow intensity, F_r = Froude number, R_e= Reynolds number and d_{se}= maximum scour depth around the pier without collar.

Table 4.2: Hydraulic conditions and experimental outcomes for the pier with airfoil collar.

ER	d_{50} (m)	b (m)	b_c(m)	L_c(m)	z (m)	$V(m)$	V/V_c	$y(m)$	d_{sec} (m)
1	0.00032	0.05	0.075	0.15	0	0.247	0.98	0.10	0.027
2	0.00032	0.05	0.075	0.15	0.025	0.247	0.98	0.10	0.036
3	0.00032	0.05	0.075	0.15	0.05	0.247	0.98	0.10	0.055
4	0.00032	0.05	0.075	0.15	0.075	0.247	0.98	0.10	0.061
5	0.00032	0.05	0.10	0.20	0	0.247	0.98	0.10	0.012
6	0.00032	0.05	0.10	0.20	0.025	0.247	0.98	0.10	0.031
7	0.00032	0.05	0.10	0.20	0.05	0.247	0.98	0.10	0.04

8	0.00032	0.05	0.10	0.20	0.075	0.247	0.98	0.10	0.052
9	0.00032	0.05	0.125	0.25	0	0.247	0.98	0.10	0
10	0.00032	0.05	0.125	0.25	0.025	0.247	0.98	0.10	0.029
11	0.00032	0.05	0.125	0.25	0.05	0.247	0.98	0.10	0.037
12	0.00032	0.05	0.125	0.25	0.075	0.247	0.98	0.10	0.048
13	0.00032	0.05	0.15	0.30	0	0.247	0.98	0.10	0
14	0.00032	0.05	0.15	0.30	0.025	0.247	0.98	0.10	0.027
15	0.00032	0.05	0.15	0.30	0.05	0.247	0.98	0.10	0.031
16	0.00032	0.05	0.15	0.30	0.075	0.247	0.98	0.10	0.04
17	0.00032	0.05	0.075	0.15	0	0.195	0.75	0.10	0.02
18	0.00032	0.05	0.075	0.15	0.025	0.195	0.75	0.10	0.031
19	0.00032	0.05	0.075	0.15	0.05	0.195	0.75	0.10	0.048
20	0.00032	0.05	0.075	0.15	0.075	0.195	0.75	0.10	0.049
21	0.00032	0.05	0.10	0.20	0	0.195	0.75	0.10	0.005
22	0.00032	0.05	0.10	0.20	0.025	0.195	0.75	0.10	0.028
23	0.00032	0.05	0.10	0.20	0.05	0.195	0.75	0.10	0.04
24	0.00032	0.05	0.10	0.20	0.075	0.195	0.75	0.10	0.043
25	0.00032	0.05	0.125	0.25	0	0.195	0.75	0.10	0
26	0.00032	0.05	0.125	0.25	0.025	0.195	0.75	0.10	0.024
27	0.00032	0.05	0.125	0.25	0.05	0.195	0.75	0.10	0.031
28	0.00032	0.05	0.125	0.25	0.075	0.195	0.75	0.10	0.04

29	0.00032	0.05	0.15	0.30	0	0.195	0.75	0.10	0
30	0.00032	0.05	0.15	0.30	0.025	0.195	0.75	0.10	0.02
31	0.00032	0.05	0.15	0.30	0.05	0.195	0.75	0.10	0.027
32	0.00032	0.05	0.15	0.30	0.075	0.195	0.75	0.10	0.037
33	0.00032	0.06	0.09	0.18	0	0.247	0.98	0.10	0.035
34	0.00032	0.06	0.09	0.18	0.025	0.247	0.98	0.10	0.048
35	0.00032	0.06	0.09	0.18	0.05	0.247	0.98	0.10	0.061
36	0.00032	0.06	0.09	0.18	0.075	0.247	0.98	0.10	0.073
37	0.00032	0.06	0.12	0.24	0	0.247	0.98	0.10	0.018
38	0.00032	0.06	0.12	0.24	0.025	0.247	0.98	0.10	0.043
39	0.00032	0.06	0.12	0.24	0.05	0.247	0.98	0.10	0.055
40	0.00032	0.06	0.12	0.24	0.075	0.247	0.98	0.10	0.069
41	0.00032	0.06	0.15	0.30	0	0.247	0.98	0.10	0
42	0.00032	0.06	0.15	0.30	0.025	0.247	0.98	0.10	0.041
43	0.00032	0.06	0.15	0.30	0.05	0.247	0.98	0.10	0.052
44	0.00032	0.06	0.15	0.30	0.075	0.247	0.98	0.10	0.065
45	0.00032	0.06	0.18	0.36	0	0.247	0.98	0.10	0
46	0.00032	0.06	0.18	0.36	0.025	0.247	0.98	0.10	0.038
47	0.00032	0.06	0.18	0.36	0.05	0.247	0.98	0.10	0.05
48	0.00032	0.06	0.18	0.36	0.075	0.247	0.98	0.10	0.057
49	0.00032	0.06	0.09	0.18	0	0.195	0.75	0.10	0.024

50	0.00032	0.06	0.09	0.18	0.025	0.195	0.75	0.10	0.04
51	0.00032	0.06	0.09	0.18	0.05	0.195	0.75	0.10	0.052
52	0.00032	0.06	0.09	0.18	0.075	0.195	0.75	0.10	0.061
53	0.00032	0.06	0.12	0.24	0	0.195	0.75	0.10	0.009
54	0.00032	0.06	0.12	0.24	0.025	0.195	0.75	0.10	0.038
55	0.00032	0.06	0.12	0.24	0.05	0.195	0.75	0.10	0.05
56	0.00032	0.06	0.12	0.24	0.075	0.195	0.75	0.10	0.055
57	0.00032	0.06	0.15	0.30	0	0.195	0.75	0.10	0
58	0.00032	0.06	0.15	0.30	0.025	0.195	0.75	0.10	0.037
59	0.00032	0.06	0.15	0.30	0.05	0.195	0.75	0.10	0.048
60	0.00032	0.06	0.15	0.30	0.075	0.195	0.75	0.10	0.053
61	0.00032	0.06	0.18	0.36	0	0.195	0.75	0.10	0
62	0.00032	0.06	0.18	0.36	0.025	0.195	0.75	0.10	0.036
63	0.00032	0.06	0.18	0.36	0.05	0.195	0.75	0.10	0.042
64	0.00032	0.06	0.18	0.36	0.075	0.195	0.75	0.10	0.049
65	0.00032	0.06	0.12	0.24	0	0.247	0.98	0.10	0.034

where ER= experimental runs, d_{50} = median size of sediment particles, b = pier diameter, b_c= collar diameter, L_c= length of airfoil collar, z= elevation of collar from the sediment bed, V = flow velocity, V/V_c= flow intensity, y = flow depth measured from the sediment bed and d_{sec}= maximum scour depth around the pier with collar.

4.1 Temporal variation of scour depth

4.1.1 Pier without collar

Temporal variation in the scour depth for the two piers and the two flow intensities is shown in Figure 4.1(a). During the initial stage of scouring, when flow velocity increases, the sediment transport capacity of the water also increases. Consequently, the scour depth increases rapidly as the high-velocity flow picks up and transports more sediment, leading to deeper erosion in the sediment bed. As the scouring process continues, the flow velocity reachs a point where it becomes stable and sediment transport rate approaches a constant value. At this stage, the scour depth increases smoothly or at a relatively constant rate because the flow consistently transports sediment at a steady pace. From that it is observed that initially scour depth is increases rapidly, then increases smoothly and becomes an almost stable and no increase of scour depth. For larger pier diameters with higher flow intensity, the scour is higher and for smaller pier diameters with lower flow intensity, the scour is lower. Similarly, scour is directly proportional to the discharge and vice versa. Figure 4.1(b) shows the dimensionless scour versus time. This indicates that the initial 80% of scour depth reached approximately in 20% equilibrium time. Equilibrium scour depth of 10%, 15% and 20% is reached at 70%, 75% and 81% of equilibrium time, respectively. If the value of $100\times d_{st}/d_{se}$, is equal to 10% of equilibrium scour depth, then it is equilibrium scour depth of 10%, similarly for equilibrium scour depth of 15% and 20%.

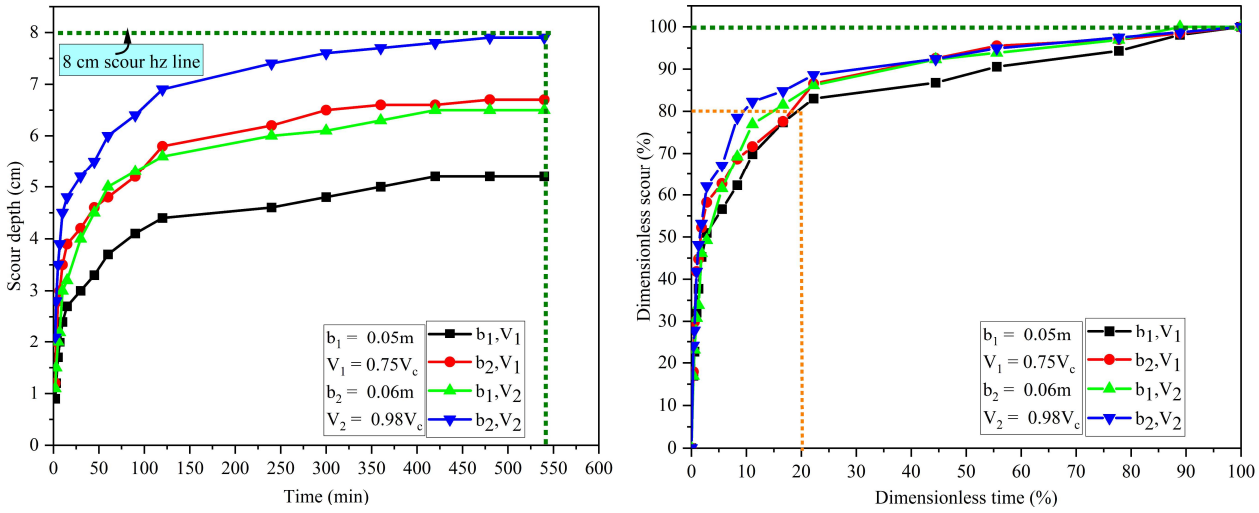

(a) (b)

Figure 4.1: (a) Temporal variation of scour depth around the pier and (b) dimensionless scour depth around the pier.

4.1.2 Pier with collar

The temporal variation of scour depth around the pier for four different collars at various locations with V/V_c= 0.98 is shown in Figure 4.2(a to d). The equilibrium scour depth around the pier without airfoil collar is 0.08 m and with b_{c1} at four locations (on bed level, y/4, y/2 and 3y/4 above the bed level), it is 0.035, 0.048, 0.061 and 0.073 m respectively, as shown in Figure 4.2 (a). With b_{c2} at five locations (on bed level, on the bed level reverse to the flow direction (b_{c2R}), y/4, y/2 and 3y/4 above the bed level), equilibrium scour depth around the pier is 0.018, 0.035, 0.043, 0.055 and 0.069 m, respectively as shown in Figure 4.2 (b).

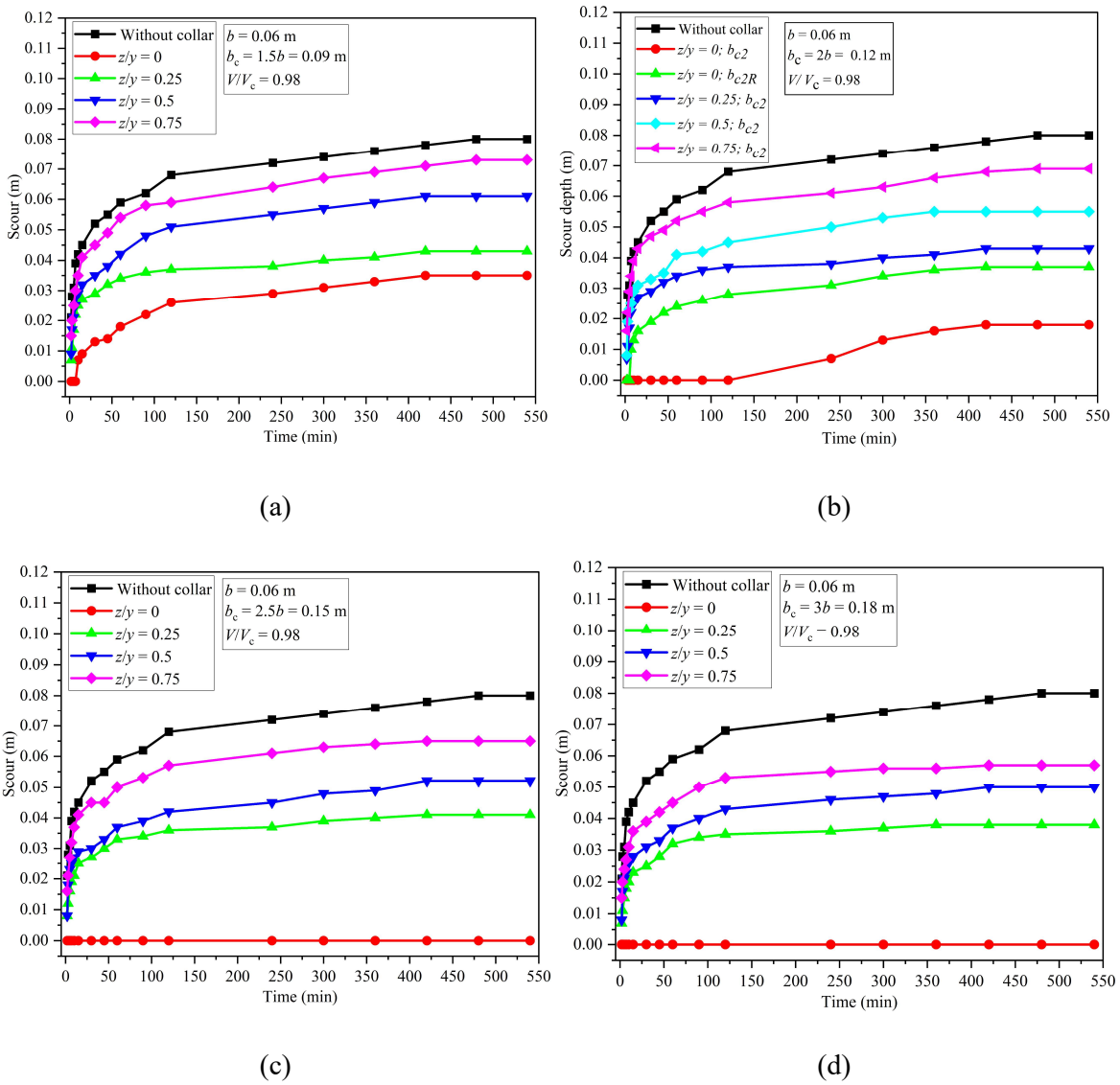

Figure 4.2: Variation of scour depth around the pier with and without four different collars (a) for b_{c1} (b) for b_{c2} (c) for b_{c3} and (d) for b_{c4}.

With b_{c3} at four locations, is 0, 0.041, 0.052 and 0.065 m respectively as shown in Figure 4.2(c). With b_{c4} at four locations, is 0, 0.038, 0.05 and 0.057 m respectively as shown in Figure 4.2 (d). When the collar b_{c2} is kept on the bed, there is almost zero scour for the first four hours (i.e., 45% of equilibrium time) and the equilibrium scour depth is 0.018 m. It is observed that for collars b_{c3} and b_{c4}, when they are kept on bed level, scouring around the pier is zero. The collar b_{c2} is 32% efficient than b_{c2R} in reducing the scour around the pier, which signify that changing the location of collar it affects the percentage of scour reduction. Changing the direction of airfoil collar (changing triangular nose facing upstream to downstream) also affects the scouring around the pier.

The percentages of scour reduction using the four collars (b_{c1}, b_{c2}, b_{c3} and b_{c4}) at bed level are 56, 77.5, nearly 100 and 100% respectively means there is no scour around the pier attached with collar b_{c3} and b_{c4}. The percentage of scour reduction when collars are kept at $y/4$ above the bed level is 40, 46.3, 48.8 and 52.5%. When the collars (b_{c1}, b_{c2}, b_{c3} and b_{c4}) are kept at elevation of $y/2$ above the bed level, percentages of scour reduction are 23.75, 31.25, 35 and 37.5% respectively and when kept at $3y/4$ above the bed level, the percentages of scour reduction are 8.75, 13.75, 18.75 and 28.75% respectively. Therefore, it can be concluded that airfoil collars at bed level are the most efficient in scour reduction compare to all other locations. Collars with diameter of b_{c2}, b_{c3} and b_{c4} are most efficient, which reduces the scour from 77.5 to 100%. For b_{c1} at bed level, scouring rate is initially low, due to protection around the pier. For collar b_{c2}, scouring started after 45% of equilibrium time. As collar diameter increases from b_{c1} to b_{c4}, scour depth around the pier is reduced. But collar diameter and length come into encroachment, so it should be optimized and cost-effective for field application. Therefore, it can be recommended that collar diameter with b_{c2}, b_{c3} and b_{c4} is the most efficient countermeasure for scour reduction. Installing the airfoil collar at bed level greatly improved the collar performance and negligible scour is observed around the pier.

The equilibrium scour depth around the pier is shown in Figure 4.3 for the collar b_{c2} after the experimental run. It is observed that scour in the directions of 0° and 180° of the pier is negligible and for 90° and 270° it is 0.018 m. The scour is significant on the sides of the pier (90° and 270°), indicating that erosion or sediment removal is occurring more prominently in those directions. Meanwhile, there is negligible scour in the front and back directions (0° and

180°), suggesting that there is minimal erosion directly in front of and behind the pier. This distribution of scour depths around the pier is an essential consideration in designing and engineering structures to ensure their stability and safety in various flow conditions.

(a) (b)

Figure 4.3: Equilibrium scour depth around the pier with airfoil collar of diameter of b_{c2} at bed level (a) rear view (b) side view.

4.2 Scour hole profile with airfoil collar

The scour hole profiles around the pier are analyzed while considering the presence of an airfoil collar positioned at four locations. The scour hole profiles in the longitudinal and transverse directions of the flow for airfoil collar b_{c2} with flow intensity of (V/V_c) 0.98 are shown in Figure 4.4. The longitudinal scour hole length along the centerline of the pier without an airfoil collar is 27 cm and with a collar on four locations is 2.2, 17, 22 and 26 cm along the centerline of the pier at four elevations (on the bed, at $y/4$, $y/2$ and $3y/4$ above the bed level respectively). When collar b_{c2} is placed on the bed, the upstream length of the scour hole is almost negligible along the centerline, but scour hole length in downstream of the pier is 1.2 cm. Moreover, the maximum scour occurs at 0° of the pier without a collar and the minimum scour length occurs when a collar is kept on the sediment bed. In case of pier without collar, the maximum deposition of 1.7 cm occurs at the downstream side of the pier at a distance of 17.5 cm from the center of the pier. The transverse scour hole profile for the

collar b_{c2} is shown in Figure 4.4(b). It is almost symmetrical around the center of the pier. The transverse length of the scour hole for the b_{c2} at four elevations (on bed level, $y/4$, $y/2$ and $3y/4$ above the bed level) is 4.5, 13, 15 and 26 cm respectively, as shown in Figure 4.4(b). The scour hole length without the airfoil is 26 cm, which is almost the same as the case where the airfoil is kept $3y/4$ above bed level. The longitudinal and transverse scour lengths vary from 24.5 and 26 cm. The transverse length of the scour hole is observed to be greater than the longitudinal scour hole length. The horizontal length of the scouring hole is greater than that of the longitudinal scouring hole because the longitudinal length (triangular part) of the airfoil collar protects the upstream face of the pier. Therefore, it is concluded that the collar on the bed reduces the scour hole volume by reducing the length, width and depth of scour hole. Ripple formation is observed in the vicinity of the pier if d_{50} <0.7 mm (Melville & Raudkivi, 1977). Ripples form as a result of the interaction between the flowing water and the wake region that emerges behind the pier. When the water encounters an obstacle, it generates turbulent eddies and vortices within the wake zone. These eddies and vortices cause fluctuations in the water surface, leading to the formation of downstream ripples.

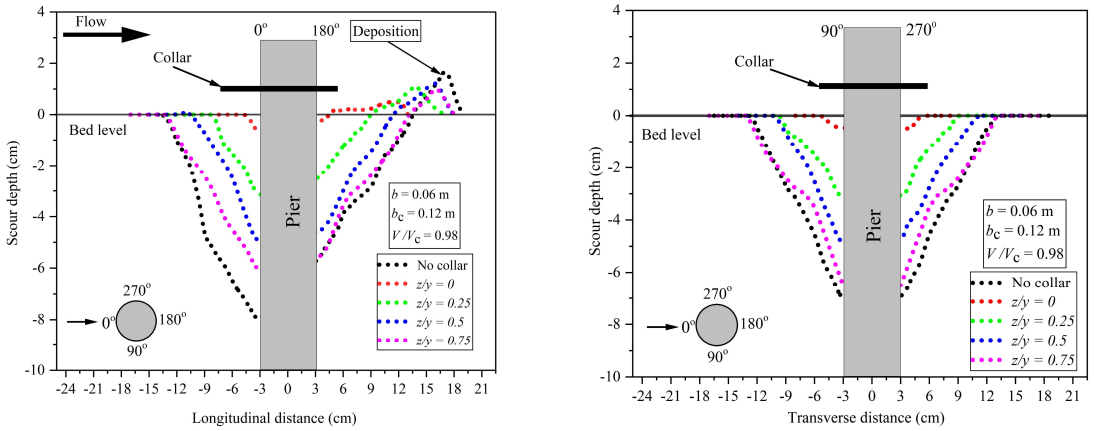

(a) (b)

Figure 4.4: Scour hole profile for collar b_{c2} (a) longitudinal and (b) transverse profile.

4.3 Time-dependent scour depth with an airfoil collar

Time-dependent scour depth changes for airfoil collar, b_{c2} with V/V_c= 0.98, is shown in Figure 4.5. The maximum scour depth at the pier without a collar is 0.08 m and in the presence of a collar, when kept at five locations (bed level, reverse to flow direction on bed level, at $y/4$, $y/2$ and $3y/4$ above the sediment bed level) are 0.018, 0.035, 0.043, 0.055 and

0.069 m respectively. Figure 4.5 shows the nondimensional scour vs nondimensional time plot for the pier without and with an airfoil collar placed at five elevations. In the case of a pier without a collar, b_{c2}, maximum scour depth is $1.33b$ and with collar is $0.3b$, $0.55b$, $0.72b$, $0.92b$ and $1.15b$ when kept five locations (on bed level, reverse to flow direction on bed level, $y/4$, $y/2$ and $3y/4$ above the sediment bed level). This indicates that if the collar elevation increases from the sediment bed, scour depth increases around the pier. So, the collar is best suited on bed level when its triangular shape of the collar is facing the upstream side of the pier. The effect of the airfoil collar location on scour depth indicates that the higher the collar's location from the sediment bed, lesser the reduction in scour depth as shown in Figure 4.5.

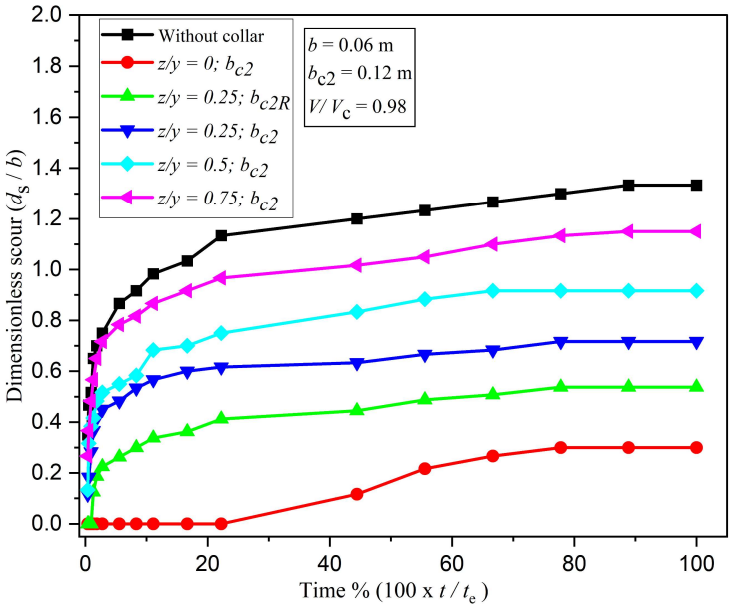

Figure 4.5: Dimensionless scour depth variation with and without airfoil collar.

4.4 Influence of collar diameter on scour depth

The effect of collar diameter on scour depth around the pier is shown in Figure 4.6 for b = 0.06 m with V/V_c = 0.98, which shows the increase in collar diameter from b_{c1} to b_{c4}, the maximum scour depth reduces from 0.05 m to 0 m. The percentage reduction in scour depth is 52% to 100% for collars b_{c1} to b_{c4}. This is because a larger collar diameter provides more resistance to the flow around the pier, thereby reducing the flow velocity of the water and erosive forces that cause scouring and prevent further deepening of the scour hole. During the initial stage of scouring, the scour depth increases more rapidly around a pier with a smaller collar diameter than that with a larger collar diameter. However, once the scouring has progressed to a certain point, the temporal variation in the scour depth becomes more stable

with a larger collar diameter. Using the collar on bed level, it is observed that maximum scour depth is reached asymptotically. From the existing literature, it is indicated that there is a positive correlation between pier diameter and variation in time-dependent scour depth (Kothyari et al., 2007; Pandey et al., 2020a). Figure 4.6(b) shows the nondimensional scour with nondimensional time plot for the pier without and with an airfoil collar placed at bed level with a flow intensity of 0.98. In the case of a pier without a collar, the maximum scour depth is 1.33b and with collars (b_{c1}, b_{c2}, b_{c3} and b_{c4}) is 0.59b, 0.33b and almost 0b and 0b (negligible) when kept on bed level.

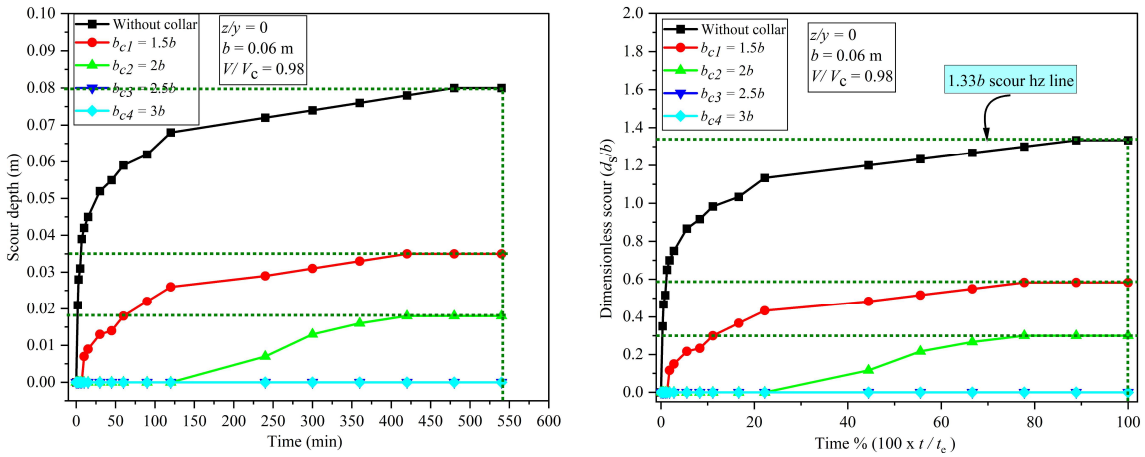

Figure 4.6: Influence of collar diameter and location (a) time-dependent variation of scour depth (b) dimensionless scour depth variation around the pier with and without airfoil collar with respect to time.

4.5 Scour depth variation for different pier diameters and flow intensities on the bed level

Time-dependent scour depth variation for different piers and flow intensities when the airfoil collar is placed on the bed level is shown in Figure 4.7(a). From the experimental results, the scour depth at pier with airfoil collars b_{c3} and b_{c4} is nearly zero when placed on the bed level. As the pier diameter and flow intensity increases, the scour depth also increases, but the increase in collar diameter reduces the scour at the pier as shown in Figure 4.7(a). The maximum scour depth at the pier is for collar b_{c1} with V/V_c=0.98 and b =0.06 m is observed and minimum for collar b_{c2} with V/V_c= 0.98 and b = 0.05m. When the diameter of the collar increases then scour at the pier decreases. At low flow intensity, smaller pier diameter with a

larger collar diameter, scour depth around the pier reached equilibrium condition earlier than all the other cases as shown in Figure 4.7(a). At threshold velocity, with small collar diameter and larger pier diameter, scour around the pier is greater. Figure 4.7(b) shows the time-dependent scour depth for two different pier diameters with the same collar diameters, location and flow intensity, indicating similar trends during initial scour hole development. However, these trends are also influenced by the collar diameter and tend to decrease as the ratio of collar width to pier width increases, as shown in Figure 4.7(b). All the analysis carried out for pier diameter of b = 0.06 m with all four collars at four elevations also shows a similar trend for b= 0.05 m with four airfoil collars at four locations.

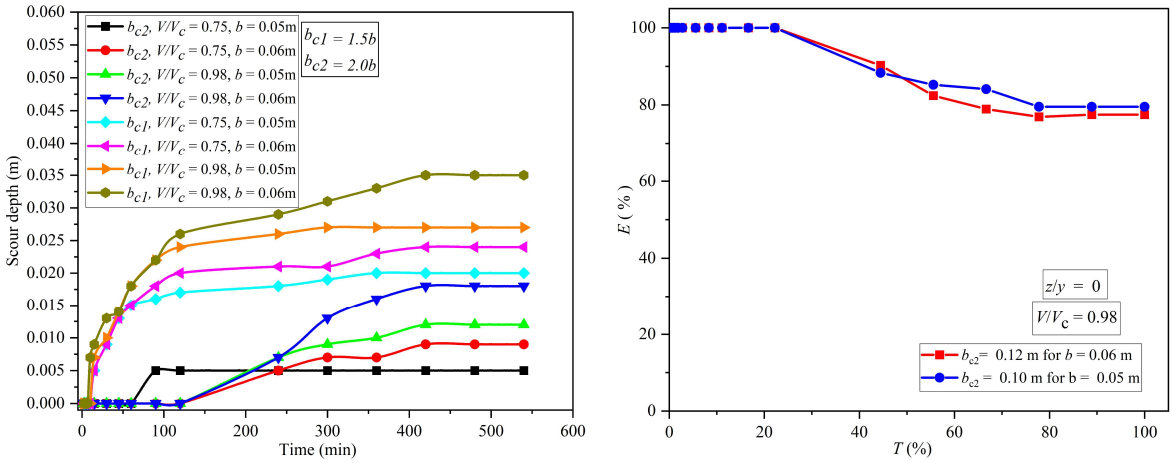

Figure 4.7: (a) Effect of flow intensity, collar diameter and pier diameter on scour depth (b) Effect of pier diameter on reduction of scour depth.

4.6 Efficiency of the airfoil collar

The efficiency of the airfoil collar is defined as:

$$E\ (\%) = \frac{d_{st} - d_{stc}}{d_{st}} * 100 \tag{4.1}$$

where d_{st} and d_{stc} are scour depth around the pier without and with airfoil collar, respectively, at any time, t.

Scour reduction using a collar at different elevations in terms of efficiency at equilibrium scour, i.e., $T(\%)$ = 100% is shown in Figure 4(a to d). The efficiency of collars b_{c1} and b_{c2} at bed level is 55 and 78% respectively and almost 100% for b_{c3} and b_{c4} as

shown in Figure 4(a). The efficiency of collars b_{c1}, b_{c2}, b_{c3} and b_{c4} at the elevation $y/4$ above the bed level is 40, 46.25, 48.75 and 52.5% respectively as shown in Figure 4(b). The efficiency of collars b_{c1}, b_{c2}, b_{c3} and b_{c4} is 23.75, 31.25, 35 and 37.5% respectively when placed at the elevation $y/2$ above the bed level as shown in Figure 4(c). When the collars are placed at the elevation of $3y/4$ above the bed level, the efficiency of collars b_{c1}, b_{c2}, b_{c3} and b_{c4} is 8.75, 13.75, 18.75% and 28.75% respectively, as shown in Figure 4(d). For all the elevations, it is observed that the maximum reduction of scour is found for collar at bed level and the efficiency of the collar increases with an increase in collar diameter as shown in Figure 4(a to d). It is observed that there is a decrement in the collar's efficiency initially and due to the protection provided by the collar around the pier, the efficiency of the collar increases with respect to time and becomes almost constant in the final stages. In addition, collars delay the scouring process and scour hole development at the perimeter of the pier.

In summary, during the initial stage of scouring, the scour depth can increase more rapidly around the pier and protection efficiency of the collar decreases rapidly. Collar provides more obstruction to the flow around the pier and thus reduces the flow velocity and the erosive forces that cause scouring and prevent further development of the scour hole. The protection efficiency of the collar is calculated when the scour is asymptotically stabilized. From it is concluded that the highest efficiency is achieved for $z = 0$ in all collars (b_{c1}, b_{c2}, b_{c3} and b_{c4}). The collar diameter also affects the amount of sediment that can be trapped by the collar, reducing the amount of sediment that is eroded from around the pier.

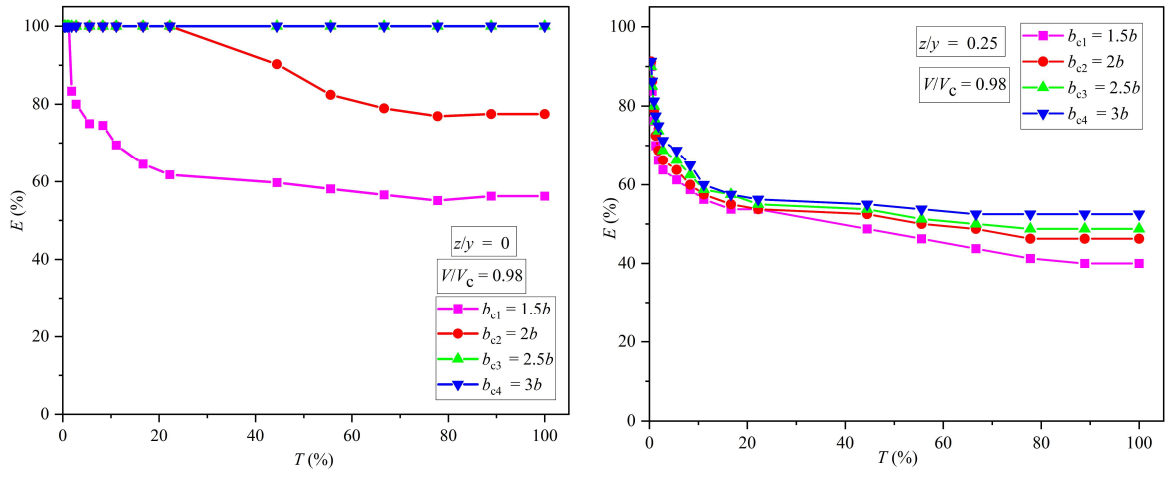

(a) (b)

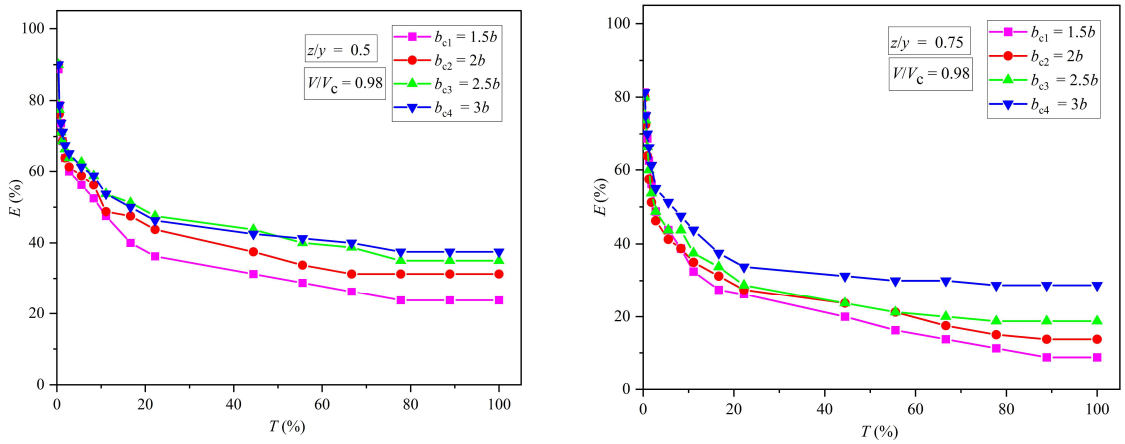

(c) (d)

Figure 4.8: Protection efficiency of collars at various locations (a) on bed level, (b) at $0.25y$, (c) at $0.5y$ and (d) at $0.75y$ above the bed level.

4.7 Proposed relationships for time-dependent scour development

Scour around the bridge pier is influenced by several factors as discussed in dimensional analysis (Chapter 3). Many researchers have proposed empirical relationship for scour around the bridge pier without scour countermeasures (Aksoy et al., 2017; Choi and Choi, 2016; Franzetti et al., 2022; Kothyari et al., 2007; Lança et al., 2013; Melville and Chiew, 1999b; Oliveto and Hager, 2002). This study proposes a relationship for scour at bridge pier without collar is given by Equation 4.2. Figure 4.9 shows temporal variation of scour depth observed and computed from proposed relationship for pier diameter of 0.06 m. Coefficient of correlation between observed and computed values, R^2=0.945.

$$\frac{d_{st}}{b} = 0.834(F_d)^{0.713} logT \tag{4.2}$$

where d_{st}= scour depth around pier at time, t, b = diameter of pier, F_d = desimetric Froude number = $\frac{V}{\sqrt{(S-1)g*d_{50}}}$, T = dimensionless time = $t\frac{\sqrt{(S-1)gd_{50}}}{(b^2y)^{1/3}}$, S = relative density, g = acceleration due to gravity, d_{50} = median particle size and y= flow depth.

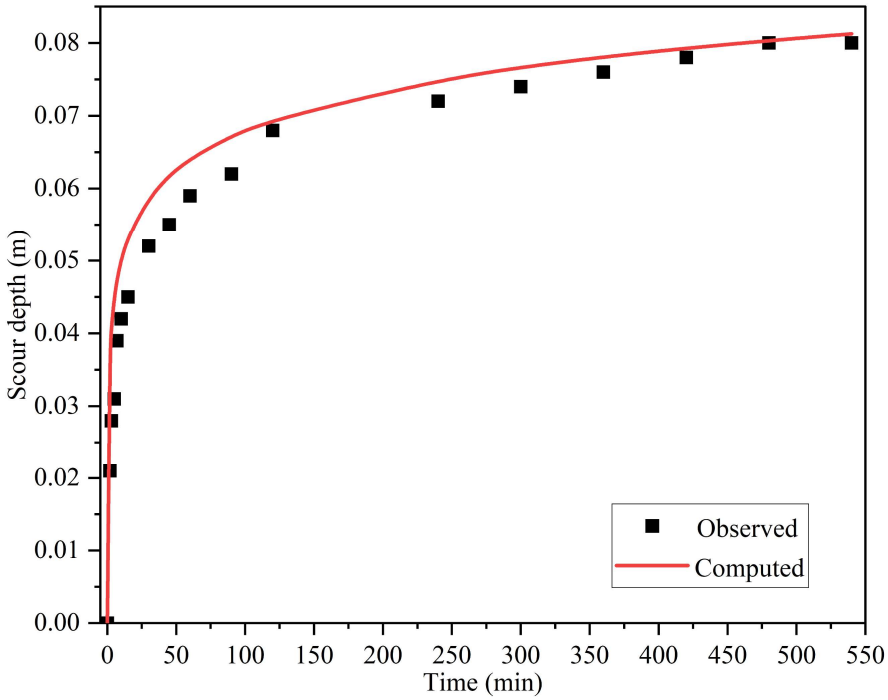

Figure 4.9: Observed and computed scour depth variation around the pier.

4.8 Proposed relationships for maximum scour depth and time-dependent scour development

Maximum scour depth around a pier with a collar depends on several factors, including the diameter and location of the collar, as well as the parameters that affect scour depth in the absence of a collar, such as the flow velocity and sediment characteristics, as discussed in earlier section (Chapter 3). Several researchers have derived relationships for maximum scour depth and temporal variation of scour depth without a collar (Aksoy et al., 2017; Choi and Choi, 2016; Franzetti et al., 2022; Kothyari et al., 2007; Lança et al., 2013; Melville and Chiew, 1999b; Oliveto and Hager, 2002) . In addition, many researchers have proposed relationships for the scour depth around the pier with protected circular and octagonal collars (Farooq et al., 2020a; Pandey et al., 2022, 2020a; Valela et al., 2022a). From dimensional analysis, scour around the pier in the presence of an airfoil collar can be expressed as follows:

$$d_{stc} = f_4(d_{st}, b, b_c, L_c, h, T_c) \tag{4.3}$$

where h is the location of the collar from the water surface, $h = y\text{-}z$, z is the location of the collar from the sediment bed, dimensionless time, $T_c = t\frac{\sqrt{(S-1)gd_{50}}}{R_L}$ in which R_L is reference

length given by $(b_c{}^2 y)^{1/3}$. By rearranging the terms and using dimensional analysis, the following relationship can be developed:

$$d_{stc} = \left(\frac{b_c}{b}, \frac{L_c}{b}, \frac{h}{y}, T_c\right) \tag{4.4}$$

Therefore, this study proposes a relationship for computing the maximum scour depth and time-dependent scour development. The experimental datasets used are 32 and 546 respectively to develop the relationships. Furthermore, nonlinear regression analysis is performed using a diverse set of datasets, resulting in the development of new relationships as given in Equations (4.5) and (4.6). By incorporating various parameters that affect the scouring process, these equations are expected to offer a more comprehensive and reliable estimation of the maximum scour depth and time-dependent scour development using an airfoil collar around the bridge pier. Most datasets show a high degree of conformity to the ideal line, with approximately 85% of them exhibiting errors within a range of ±25% when calculated using Equation (4.5) as shown in Figure 5(a). Similarly, from Figure 5(b), for Equation (4.6), most datasets showed a high degree of conformity to the ideal line, with approximately 75% of them exhibiting errors within a range of ±25% when calculated using proposed relationship as shown in Figure 5(b). Maximum scour depth around the pier with an airfoil collar:

$$\frac{d_{se} - d_{sec}}{d_{se}} = 2.22\left(\frac{b_c}{b}\right)^{2.98}\left(\frac{L_c}{b}\right)^{-2.28}\left(\frac{h}{y}\right)^{1.21} \tag{4.5}$$

where d_{se} and d_{sec} are maximum scour depth around pier without and with collar, respectively. Time-dependent scour depth variation around the pier with airfoil collar:

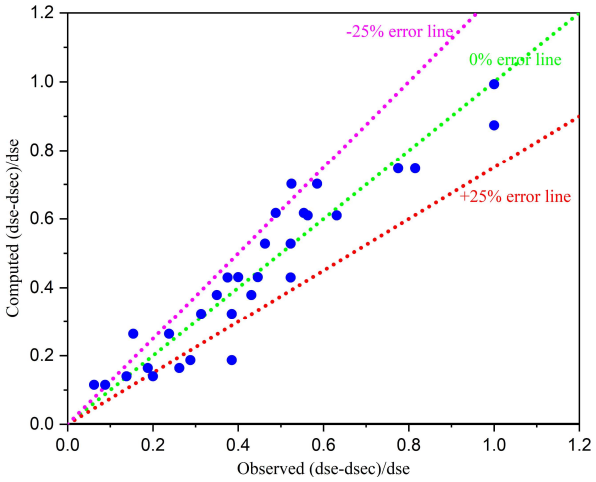

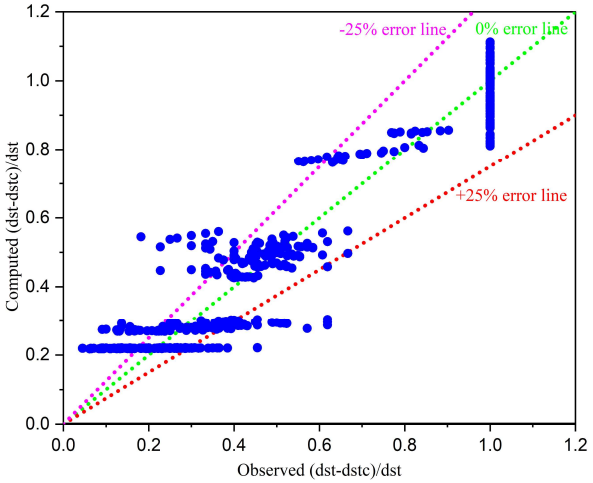

(a) (b)

Figure 4.10: shows the observed and computed scour depth, (a) for maximum scour depth around the pier with an airfoil collar and (b) time-dependent scour development around the pier with an airfoil collar.

4.8.1 Limitations of proposed relationships

These relationships consider various factors and appear to provide accurate estimates, as indicated by the high conformity of the datasets to the relationships. Some limitations of relationships (4.5 and 4.6) are:

i. Sand should be uniform.
ii. These relationships should be applied as long as wall interference is not there and end conditions are minimized.
iii. Clear-water condition should be maintained.
iv. Steady and uniform flow should be maintained.
v. Constant water depth.
vi. Scour due to the contraction effect.
vii. Collar location should be on or above the sediment bed.

4.9 Sensitivity analysis

Sensitivity analysis is a technique to understand how changes in independent variables affect the dependent variable, given a specific set of assumptions. It is commonly used to assess the robustness of empirical relationships and to examine the presence of uncertainty and its potential impact on outcomes. In sensitivity analysis, different values or ranges are assigned to the independent variables and the corresponding changes in the dependent variable are observed. Performing sensitivity analysis by taking the average values of dependent and independent variables is one approach. This method allows us to examine the impact of varying the independent variables around their average values while keeping the dependent variable constant.

The parameters of this study are b_c/b, L_c/b, h/y and T_c and their average values are 2.25, 4.5, 0.625 and 1923.1 respectively. The difference between the output obtained from the given input parameter, P_{avg} and P_{avg}+ΔP_{avg} is denoted as error Δe, where P_{avg} denotes the average value of the input parameter (P) and ΔP_{avg} is percentage change in the input parameters (Guguloth and Pandey, 2023). Absolute sensitivity (AS) is defined as $AS = \Delta e/\Delta P_{avg}$. The

relative error (RE) is defined as $\Delta e/f(P_{avg})$ and relative sensitivity (RS) is defined as $P * AS/f(P_{avg})$, where $f(P_{avg})$ is the output value corresponding to average value of the parameter and f represents the empirical relationship. Table 4.3 presents the sensitivity analysis performed by varying input parameters from ±10% to ±50%. From Table 4.3, it is observed that the most sensitive parameters are h/y, b_c/b, L_c/b and T_c, in decreasing order. By changing positive and negative increment in input parameter, RS and RE are maximum for b_c/b, AS is maximum for h/y. The most and least sensitive parameters are h/y and T_c. Therefore, it can be concluded that most sensitive parameters are h/y and b_c/b.

4.10 Statistical analysis

Statistical analysis is performed to check the accuracy of relationships (4.5) and (4.6). The various statistical indices, such as the coefficient of determination (R^2) indicates the proportion of the variance in the dependent variable that can be explained by the independent variable(s) in a regression model. It is a common tool for assessing the goodness of fit of a regression model. Root Mean Square Error ($RMSE$) measures the performance of derived relationships. Mean Absolute Error (MAE) measures the average magnitude of errors between computed and observed values. It provides a measure of how far, on average, the computed values deviate from the observed values. Mean Absolute Percentage Error ($MAPE$) measures the performance of a computed against the observed values. For maximum scour depth, the value of R^2, $RMSE$, MAE and $MAPE$ are 0.91, 0.081, 0.064 and 17%, respectively. For time-dependent scour depth, the value of R^2, $RMSE$, MAE and $MAPE$ are 0.887, 0.099, 0.078 and 24.5%, respectively.

$$R^2 = \left[\frac{(N\sum M_{obs}M_{com}) - (\sum M_{obs})(\sum M_{com})}{\sqrt{N(\sum {M_{obs}}^2) - (\sum M_{obs})^2}\sqrt{N(\sum {M_{com}}^2) - (\sum M_{com})^2}}\right]^2 \tag{4.7}$$

$$RMSE = \sqrt{\frac{1}{N}\sum_{i=1}^{N}(M_{obs} - M_{com})^2} \tag{4.8}$$

$$MAE = \frac{\sum |M_{obs} - M_{com}|}{N} \tag{4.9}$$

$$MAPE = \frac{100}{N}\sum_{i=1}^{N}\left|\frac{M_{obs} - M_{com}}{M_{obs}}\right| \tag{4.10}$$

where M_{obs} and M_{com} are observed and computed values of scour depth. N is the number of datasets.

Table 4.3: Sensitivity analysis of positive and negative increments in parameters.

% change	P	P_{avg}	ΔP_{avg}	$P_{avg} \pm \Delta P_{avg}$	$f(P_{avg})$	$f(P_{avg} \pm \Delta P_{avg})$	Δe	AS	RE	RS
+10%	b_c/b	2.250	0.225	2.475	0.361	0.376	0.015	0.067	0.042	0.418
	L_c/b	4.5	0.450	4.950	0.361	0.353	-0.007	-0.016	-0.020	-0.202
	h/y	0.625	0.063	0.688	0.361	0.416	0.055	0.885	0.153	1.533
	T_c	1923.1	192.31	2115.41	0.361	0.360	0.000	0.000	-0.001	-0.009
-10%	b_c/b	2.250	0.225	2.025	0.361	0.346	-0.015	-0.067	-0.042	-0.418
	L_c/b	4.5	0.450	4.050	0.361	0.369	0.008	0.019	0.024	0.235
	h/y	0.625	0.063	0.563	0.361	0.317	-0.044	-0.704	-0.122	-1.220
	T_c	1923.1	192.31	1730.79	0.361	0.361	0.000	0.000	0.001	0.010
+20	b_c/b	2.250	0.450	2.700	0.361	0.391	0.030	0.067	0.084	0.418
	L_c/b	4.5	0.900	5.400	0.361	0.347	-0.014	-0.015	-0.038	-0.189

	h/y	0.625	0.125	0.750	0.361	0.484	0.123	0.986	0.342	1.709
	T_c	1923.1	384.620	2307.72	0.361	0.360	-0.001	0.000	-0.002	-0.009
-20	b_c/b	2.250	0.450	1.800	0.361	0.331	-0.030	-0.067	-0.084	-0.418
	L_c/b	4.5	0.900	3.600	0.361	0.379	0.019	0.021	0.051	0.257
	h/y	0.625	0.125	0.500	0.361	0.282	-0.078	-0.625	-0.217	-1.084
	T_c	1923.1	384.620	1538.48	0.361	0.361	0.001	0.000	0.002	0.011
+30	b_c/b	2.250	0.675	2.925	0.361	0.406	0.045	0.067	0.125	0.418
	L_c/b	4.5	1.350	5.850	0.361	0.341	-0.019	-0.014	-0.053	-0.178
	h/y	0.625	0.188	0.813	0.361	0.566	0.206	1.096	0.570	1.900
	T_c	1923.1	576.930	2500.03	0.361	0.360	-0.001	0.000	-0.002	-0.008
-30	b_c/b	2.250	0.675	1.575	0.361	0.315	-0.045	-0.067	-0.125	-0.418
	L_c/b	4.5	1.350	3.150	0.361	0.391	0.031	0.023	0.085	0.284
	h/y	0.625	0.188	0.438	0.361	0.257	-0.104	-0.554	-0.288	-0.960
	T_c	1923.1	576.930	1346.17	0.361	0.362	0.001	0.000	0.004	0.012

+40	b_c/b	2.250	0.900	3.150	0.361	0.421	0.060	0.067	0.167	0.418
	L_c/b	4.5	1.800	6.300	0.361	0.336	-0.024	-0.013	-0.067	-0.168
	h/y	0.625	0.250	0.875	0.361	0.664	0.304	1.214	0.842	2.104
	T_c	1923.1	769.240	2692.34	0.361	0.360	-0.001	0.000	-0.003	-0.008
-40	b_c/b	2.250	0.900	1.350	0.361	0.300	-0.060	-0.067	-0.167	-0.418
	L_c/b	4.5	1.800	2.700	0.361	0.406	0.046	0.025	0.127	0.318
	h/y	0.625	0.250	0.375	0.361	0.238	-0.122	-0.490	-0.340	-0.849
	T_c	1923.1	769.240	1153.86	0.361	0.362	0.002	0.000	0.005	0.013
+50	b_c/b	2.250	1.125	3.375	0.361	0.436	0.075	0.067	0.209	0.418
	L_c/b	4.5	2.250	6.750	0.361	0.332	-0.029	-0.013	-0.079	-0.159
	h/y	0.625	0.313	0.938	0.361	0.780	0.419	1.340	1.162	2.323
	T_c	1923.1	961.550	2884.65	0.361	0.359	-0.001	0.000	-0.004	-0.008
-50	b_c/b	2.250	1.125	1.125	0.361	0.285	-0.075	-0.067	-0.209	-0.418
	L_c/b	4.5	2.250	2.250	0.361	0.426	0.065	0.029	0.181	0.363

	h/y	0.625	0.313	0.313	0.361	0.226	-0.135	-0.432	-0.375	-0.749
	T_c	1923.1	961.550	961.550	0.361	0.363	0.003	0.000	0.007	0.014

4.11 Simulation results

4.11.1 Validation of Large Eddy Simulation (LES) model from previous research

The experimental data of Melville & Raudkivi (1977) is utilized to verify the accuracy of the Large Eddy Simulation (LES) model. This same data was also utilized by Qi et al. (2021) in their numerical simulation validation process. The experiments are carried out in a rectangular flume of 19 m in length, 0.456 m in width and 0.44 m in depth. A cylindrical pier of diameter 0.0508 m is used as bridge pier with uniform sediment of median size (d_{50}) of 0.000385 m. The approach velocity and flow depth are 0.25 m/s and 0.15 m respectively. The experiment continued for several hours and during the first 30 minutes, the depth of the scour hole increased rapidly but subsequently progressed at a slower rate. The simulation has same conditions as in experimental setup. The velocity, continuity, wall, wall and symmetry boundary conditions are applied to the upstream, downstream, floor, lateral side and free surface respectively. To validate the observed data of Melville & Raudkivi (1977) in a simulation model, the parameters such as critical Shields number, entrainment coefficient, angle of repose, bed roughness and bed load coefficient of 0.033, 0.018, 32°, 2.5 and 0.050 respectively are considered. The study uses nested mesh configuration of coarse and fine cell sizes of 0.8 and 0.4 cm respectively.

4.11.2 Results of LES model from previous research

The maximum scour depth around the pier is 4.073 cm and 3.89 cm from Melville & Raudkivi, (1977) and this simulation respectively. The error between simulated and observed results is below 6%. Melville & Raudkivi (1977) findings indicate that the point of maximum scour depth is located at the upstream face (0°) of the pier. However, simulations suggest that it is situated within the range of 0° to 45°. The comparison between Melville & Raudkivi (1977) and the simulated are shown in Figure 4.11 for scour profiles. Figure 4.11(a) shows the longitudinal scour profile in which maximum scour occurs at the upstream face of the pier along the center line of the pier and deposition occurs behind the downstream face of the pier. Traverse scour hole profile is symmetrical about the pier's center line as shown in Figure 4.11(b). The findings of this study align more closely with previous research, as evidenced by the comparable maximum depth of local scour and the similar shape of the scour hole

observed. From the Melville & Raudkivi (1977) and simulated results, it is observed that both profiles are significantly similar. It can be concluded that LES model utilized is both reasonable and accurate, indicating its suitability for computing the utmost scouring depth surrounding the bridge pier.

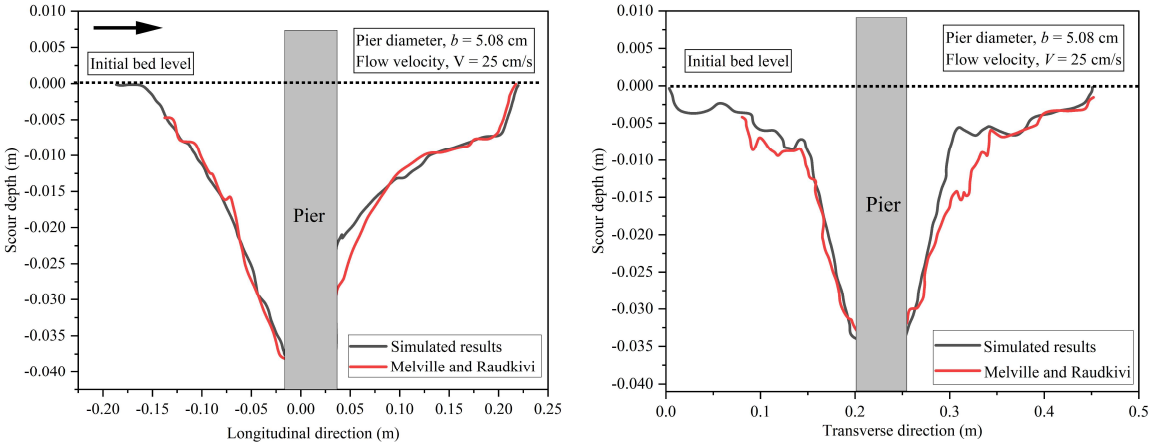

(a) Scour hole profile in the longitudinal direction

(b) Scour hole profile in the transverse direction

Figure 4.11: Scour hole profile from Melville & Raudkivi (1977) and simulated results.

4.12 Validation of numerical result with the present experimental results

It is important to indicate the uncertainties of the experiment when reporting the results, particularly in the case of a movable bed experiment where repeatability can be low. The uncertainties or errors associated with the experiment can be due to a variety of factors, such as variations in measurement error, experimental setup, instrumentation error, variability of system, environmental factors and human error. By reporting the uncertainties, researchers have provided a measure of the reliability of the results and the degree of confidence that can be placed in the findings. This information can help other researchers to evaluate and build upon the results of the experiment and can also aid in the design of future experiments. To determine the uncertainties, researchers typically conduct a series of measurements and calculate the standard deviation or other statistical measures of the data. This provides a measure of the variability of the data and can help to identify potential sources of error. By acknowledging and reporting the uncertainties, researchers can provide a more complete and transparent account of their work, which can ultimately contribute to the advancement of

scientific knowledge.

Experiment is conducted to validate the maximum scour depth around the pier without collar, which is found to be 6.8 cm and numerical simulation for the similar condition is 6.33 cm. Thus, an error of 7% is observed, with simulation underestimating the scour depth as shown in Figure 4.12.

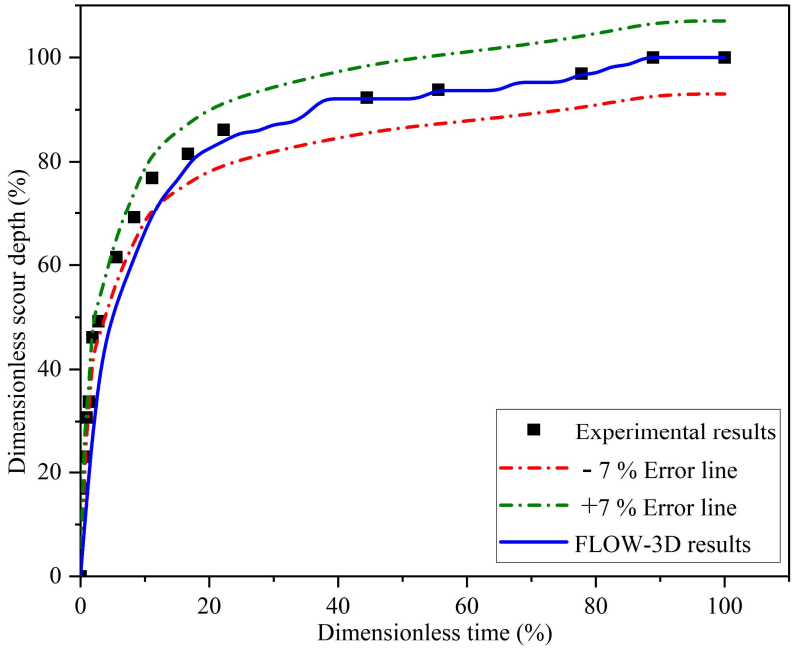

Figure 4.12: Dimensionless scour vs time for experimental and simulation results.

A 7% error is generally considered acceptable in many scientific and engineering disciplines, including river engineering, as it is often challenging to precisely account for all the complexities and uncertainties present in real-world systems. The ability of the numerical model to achieve such a level of agreement indicates that it can provide valuable insights and predictions for practical applications. The 7% error range allows for minor discrepancies that could arise due to various factors, such as measurement uncertainties, boundary condition assumptions, or simplifications in the model. Nevertheless, the small magnitude of the error suggests that the model is robust and can be relied upon for decision-making purposes. The good agreement within a 7% error between the simulated and experimental results demonstrates the effectiveness of the numerical model in replicating the observed phenomena. It signifies the model's reliability and accuracy, suggesting that it can serve as a valuable tool for analyzing and predicting river behavior, guiding engineering designs and informing decision-making processes in the field of river engineering.

From the numerical simulation, 67% and 83% of equilibrium scour depths are obtained at 10 and 20% of equilibrium time as shown in Figure 4.12. From the experimental results, the maximum scour depth location is at the pier's upstream face (0°). But, in simulation, it is between 0°–45°. Simulation did not estimate the location of maximum scour depth accurately because, it does not measure the velocity of turbulent pulsation. Also, the smallest mesh cell size is not capable of capturing the actual scour hole location. The second reason might be that it does not consider the sliding, rolling and jumping of sediment particles as in real-world scenarios.

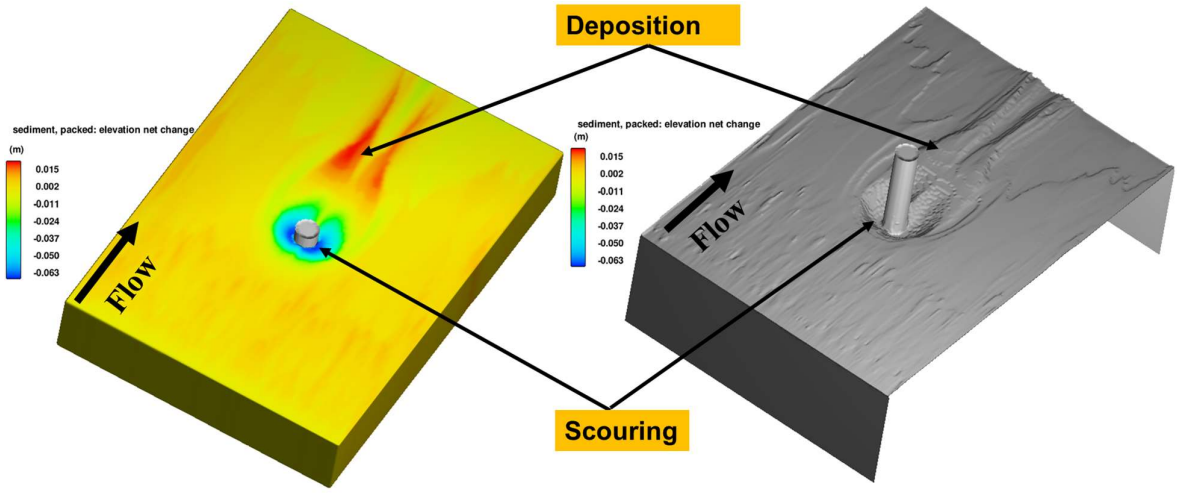

Figure 4.13: Scouring around the pier without collar.

To check the accuracy of the numerical results, various statistical indices are evaluated by comparing the numerical and experimental results. The coefficient of correlation (R^2) is calculated to assess the strength of the linear relationship between the numerical and experimental results. Additionally, the Mean Absolute Error (MAE) is computed to determine the average magnitude of the errors in the numerical simulations (Guguloth and Pandey, 2023). The Root Mean Square Error (RMSE) is also employed to measure the magnitude of the errors in the simulated results. The model's performance is evaluated using the Nash-Sutcliffe Efficiency (NSE) coefficient, which compares the model's performance to the experimental results based on the mean squared error of the residuals. The value of R^2, MAE, RMSE and NSE are evaluated using the following Equations (4.9 to 4.12), which are found to be 0.981, 3.65, 6.30 and 0.924, respectively. Overall, the results of the study indicated that the simulation has a high level of accuracy, as demonstrated by the low values of MAE and

RMSE and the high value of the R^2 and NSE.

$$R^2 = \left[\frac{(N\sum M_{exp}M_{sim}) - (\sum M_{exp})(\sum M_{sim})}{\sqrt{N(\sum {M_{exp}}^2) - (\sum M_{exp})^2}\sqrt{N(\sum {M_{sim}}^2) - (\sum M_{sim})^2}}\right]^2 \quad (4.9)$$

$$MAE = \frac{\sum |M_{exp} - M_{sim}|}{N} \quad (4.10)$$

$$RMSE = \sqrt{\frac{1}{N}\sum_{i=1}^{N}(M_{exp} - M_{sim})^2} \quad (4.11)$$

$$NSE = 1 - \frac{\sum_{i=1}^{N}(M_{exp} - M_{sim})^2}{\sum_{i=1}^{N}(M_{exp} - \overline{M_{exp}})^2} \quad (4.12)$$

where M_{exp} and M_{sim} are experimental and simulated values, N and $\overline{M_{exp}}$ are total no of data and average experimental values respectively.

4.13 Temporal variation of scour depth with and without AFC

The equilibrium scour depth around the pier without AFC is 6.33 cm and with collars b_{c2}, b_{c2R} and b_{c4} , it is 1.4, 3.5 and 0 cm, respectively, when they are on the sediment bed, as shown in Figure 4.14. When b_{c2} and b_{c4} are at $y/2$ above the sediment bed then the equilibrium scour depth around the pier is 5.6 and 3.6 cm respectively. The percentage of scour reduction using b_{c2}, b_{c2R}, b_{c4} on sediment bed is 77.78, 46 and 100% and for b_{c2} and b_{c4} at $y/2$ above sediment bed is 11.12 and 42.86%. It is observed that the collar b_{c4} on sediment bed is the best suited for reducing local scour around the bridge pier. The increasing order of percentages of scour reduction for collars are b_{c2} at $y/2$, b_{c4} at $y/2$ and b_{c2R}, b_{c2} and b_{c4} on sediment bed respectively. It is observed that the location of AFC also affects the scour depth around the pier. The collar b_{c2} is 31.78% more efficient than b_{c2R} in reducing the scour around the pier. The streamlined geometry of the AFC reduces the turbulent intensity of the flow, leading to a decrease in the strength of horseshoe and wake vortices and a reduction in the transportation of sediment particles downstream of the pier.

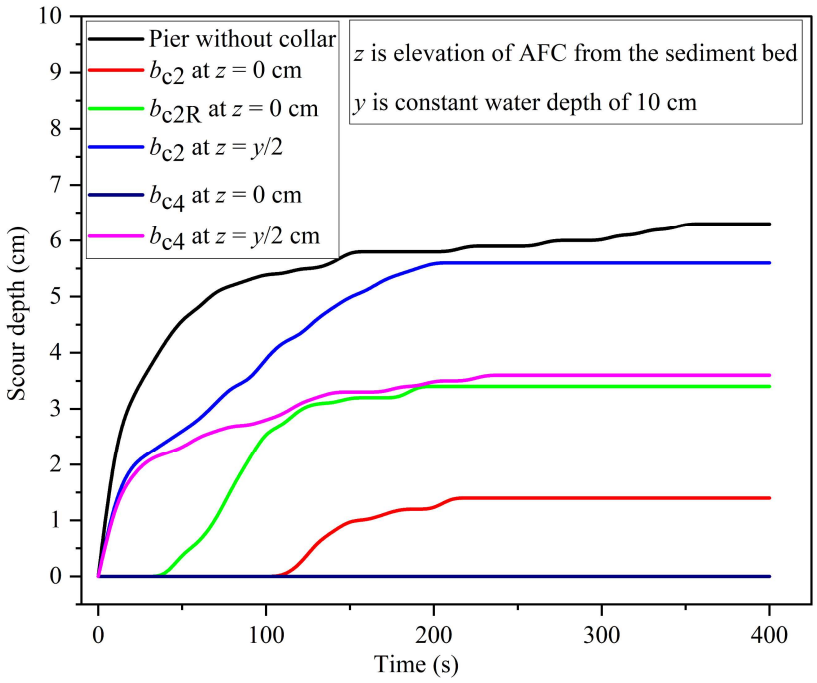

Figure 4.14: Temporal variation of scour depth around the pier using AFC.

4.14 Morphological changes and scour depth contours

Bed morphological changes around the pier with different collar sizes placed at different elevations as shown in Figure 4.15. These figures show equilibrium scour hole shapes, reflecting the scouring and deposition area. Using the collar, minimum scour is observed at b_{c4} on sediment bed as shown in Figure 4.15 (e) and maximum scour depth at b_{c2} at $y/2$ above the sediment bed as shown in Figure 4.15 (d). The maximum depositions of 1.54, 1.6, 1.64, 1.55, 2.02 and 0.6 cm occurred at the distances of 33.5, 22, 23.4, 32.6, 19.2 and 31.9 cm from the centre of the pier respectively.

Scour depth contours are developed in six cases as shown in Figure. 4.16. Figure 4.16(b) and (e) show that in the longitudinal direction, no scouring occurred around the pier respectively. There is no scouring in the downstream face of the pier as shown in Figure 4.16(c). Also, no scour is developed around the pier with collar b_{c4} on bed level as shown in Figure 4.16(e). Similar pattern in contour profiles is observed when the pier is without the collar and when the collar is placed above the sediment bed. Collars b_{c2} and b_{c4} on the sediment bed have similar profile and differ when the collar b_{c2} is placed in reverse to the flow direction.

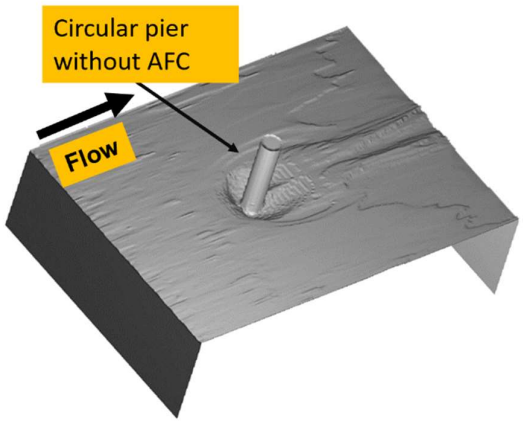

(a) Circular pier without AFC

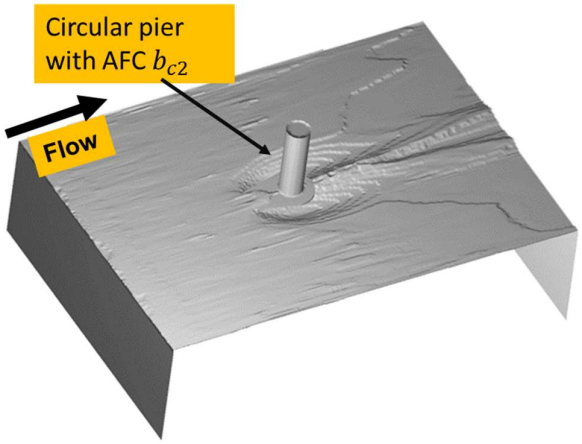

(b) Circular pier with AFC having diameter $2b$ on sediment bed (b_{c2})

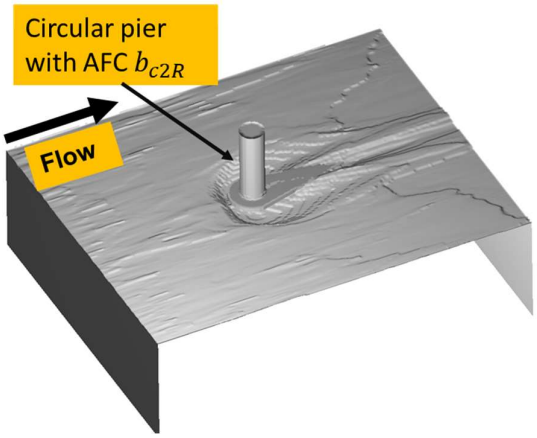

(c) Circular pier with AFC having diameter $2b$ on sediment bed in reverse to the flow direction (b_{c2R})

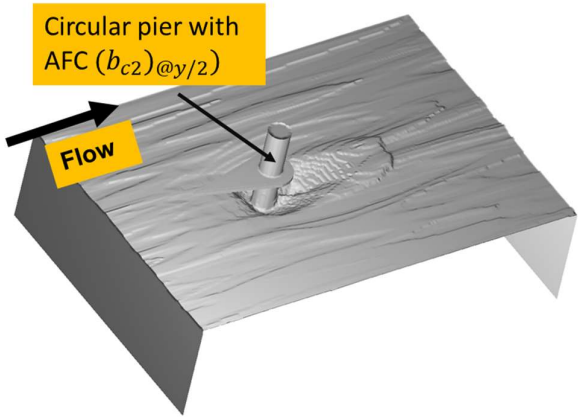

(d) Circular pier with AFC having diameter $2b$ at $y/2$ above the sediment bed $(b_{c2})_{@\,y/2}$

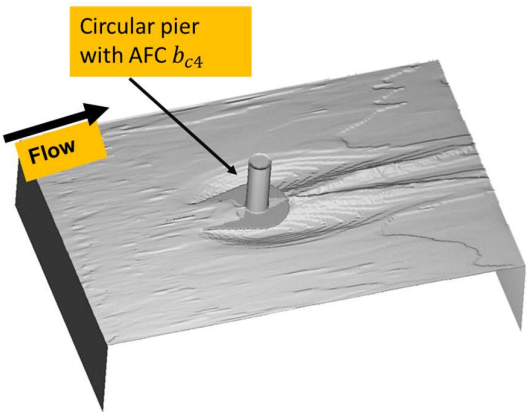

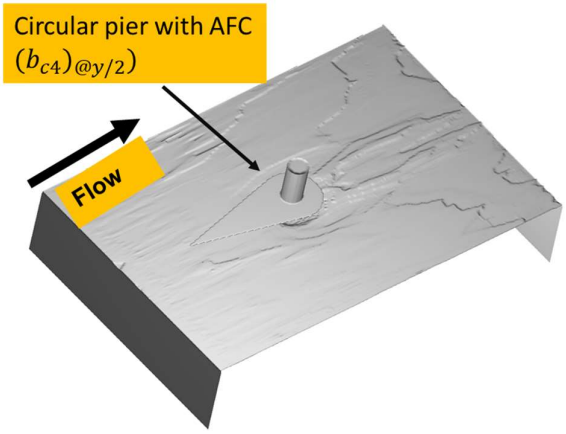

(e) Circular pier with AFC having diameter $3b$ on the sediment bed (b_{c4})

(f) Circular pier with AFC having diameter $3b$ at $y/2$ above the sediment bed $(b_{c4})_{@\ y/2}$

Figure 4.15: Morphological changes in six different cases.

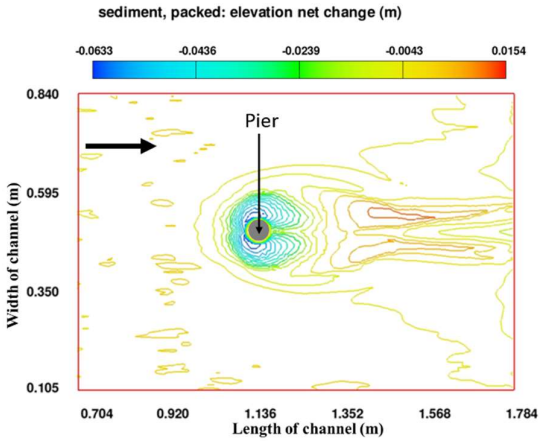

(a) Circular pier without AFC

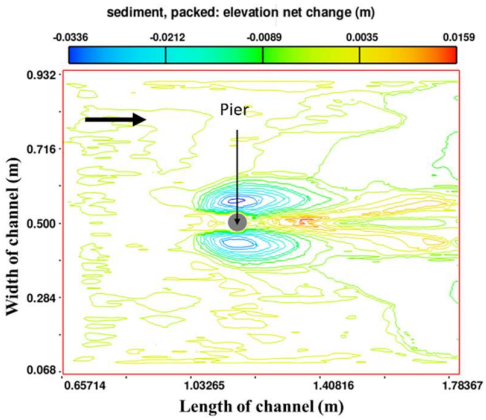

(b) Circular pier with AFC having diameter $2b$ on sediment bed (b_{c2})

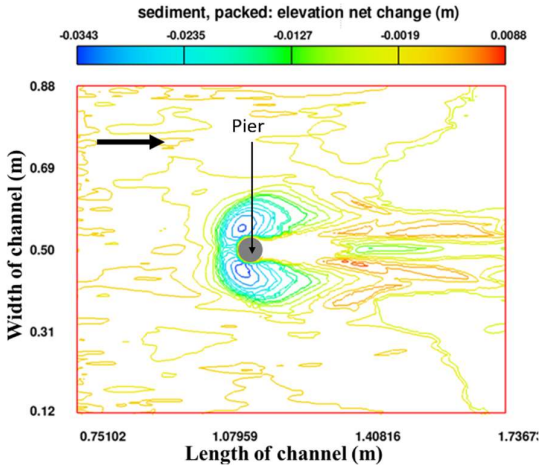

(c) Circular pier with AFC having diameter $2b$ on sediment bed in reverse to the flow direction (b_{c2R})

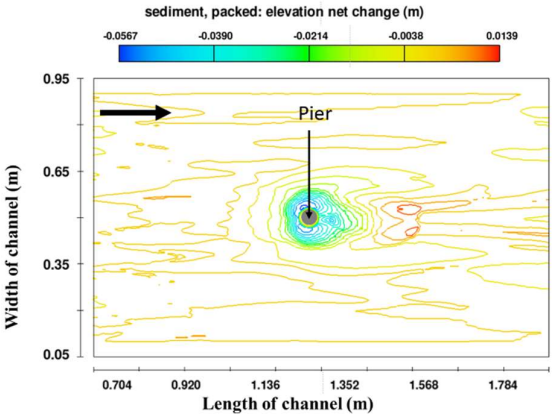

(d) Circular pier with AFC having diameter $2b$ at $y/2$ above the sediment bed $(b_{c2})_{@\ y/2}$

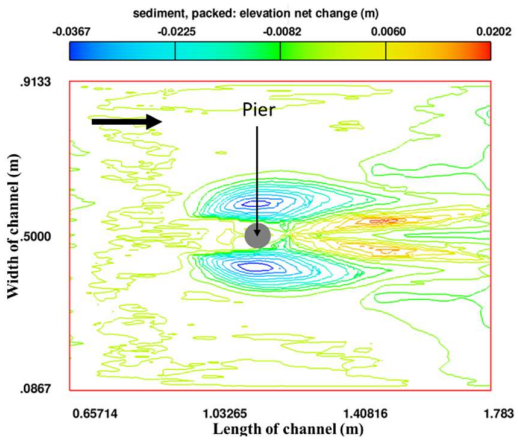

(e) Circular pier with AFC having diameter $3b$ on the sediment bed (b_{c4})

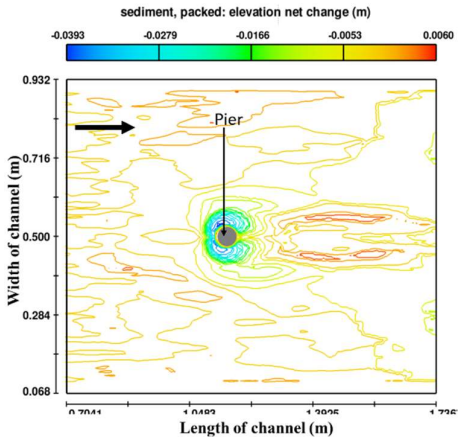

(f) Circular pier with AFC having diameter $3b$ at $y/2$ above the sediment bed (b_{c4})$_{@\, y/2}$

Figure 4.16: Scour depth contours developed around the pier in six cases.

4.15 Scour hole profiles

Longitudinal profiles of six cases are shown in Figure 4.17. Scour occurs at the upstream face of pier and deposition at the downstream face of the pier. Length of the longitudinal scour hole in six cases is 30.7, 2.17, 8.67, 26.5, 0 and 16 cm respectively. Longitudinal scour profile around the pier without collar is shown in Figure 4.17(a) and it is observed that maximum scour occurs at upstream face of the pier and minimum scour at downstream face of the pier. The longitudinal scour hole profile at the upstream and downstream face of the pier is not symmetrical around the pier owing to the upstream face of the pier being affected by the downflow and horseshoe vortices, but the downstream face of the pier is affected by wake vortices, which is also observed in the experimental scour hole profile. When collar b_{c2} is placed on the bed level, it is observed that no scouring at upstream face of the pier and minimal scour (5 mm) at downstream face of the pier as shown in Figure 4.17(b). When collar b_{c2R} is placed on the bed level it is observed that no scouring at downstream face of the pier and scouring at upstream face of the pier as shown in Figure 4.17(c). When collar b_{c4} is placed on the bed level it is observed that no scouring around the pier as shown Figure 4.17(e). When collar b_{c2} and b_{c4} is placed at $y/2$ then scouring around the pier is observed as shown in Figure 4.17(d and f).

Length of transverse scour hole in six cases is 22.23, 4.1, 25.5, 22, 0 and 18 cm respectively.

Transverse profiles are symmetrical because of the circular shape of the collar in downstream face of the pier as shown in Figure 4.18. Transverse scour profile without collar as shown in Figure 4.18(a) which can be observed that maximum scour occurs at lateral side of the pier and symmetrical about the center of the pier, which is also observed from the experimental scour hole profile. When collar b_{c2} and b_{c2R} are placed on the bed level it is observed that scouring at the lateral face of the pier as shown in Figure 4.18(b and c). When collar b_{c4} is placed on the bed level it is observed that no scouring around the pier as shown in Figure 4.18(e). When collar b_{c2} and b_{c4} is placed at $y/2$ then scouring at lateral side of the pier is observed as shown in Figure 4.18(d and f).

The van Rijn model provides an estimate of the sediment transport rate over the entire flow depth and does not explicitly account for variations in sediment transport near the bed. Therefore, it does not represent the spanwise-averaged sediment transport rate but rather the total sediment transport rate in the channel. It is based on the concept of an equilibrium boundary layer, where the sediment transport rate is balanced by the settling velocity of sediment particles and turbulent diffusion of particles in the water column. The scour hole profile is typically calculated using a sediment transport model. This model simulates the movement of sediment particles in water and predicts how they interact with the river bed or channel. This involves solving the Navier-Stokes equations for the fluid flow, as well as the equations of motion for the sediment particles (morphological equation). As sediment is transported downstream, it can cause erosion and deposition of sediment on the bed. The scour hole profile is the final result of this process. Overall, the method used to calculate local scour profile depends on the specific situation and available data and may require a combination of empirical relationships and numerical modelling.

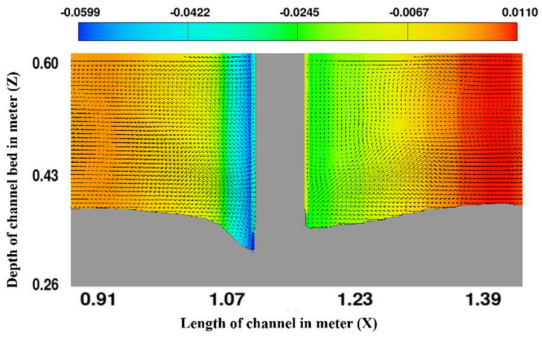

(a) Circular pier without AFC

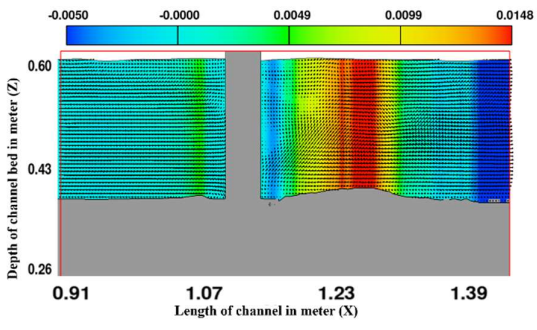

(b) Circular pier with AFC having diameter $2b$ on sediment bed (b_{c2})

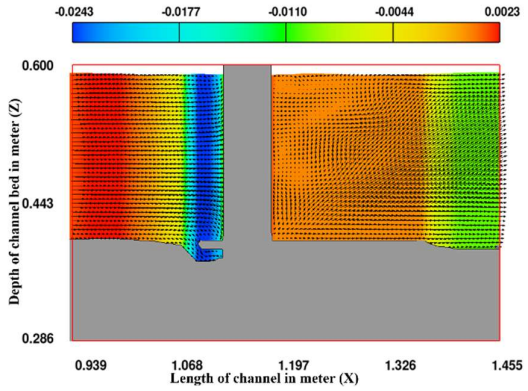

(c) Circular pier with AFC having diameter $2b$ on sediment bed in reverse to the flow direction (b_{c2R})

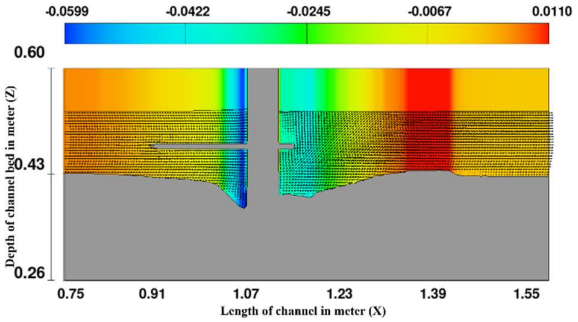

(d) Circular pier with AFC having diameter $2b$ at $y/2$ above the sediment bed $(b_{c2})_{@\ y/2}$

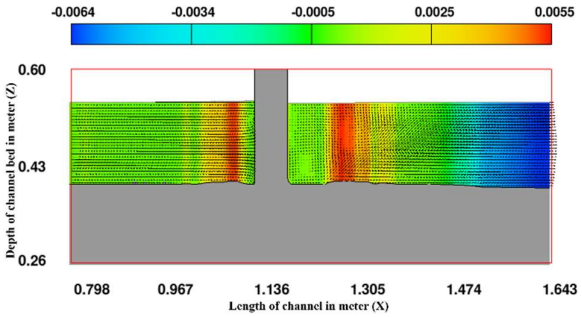

(e) Circular pier with AFC having diameter $3b$ on the sediment bed (b_{c4})

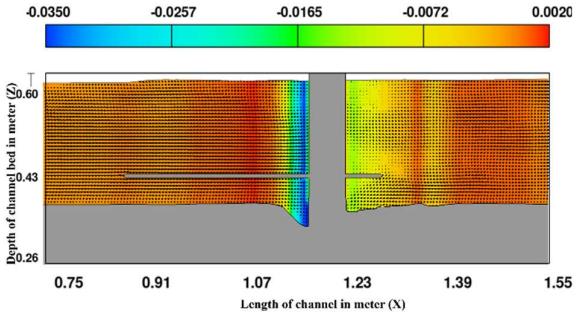

(f) Circular pier with AFC having diameter $3b$ at $y/2$ above the sediment bed $(b_{c4})_{@\ y/2}$

Figure 4.17: Longitudinal scour hole profiles for six cases.

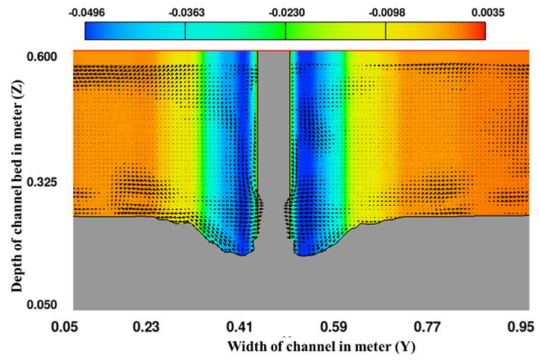

(a) Circular pier without AFC

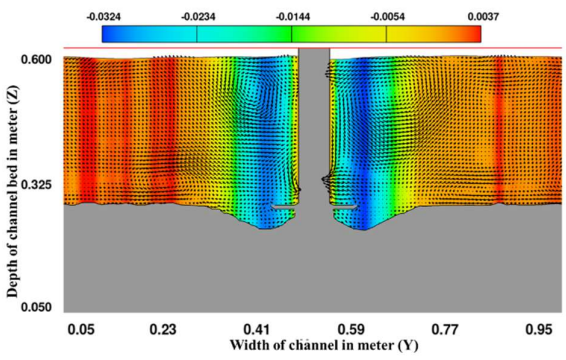

(b) Circular pier with AFC having diameter $2b$

on sediment bed (b_{c2})

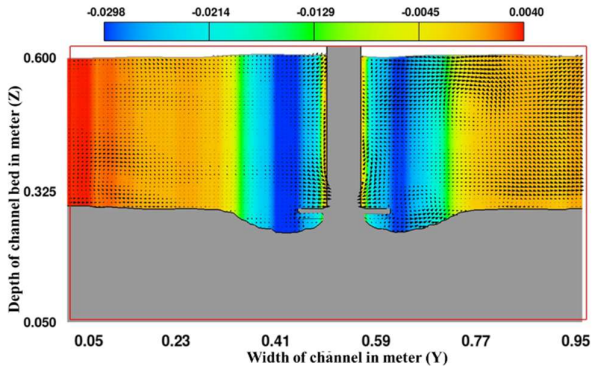

(c) Circular pier with AFC having diameter $2b$ on sediment bed in reverse to the flow direction (b_{c2R})

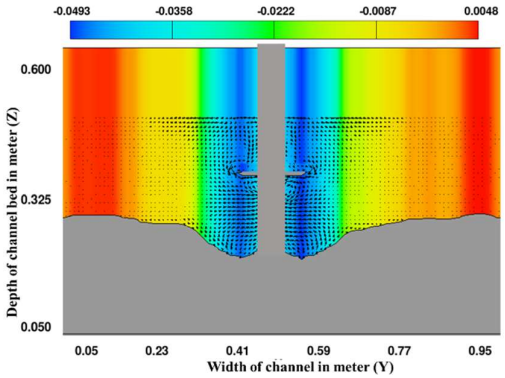

(d) Circular pier with AFC having diameter $2b$ at $y/2$ above the sediment bed $(b_{c2})_{@\ y/2}$

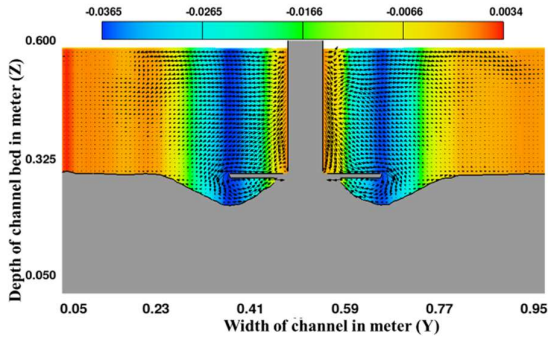

(e) Circular pier with AFC having diameter $3b$ on the sediment bed (b_{c4})

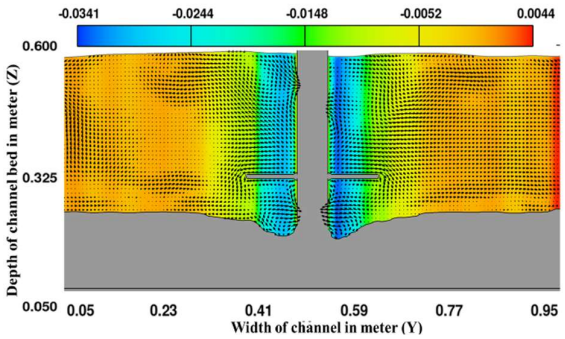

(f) Circular pier with AFC having diameter $3b$ at $y/2$ above the sediment bed $(b_{c4})_{@\ y/2}$

Figure 4.18: Transverse scour hole profiles for six cases.

4.16 Flow Structure

The flow structures are uniform in the vertical direction in Figures 4.19 to 4.22. The "flow structures" refers to the patterns and features of fluid motion in a particular flow field. It means that the flow patterns are consistent throughout the vertical extent of the fluid. The flow is steady and is not accelerating in the vertical direction. In other words, there is no variation in the flow properties, such as velocity or pressure, in the vertical direction. This is important because it simplifies the modeling and analysis of fluid flows, allowing researchers to make assumptions about the flow based on measurements at a single height or depth. This

concept is known as homogeneity in the vertical direction and is relevant in fields such as fluid mechanics, atmospheric science and oceanography.

The effects of AFC are shown in Figures 4.19 and 4.20, which show longitudinal scour hole profile for collar b_{c4} at $y/2$ and on the bed level. The velocity magnitude into the scour hole is negligible and vortex shedding occurs behind the pier, as shown in Figure 4.19. When collar b_{c4} is placed at the bed level, the effect of downflow is observed on the upstream side of the pier and the formation of wake vortices is observed on the lateral side of the pier, as shown in Figure 4.20. Please note if the author wants to increase the arrow length and head, the arrow moves out of the frame in the horizontal direction and into the sediment bed in the downward direction.

The transverse scour profiles for collar $b_{c4}$when placed on bed level and at $y/2$ are shown in Figures 4.21 and 4.22. In addition, the formation of wake vortices around the collared pier system is observed. Flow velocity in the wake regions behind the pier is very low, whereas maximum flow velocity is observed at the side of the pier. For the pier with collar b_{c4}, gradual flow separation is observed, thereby avoiding sudden flow separation. There are more zero velocity magnitude vectors around the pier in the presence of a collar, which implies a reduction in the intensity of the horseshoe and wake vortices.

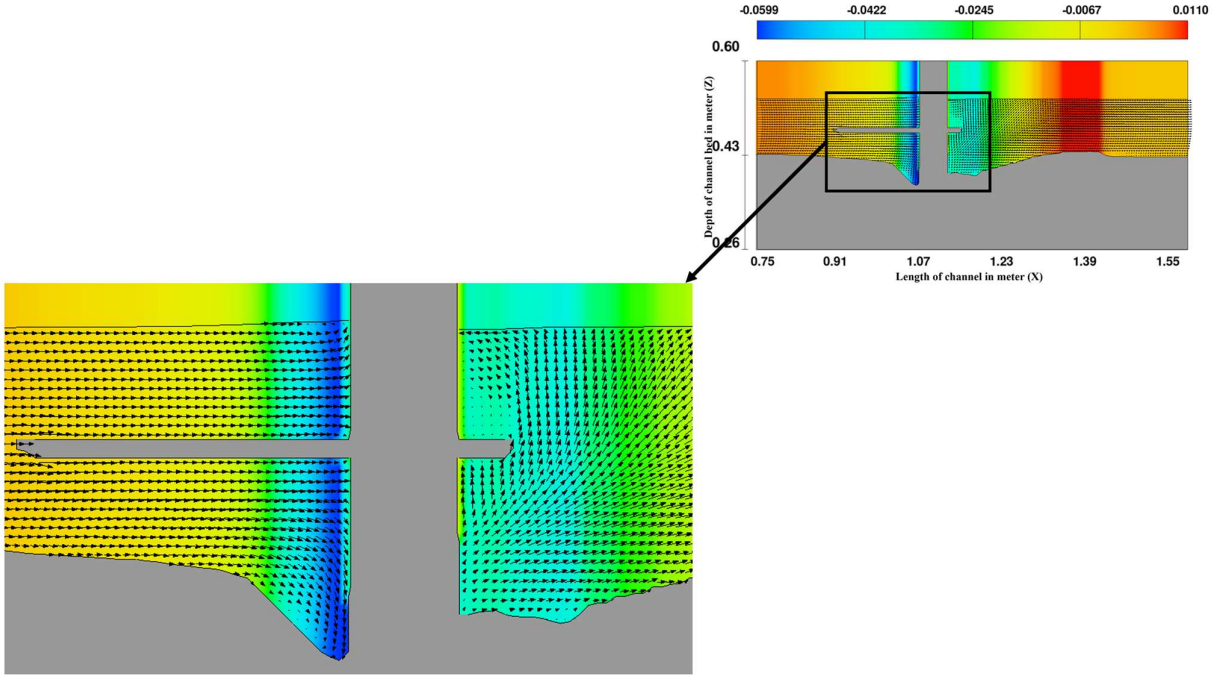

Figure 4.19: Longitudinal scour hole profile of pier with AFC having diameter $2b$ at $y/2$ above the sediment bed $(b_{c2})_{@\, y/2}$.

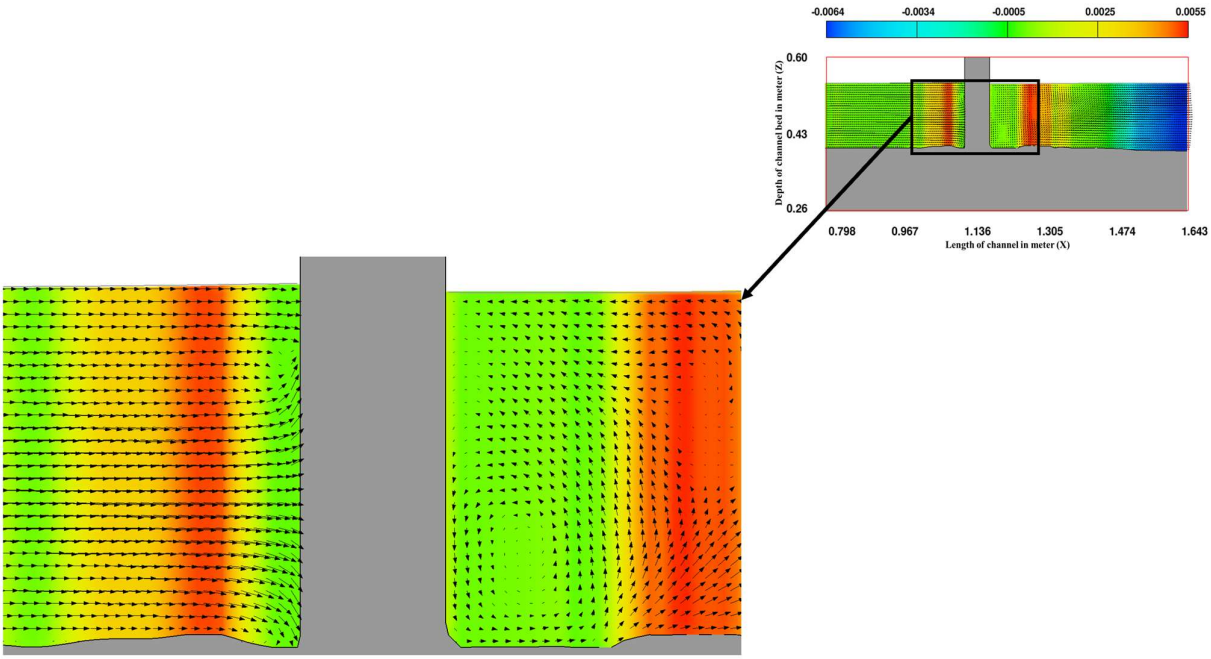

Figure 4.20: Longitudinal scour hole profile of pier with AFC having diameter $3b$ on the sediment bed (b_{c4}).

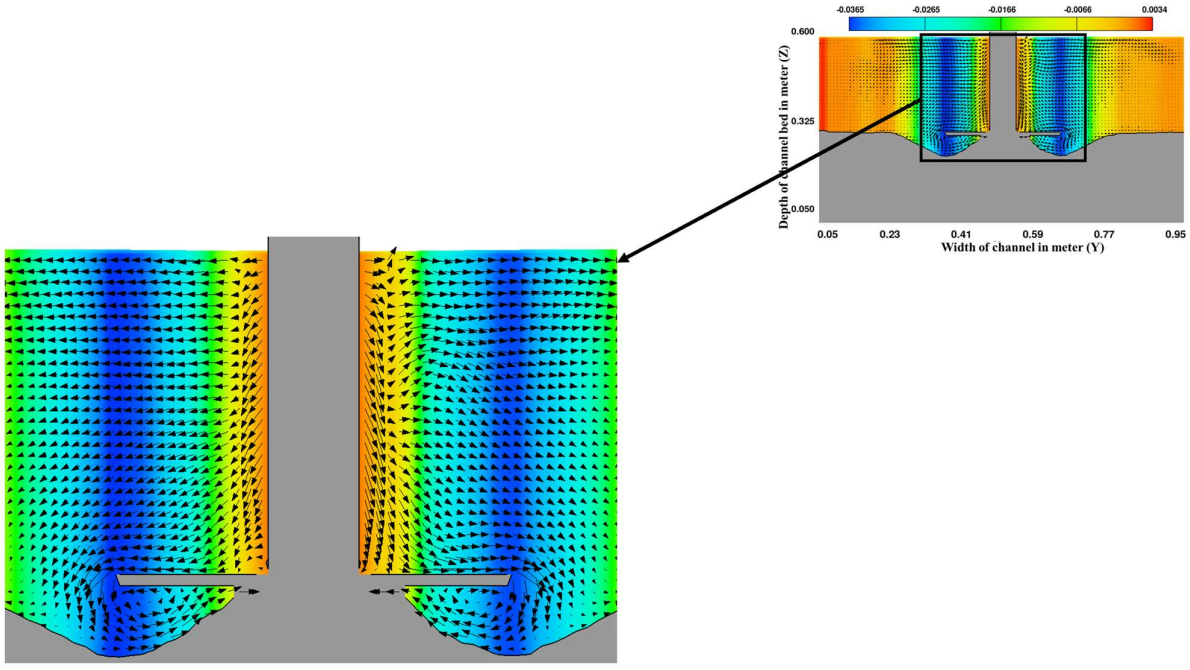

Figure 4.21: Transverse scour hole profile of Pier with AFC having diameter $3b$ on the sediment bed (b_{c4}).

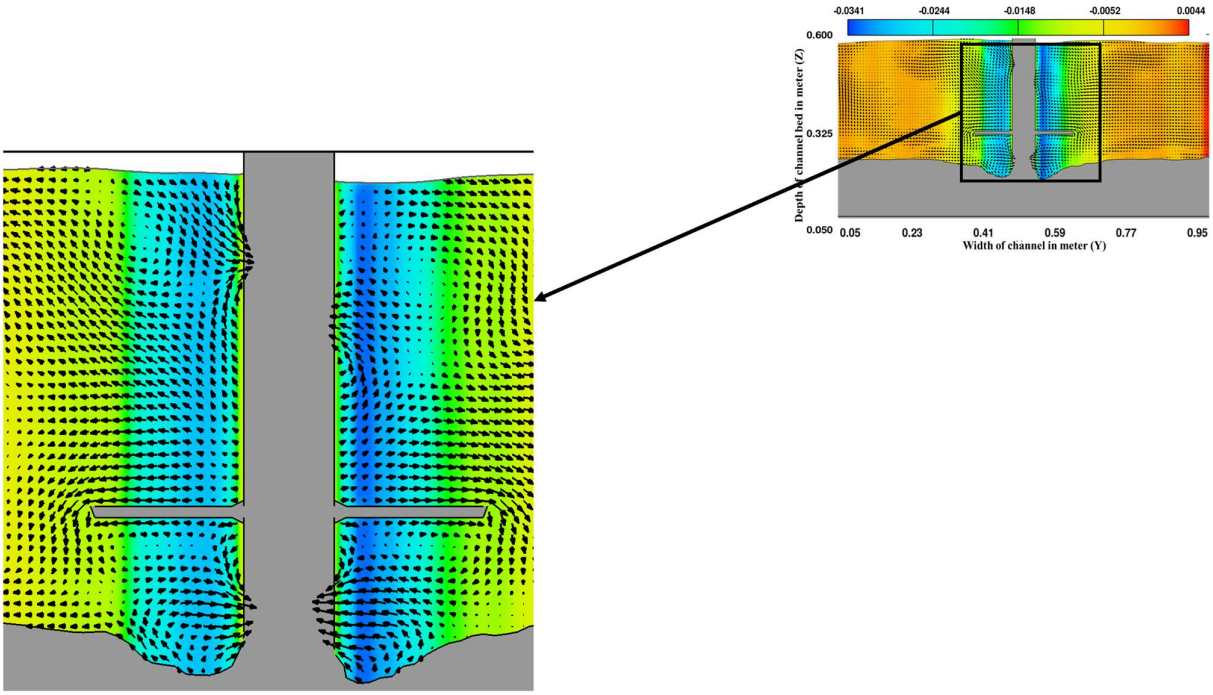

Figure 4.22: Transverse scour hole profile of pier with AFC having diameter $3b$ at $y/2$ above the sediment bed $(b_{c4})_{@\,y/2}$.

4.17 Plotting of the streamlines

Streamlines pattern around the pier with AFC in six cases is shown in Figure 4.23. The wake regions behind the pier exhibit low flow velocity, whereas the maximum flow velocity is observed at the pier's side. When pier is attached with AFC, results in a gradual flow separation, thereby avoiding sudden flow separation. Reduction of intensity of vortices is directly related to scour reduction. Furthermore, the collar increases the number of zero velocity streamlines around the pier, which signifies a reduction in the intensity of horseshoe and wake vortices. AFC is similar to streamline body and greatly influences the vortex system i.e., horseshoe and wake vortices. When flow bypassed the pier attached with collar, vortex system is divided the into two parts; vortex above the collar and below the collar. As the local scour hole around the pier increases, the number of streamlines also increases. As a result, the vortex below the collar also increases. Number of streamlines are lesser below the collar because of the smaller scour hole.

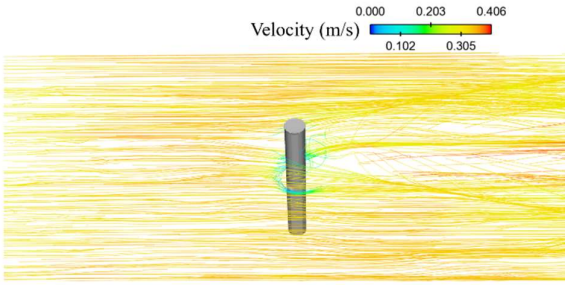

(a) Circular pier without AFC

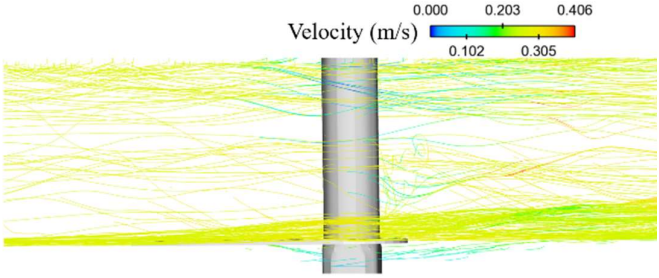

(b) Circular pier with AFC having diameter $2b$ on sediment bed (b_{c2})

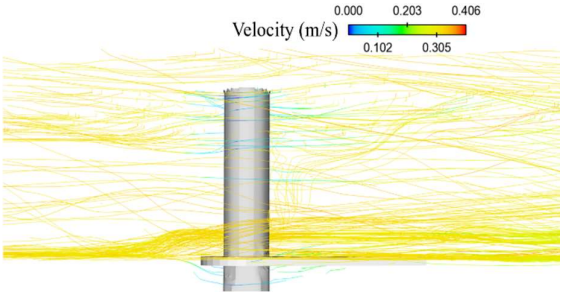

(c) Circular pier with AFC having diameter $2b$ on sediment bed in reverse to the flow direction (b_{c2R})

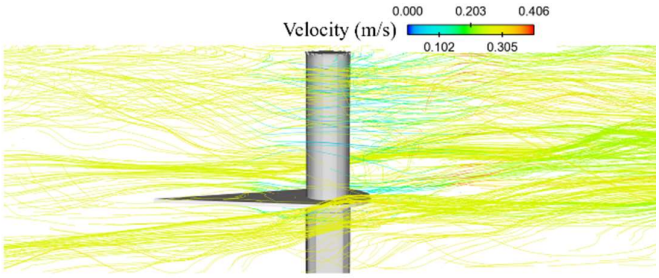

(d) Circular pier with AFC having diameter $2b$ at $y/2$ above the sediment bed $(b_{c2})_{@\, y/2}$

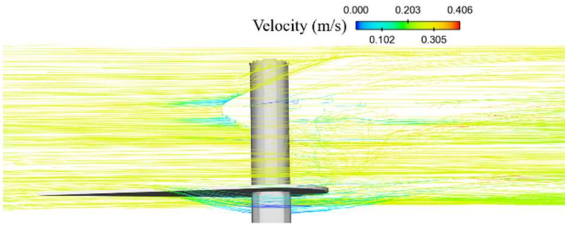

(e) Circular pier with AFC having diameter $3b$ on the sediment bed (b_{c4})

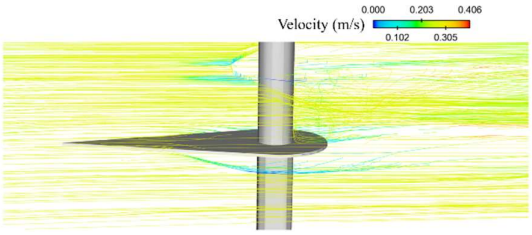

(f) Circular pier with AFC having diameter $3b$ at $y/2$ above the sediment bed $(b_{c4})_{@\, y/2}$

Figure 4.23: Streamlines pattern around the pier with collar in six cases.

Chapter 5

Conclusions

5.1 Introduction

Scouring around hydraulic structures is a severe problem with devastating consequences, particularly on abutments, bridge piers, caissons and dams. It occurs because of river erosion, sedimentation and flooding, weakening the foundation of a structure to the point of collapse. Designing structures to resist scouring is preferable; however, it is not always possible to foresee all potential scour scenarios. Climate change and frequent flooding lead to scouring resulting in bridge failure, affecting socioeconomic activities and environmental issues. The challenging problem for hydraulic engineers is to reduce the scour around the bridge pier owing to changes in flow patterns to ensure stability and cost-effectiveness in design considerations. Therefore, it is necessary to mitigate or delay scouring using scour countermeasures. One of the major research areas is pier modification using collars. Study of

collars is an area of active research in the field of scour countermeasures that aim to protect bridge piers by mitigating scour. The collar installation is also known as a flow-altering countermeasure that reduces the amount of water flowing around the pier and directs it sideward. It is typically a flat horizontal disk made of sturdy material, such as concrete or steel, attached to the pier. The idea of utilizing collars was first proposed in the 1960s. The diameter and location of the collar on the pier are the two primary factors that determine its performance. Several researchers have investigated the effects of collars on the scour depth around bridge piers.

5.2 Experimental and numerical setup

To achieve the objectives of this thesis, experiments are conducted in a rectangular flume with dimensions of 10.3x0.8x0.5 m. The working section is located 4 m from the channel inlet and outlet. The dimension of the working section is 2.3x0.8x0.5 m. Two circular pier models of 0.05 and 0.06 m diameters are fixed (one at time) at the centre, both in the longitudinal and transverse directions of the working section. The working section is filled with uniform sediment of diameter (d_{50}) 0.00032 m, σ_g of 1.31 and relative density (S) of 2.65. Four different airfoil collars with diameters (b_{c1}, b_{c2}, b_{c3} and b_{c4}) of $1.5b$, $2b$, $2.5b$ and $3b$ respectively are considered in this study. The longitudinal length of the collar is twice the collar's diameter and its thickness is 0.004 m. The total number of experiments conducted without and with collar is sixty-nine. The experimental results are also validated with the numerically simulated results using FLOW-3D. The circular pier of diameter (b) of 0.05 m is considered in the simulation and is kept at the center in the longitudinal and transverse directions of the working section. The turbulence model used in this study is Large Eddy Simulation and the bed-load transport model utilized is the van Rijn model. A nested mesh configuration is used with 12.234 million mesh cells. A nested mesh configuration in which coarse mesh cells cover the entire geometry and finer meshing is used near the pier with airfoil collar. The upstream and downstream boundary conditions are velocity (V) and continuative (C) respectively. The boundary conditions for floor, both laterals and free surface are laterals wall (W) and symmetry (S) respectively. The initial water depth used in this study is 0.5 m and hydrostatic pressure distribution is assumed.

5.3 Outcomes of the study

This study investigates the influence of airfoil collar on the local scour around a circular pier.

It is observed that the presence of an airfoil collar disturbed the formation and intensity of vortices and reduces the destructive impact on the sediment around the pier. This can be attributed to the enfeeblement of the vortices and protection offered by the collar. From this study, the following conclusions are drawn:

i. When the collar is placed at bed level (i.e., $y = 0$ where y is the depth of flow), $y/4$, $y/2$ and $3y/4$ above the bed level, the protection efficacies are found to be ranging between 55 to 100%, 40 to 53%, 23 to 38% and 8 to 29% for b_{c1}, b_{c2}, b_{c3} and b_{c4} respectively.

ii. In the case of a pier without a collar, maximum scour depth is $1.33b$ and with collar, b_{c2}, the maximum scour depths are $0.3b$, $0.6b$, $0.72b$, $0.92b$ and $1.15b$ when it is placed on bed level, reverse to flow direction (b_{c2R}) on bed level, $y/4$, $y/2$ and $3y/4$, respectively.

iii. The effect of collar diameter on scour depth is 52% to 100% for all collars on bed level. This is because, a larger diameter collar provides more resistance to the flow around the pier, thereby reducing the flow velocity of the water and erosive forces that cause scouring and prevent further deepening of the scour hole.

iv. It is observed that there is a positive correlation between pier diameter and scour depth. The collar diameter also affects the amount of sediment that can be trapped by the collar, reducing the amount of sediment eroded from around the pier.

v. When collar b_{c2} is placed on the bed, the upstream scour hole length is almost negligible along the centerline, but in downstream of the pier, it is 1.2 cm.

vi. It is noticed that the length of longitudinal scour hole is less than that of the transverse scour hole. Therefore, it is concluded that the collar on the bed reduces the scour hole volume by reducing the length, width and depth of the scour hole.

vii. From the experimental results, the scour depth at the pier with airfoil collars b_{c3} and b_{c4} is nearly zero when placed on the bed level.

viii. Time-dependent scour depth for two different pier diameters with the same collar diameter, location and flow intensity are indicating similar trends during scour hole development.

ix. A relationship for scour at pier without a collar is proposed and is given by

$$\frac{d_{st}}{b} = 0.834(F_d)^{0.713} logT$$

where d_{st}= scour depth around the pier at time, t, b = diameter of pier, F_d = densimetric Froude number = $\frac{V}{\sqrt{(S-1)g*d_{50}}}$, T = dimensionless time = $t\frac{\sqrt{(S-1)gd_{50}}}{(b^2y)^{1/3}}$, S = relative density, g = acceleration due to gravity, d_{50} = median particle size and y= flow depth.

x. Nonlinear regression analysis is performed to propose a relationship for maximum scour depth and time-dependent scour depth variations around the pier in the presence of an airfoil collar. The relationships for the maximum scour depth with an airfoil collar and time-dependent scour depth variation around the pier with an airfoil collar are given by

$$\frac{d_{se} - d_{sec}}{d_{se}} = 2.22\left(\frac{b_c}{b}\right)^{2.98}\left(\frac{L_c}{b}\right)^{-2.28}\left(\frac{h}{y}\right)^{1.21}$$

$$\frac{d_{st} - d_{sct}}{d_{st}} = 0.84\left(\frac{b_c}{b}\right)\left(\frac{L_c}{b}\right)^{-0.52}\left(\frac{h}{y}\right)^{3.28}(logT_c)^{-0.173} + 0.21$$

where d_{se} and d_{sec} are maximum scour depth around the pier without and with collar respectively and d_{st} and d_{stc} are time-dependent scour development around the pier without and with airfoil collar respectively.

xi. Statistical sensitivity analyses reveals that the most and least sensitive parameters are the collar location and dimensionless time.

xii. The percentage error between the experimental and simulation results is around 7%, indicating a good correlation between the experimental (observed) and simulation results.

xiii. The percentage of scour reduction using the collar b_{c2}, b_{c2R}, b_{c4} on sediment bed are 77.78, 46 and 100%, respectively. For b_{c2} and b_{c4} at $y/2$ from sediment bed, it is 11.12 and 42.86%, respectively.

xiv. The increasing order of percentages of scour reduction for collars are b_{c2} at $y/2$, b_{c4} at $y/2$ and b_{c2R}, b_{c2} and b_{c4} on sediment bed. The collar b_{c2} is 31.78% efficient than b_{c2R} in reducing the scour around the pier.

xv. When the collars b_{c2}, b_{c2R} and b_{c4} are placed on the sediment bed, no scouring is observed at the upstream face, downstream face and around the pier respectively.

xvi. Lengths of the longitudinal scour hole in six cases are 30.7, 2.17, 8.67, 26.5, 0 and 16 cm, respectively. Lengths of the transverse scour hole in six cases are 22.23, 4.1, 25.5, 22, 0 and 18 cm respectively.

xvii. The presence of airfoil collar significantly reduces horseshoe and wake vortices, as evidenced by the higher number of zero-velocity streamlines around the pier. When the pier is attached with collar, it results in a gradual flow separation, thereby avoiding sudden flow separation.

xviii. Reduction of the intensity of vortices is directly related to scour reduction. Furthermore, the collar increases the number of zero-velocity streamlines around the pier, which signifies a reduction in the intensity of horseshoe and wake vortices.

5.4 Scope for future studies

i. The flow and scour pattern around the bridge pier in the presence of an heart-shape collar.

ii. Numerical simulation of scour around bridge pier with and without airfoil shape collar with different locations.

iii. The scour and flow pattern around the bridge pier in the presence of a streamlined tapered sheath.

iv. Reduction of pier scour using different collars (hexagonal, octagonal and lenticular) in non-uniform sediment sand. Reduction of pier scour using sacrificial piles, vanes and collars.

v. Scour around the bridge pier using solid and permeable collars.

vi. Many investigators prefer to perform experiments in the case of clear-water flow. However, the flow in nature often tends to carry sediment, so more studies should be carried out in live-bed conditions.

vii. A minimal amount of work is being done with the combination of countermeasures.

viii. More studies should be under taken on eco-friendly scour countermeasures.

References

1. Acharya, A., & Duan, J. G. (2011). Three-dimensional simulation of flow field around series of spur dikes. In *World Environmental and Water Resources Congress 2011: Bearing Knowledge for Sustainability* (pp. 2085-2094). https://doi.org/10.1061/41173(414)218
2. Afaridegan, E., Heidarpour, M., Goodarzi, M., & Fallahi, B. (2022). Influence of suction and collar on reducing local scouring in cylindrical pier. *Journal of Applied Water Engineering and Research*, *10*(1), 27-38. https://doi.org/10.1080/23249676.2021.1919225
3. Agrawal, A. K., Khan, M. A., Yi, Z., & Aboobaker, N. (2007). *Handbook of scour countermeasures designs* (No. FHWA-NJ-2005-027). New Jersey Department of Transportation.
4. Ahmad, N., Afzal, S., Bihs, H., & Arntsen, Ø. A. (2015, June). Three-dimensional numerical modeling of local scour around a non-slender cylinder under varying wave conditions. In *36th IAHR world congress*.
5. Aksoy, A. O., Bombar, G., Arkis, T., & Guney, M. S. (2017). Study of the time-dependent clear water scour around circular bridge piers. *Journal of hydrology and hydromechanics*, *65*(1), 26. https://doi.org/10.1515/johh-2016-0048
6. Al-Shukur, A. H. K., & Obeid, Z. H. (2016). Experimental study of bridge pier shape to minimize local scour. *International Journal of Civil Engineering and Technology*, *7*(1), 162-171.
7. Anand, N., 2022. Video: Chakki railway bridge in Himachal collapses amid flash floods. Hindustan Times. https://www.hindustantimes.com/india-news/video-chakki-railway-bridge-in-himachal-collapses-amid-flash-floods-101660984406499.html.
8. Armenio, V. (2017). Large eddy simulation in hydraulic engineering: Examples of laboratory-scale numerical experiments. *Journal of Hydraulic Engineering*, *143*(11), 03117007. https://doi.org/10.1061/(asce)hy.1943-7900.0001357
9. Ballegooy, Van, S., Meville, B. W., & Coleman, S. E. Riprap and Cable-tied Block Performance as Scour Protection for Wing-wall Abutments Under Live Bed Conditions.
10. Barbhuiya, A. K., & Mazumder, M. H. (2014). Live-bed local scour around vertical-wall abutments. *ISH Journal of Hydraulic Engineering*, *20*(3), 339-351. https://doi.org/10.1080/09715010.2014.925331

11. Barkdoll, B. D., Melville, B. W., & Ettema, R. (2006). A Review of bridge abutment scour countermeasures. In *World Environmental and Water Resource Congress 2006: Examining the Confluence of Environmental and Water Concerns* (pp. 1-9). https://doi.org/10.1061/40856(200)173

12. Bathurst, R. J., & Knight, M. A. (1998). Analysis of geocell reinforced-soil covers over large span conduits. *Computers and Geotechnics*, *22*(3-4), 205-219. https://doi.org/10.1016/S0266-352X(98)00008-1

13. Bestawy, A., Eltahawy, T., Alsaluli, A., Almaliki, A., & Alqurashi, M. (2020). Reduction of local scour around a bridge pier by using different shapes of pier slots and collars. *Water Supply*, *20*(3), 1006-1015. https://doi.org/10.2166/ws.2020.022.

14. Bhalerao, A. R., & Garde, R. J. (2010). Design of Riprap for protection against scour around bridge pier. *ISH Journal of Hydraulic Engineering*, *16*(1), 79-92. https://doi.org/10.1080/09715010.2010.10514990

15. Bhide, K., & Abdallah, S. (2022). High-Order Accurate Numerical Simulation of Supersonic Flow Using RANS and LES Guided by Turbulence Anisotropy. *Fluids*, *7*(12), 385. https://doi.org/10.3390/fluids7120385

16. Brandimarte, L., Paron, P., & Di Baldassarre, G. (2012). Bridge pier scour: A review of processes, measurements and estimates. *Environmental Engineering and Management Journal*, *11*(5), 975-989. https://doi.org/10.30638/eemj.2012.121

17. Melville, B. W., & Coleman, S. E. (2000). *Bridge scour*. Water Resources Publication.

18. Chamani, M. R., Rajaratnam, N., & Beirami, M. K. (2008). Turbulent jet energy dissipation at vertical drops. *Journal of hydraulic engineering*, *134*(10), 1532-1535. https://doi.org/10.1061/(ASCE)0733-9429(2008)134.

19. Chang, W. Y., Lai, J. S., & Yen, C. L. (2004). Evolution of scour depth at circular bridge piers. *Journal of Hydraulic Engineering*, *130*(9), 905-913. https://doi.org/10.1061/(asce)0733-9429(2004)130:9(905).

20. Chaudhuri, S., Singh, S. K., Debnath, K., & Manik, M. K. (2018). Pier scour within long contraction in cohesive sediment bed. *Environmental Fluid Mechanics*, *18*, 417-441. https://doi.org/10.1007/s10652-017-9560-x.

21. Chen, S. C., Tfwala, S., Wu, T. Y., Chan, H. C., & Chou, H. T. (2018). A hooked-collar for bridge piers protection: Flow fields and scour. *Water*, *10*(9), 1251. https://doi.org/10.3390/w10091251.

22. Chiew, Y. M. (1992). Scour protection at bridge piers. *Journal of Hydraulic Engineering*, *118*(9), 1260-1269. https://doi.org/10.1061/(asce)0733-9429(1992)118:9(1260).

23. Chiew, Y. M. (1995). Mechanics of riprap failure at bridge piers. *Journal of hydraulic engineering*, *121*(9), 635-643. https://doi.org/10.1061/(asce)0733-9429(1995)121:9(635).

24. Choi, S. U., & Choi, B. (2016). Prediction of time-dependent local scour around bridge piers. *Water and Environment Journal*, *30*(1-2), 14-21. https://doi.org/10.1111/wej.12157.

25. Choufu, L., Abbasi, S., Pourshahbaz, H., Taghvaei, P., & Tfwala, S. (2019). Investigation of flow, erosion, and sedimentation pattern around varied groynes under different hydraulic and geometric conditions: a numerical study. *Water*, *11*(2), 235. https://doi.org/10.3390/w11020235.

26. Lauchlan, C. S., & Melville, B. W. (2001). Riprap protection at bridge piers. *Journal of Hydraulic Engineering*, *127*(5), 412-418. https://doi.org/10.1061/(ASCE)0733-9429(2001)127:5(412).

27. Valela, C. (2021). *Reduction of bridge pier scour through the use of a novel collar design* (Doctoral dissertation, Université d'Ottawa/University of Ottawa). http://dx.doi.org/10.20381/ruor-26471.

28. Churchfield, M. J., Li, Y., & Moriarty, P. J. (2013). A large-eddy simulation study of wake propagation and power production in an array of tidal-current turbines. *Philosophical Transactions of the Royal Society A: Mathematical, Physical and Engineering Sciences*, *371*(1985), 20120421. https://doi.org/10.1098/rsta.2012.0421.

29. Clopper, P. E., Lagasse, P. F., & Zevenbergen, L. W. (2007). Bridge pier scour countermeasures. In *World Environmental and Water Resources Congress 2007: Restoring Our Natural Habitat* (pp. 1-13). https://doi.org/10.1061/40927(243)380.

30. Daneshfaraz, R., Ghaderi, A., Sattariyan, M., Alinejad, B., Asl, M. M., & Di Francesco, S. (2021). Investigation of local scouring around hydrodynamic and circular pile groups under the influence of river material harvesting pits. *Water*, *13*(16), 2192. https://doi.org/10.3390/w13162192.

31. Deng, L., Wang, W., & Yu, Y. (2016). State-of-the-art review on the causes and mechanisms of bridge collapse. *Journal of Performance of Constructed Facilities*, *30*(2), 04015005. https://doi.org/10.1061/(asce)cf.1943-5509.0000731.

32. Dey, S., Sumer, B. M., & Fredsøe, J. (2006). Control of scour at vertical circular piles under waves and current. *Journal of Hydraulic Engineering*, *132*(3), 270-279. https://doi.org/10.1061/(ASCE)0733-9429(2006)132.

33. Dey, S. (1995). Three-dimensional vortex flow field around a circular cylinder in a quasi-equilibrium scour hole. *Sadhana*, *20*, 871-885. https://doi.org/10.1007/BF02745871.

34. Dey, S., Bose, S. K., & Sastry, G. L. (1995). Clear water scour at circular piers: a model. *Journal of Hydraulic Engineering*, *121*(12), 869-876. https://doi.org/10.1061/(asce)0733-9429(1995)121:12(869).

35. Dhamankar, N. S., Blaisdell, G. A., & Lyrintzis, A. S. (2018). Overview of turbulent inflow boundary conditions for large-eddy simulations. *Aiaa Journal*, *56*(4), 1317-1334. https://doi.org/10.2514/1.J055528.

36. Sheppard, D. M., Demir, H., & Melville, B. W. (2011). *Scour at wide piers and long skewed piers* (Vol. 682). Transportation Research Board.

37. Ettema, R., Nakato, T., & Muste, M. V. I. (2006). *An illustrated guide for monitoring and protecting bridge waterways against scour* (No. Project TR-515). IIHR-Hydroscience & Engineering, University of Iowa. https://publications.iowa.gov/id/eprint/3752.

38. Express Web Desk, 2016. Watch video: 44-year-old bridge collapses in Himachal, no casualties. The Indian Express. https://indianexpress.com/article/india/india-news-india/watch-video-44-year-old-bridge-collapses-in-kangra-nobody-injured-2970020.

39. Farooq, R., Azimi, A. H., Tariq, M. A. U. R., & Ahmed, A. (2023). Effects of hooked-collar on the local scour around a lenticular bridge pier. *International Journal of Sediment Research*, *38*(1), 1-11. https://doi.org/10.1016/j.ijsrc.2022.07.002.

40. Farooq, R., Azimi, A. H., Tariq, M. A. U. R., & Ahmed, A. (2023). Effects of hooked-collar on the local scour around a lenticular bridge pier. *International Journal of Sediment Research*, *38*(1), 1-11. https://doi.org/10.1016/j.ijsrc.2022.07.002.

41. Farooq, R., & Ghumman, A. R. (2019). Impact assessment of pier shape and modifications on scouring around bridge pier. *Water*, *11*(9), 1761. https://doi.org/10.3390/w11091761.

42. Farooq, R., Ghumman, A. R., Tariq, M. A. U. R., Ahmed, A., & Jadoon, K. Z. (2020). Optimal octagonal hooked collar countermeasure to reduce scour around a single bridge pier. *Periodica Polytechnica Civil Engineering*, *64*(4), 1026-1037. https://doi.org/10.3311/PPci.15966.

43. Flow Science, I. *Flow-3d User Manual*, V11.2., Flow Science: Santa Fe, NM, USA, 2016.

44. Franzetti, S., Radice, A., Rebai, D., & Ballio, F. (2022). Clear Water Scour at Circular Piers: A New Formula Fitting Laboratory Data with Less Than 25% Deviation. *Journal of Hydraulic Engineering*, *148*(10), 04022021. https://doi.org/10.1061/(asce)hy.1943-7900.0002009.

45. Garg, V., Setia, B., & Verma, D. V. S. (2005). Reduction of scour around a bridge pier by multiple collar plates. *ISH Journal of Hydraulic Engineering*, *11*(3), 66-80. https://doi.org/10.1080/09715010.2005.10514802.

46. Gaudio, R., Tafarojnoruz, A., & Calomino, F. (2012). Combined flow-altering countermeasures against bridge pier scour. *Journal of Hydraulic Research*, *50*(1), 35-43. https://doi.org/10.1080/00221686.2011.649548.

47. Gautam, S., Dutta, D., Bihs, H., & Afzal, M. S. (2021). Three-dimensional Computational Fluid Dynamics modelling of scour around a single pile due to combined action of the waves and current using Level-Set method. *Coastal Engineering*, *170*, 104002. https://doi.org/10.1016/j.coastaleng.2021.104002.

48. Gazi, A. H., & Afzal, M. S. (2020). A review on hydrodynamics of horseshoe vortex at a vertical cylinder mounted on a flat bed and its implication to scour at a cylinder. *Acta Geophysica*, *68*, 861-875. https://doi.org/10.1007/s11600-020-00439-8.

49. Gazi, A. H., Purkayastha, S., & Afzal, M. S. (2020). The equilibrium scour depth around a pier under the action of collinear waves and current. *Journal of Marine Science and Engineering*, *8*(1), 36. https://doi.org/10.3390/JMSE8010036.

50. Ghaderi, A., & Abbasi, S. (2019). CFD simulation of local scouring around airfoil-shaped bridge piers with and without collar. *Sādhanā*, *44*, 1-12. https://doi.org/10.1007/s12046-019-1196-8.

51. Ghaderi, A., Dasineh, M., Aristodemo, F., & Aricò, C. (2021). Numerical simulations of the flow field of a submerged hydraulic jump over triangular macroroughnesses. *Water*, *13*(5), 674. https://doi.org/10.3390/w13050674.

52. Ghazvinei, P. T., Ariffin, J., Abdullah, J., & Mohamed, T. A. (2014). Comparative Analysis between Observed and Predicted Contraction Scour at Bridges Abutments. *Research Journal of Applied Sciences, Engineering and Technology*, *8*(4), 452-459. https://doi.org/10.19026/rjaset.8.993.

53. Ghodsi, H., Najafzadeh, M., Khanjani, M. J., & Beheshti, A. (2021). Effects of different geometric parameters of complex bridge piers on maximum scour depth: Experimental study. *Journal of Waterway, Port, Coastal, and Ocean Engineering*, *147*(5), 04021021. https://doi.org/10.1061/(asce)ww.1943-5460.0000645.

54. Ghorbani, B., & Kells, J. A. (2008). Effect of submerged vanes on the scour occurring at a cylindrical pier. *Journal of Hydraulic Research*, *46*(5), 610-619. https://doi.org/10.3826/jhr.2008.3003.

55. Giglou, A. N., Mccorquodale, J. A., & Solari, L. (2018). Numerical study on the effect of the spur dikes on sedimentation pattern. *Ain Shams Engineering Journal*, *9*(4), 2057-2066. https://doi.org/10.1016/j.asej.2017.02.007.

56. Grimaldi, C., Gaudio, R., Calomino, F., & Cardoso, A. H. (2009). Control of scour at bridge piers by a downstream bed sill. *Journal of Hydraulic Engineering*, *135*(1), 13-21. https://doi.org/10.1061/(asce)0733-9429(2009)135:1(13).

57. Grimaldi, C., Gaudio, R., Calomino, F., & Cardoso, A. H. (2009). Control of scour at bridge piers by a downstream bed sill. *Journal of Hydraulic Engineering*, *135*(1), 13-21. https://doi.org/10.1061/(asce)0733-9429(2009)135:1(13).

58. Gris, R. B. (2010). Sheath for reducing local scour in bridge piers. In *Scour and Erosion* (pp. 987-996). https://doi.org/10.1061/41147(392)99.

59. Guguloth, S., & Pandey, M. (2023). Accuracy evaluation of scour depth equations under the submerged vertical jet. *AQUA-Water Infrastructure, Ecosystems and Society*, *72*(4), 557-575. https://doi.org/10.2166/aqua.2023.015.

60. Guo, J. (2012). Pier scour in clear water for sediment mixtures. *Journal of hydraulic research*, *50*(1), 18-27. https://doi.org/10.1080/00221686.2011.644418.

61. Guo, J., Suaznabar, O., Shan, H., & Shen, J. (2012). Pier scour in clear-water conditions with non-uniform bed materials. https://rosap.ntl.bts.gov/view/dot/24982/dot_24982_DS1.pdf.

62. Gupta, L. K., Pandey, M., Raj, P. A., & Shukla, A. K. (2023). Fine sediment intrusion and its consequences for river ecosystems: A review. *Journal of Hazardous, Toxic, and Radioactive Waste*, *27*(1), 04022036. https://doi.org/10.1061/(ASCE)HZ.2153-5515.0000729.

63. Hamidifar, H., Shahabi-Haghighi, S. M. B., & Chiew, Y. M. (2022). Collar performance in bridge pier scour with debris accumulation. *International Journal of Sediment Research*, *37*(3), 328-334. https://doi.org/10.1016/j.ijsrc.2021.10.002.

64. Heidarpour, M., Afzalimehr, H., & Izadinia, E. (2010). Reduction of local scour around bridge pier groups using collars. *International Journal of Sediment Research*, *25*(4), 411-422. https://doi.org/10.1016/S1001-6279(11)60008-5.

65. Hinterberger, C., Fröhlich, J., & Rodi, W. (2007). Three-dimensional and depth-averaged large-eddy simulations of some shallow water flows. *Journal of Hydraulic Engineering*, *133*(8), 857-872. https://doi.org/10.1061/(ASCE)0733-9429(2007)133:8(857).

66. Hong, J. H., Chiew, Y. M., Lu, J. Y., Lai, J. S., & Lin, Y. B. (2012). Houfeng bridge failure in Taiwan. *Journal of Hydraulic Engineering*, *138*(2), 186-198. https://doi.org/10.1061/(asce)hy.1943-7900.0000430.

67. Hong, J. H., Chiew, Y. M., Yeh, P. H., & Chan, H. C. (2017). Evolution of local pier-scour depth with dune migration in subcritical flow conditions. *Journal of Hydraulic Engineering*, *143*(4), 04016098. https://doi.org/10.1061/(asce)hy.1943-7900.0001261.

68. Hunt, B. E. (2009). Monitoring scour critical bridges: a synthesis of highway practice. *Synthesis of highway practice*, *396*.

69. Izadinia, E., & Heidarpour, M. (2023). Parametric study for hydraulic design of air-bubble injections to control scour around circular bridge piers. *ISH Journal of Hydraulic Engineering*, *29*(3), 281-288. https://doi.org/10.1080/09715010.2022.2058331.

70. Izadinia, E., & Heidarpour, M. (2012). Simultaneous use of cable and collar to prevent local scouring around bridge pier. *International Journal of Sediment Research*, *27*(3), 394-401. https://doi.org/10.1016/S1001-6279(12)60044-4.

71. Jahangirzadeh, A., Basser, H., Akib, S., Karami, H., Naji, S., & Shamshirband, S. (2014). Experimental and numerical investigation of the effect of different shapes of collars on the reduction of scour around a single bridge pier. *PloS one*, *9*(6), e98592. https://doi.org/10.1371/journal.pone.0098592.

72. Jalal, H. K., & Hassan, W. H. (2020). Effect of bridge pier shape on depth of scour. In *IOP conference series: materials science and engineering* (Vol. 671, No. 1, p. 012001). IOP Publishing. https://doi.org/10.1088/1757-899X/671/1/012001.

73. Jalal, H. K., & Hassan, W. H. (2020). Effect of bridge pier shape on depth of scour. In *IOP conference series: materials science and engineering* (Vol. 671, No. 1, p. 012001). IOP Publishing. https://doi.org/10.1088/1757-899X/671/1/012001.

74. Jones, J. S., Bertoldi, D., & Stein, S. (1995). Alternatives to Riprap as a Scour Countermeasure. In *Transportation Research Board Conference Proceedings* (No. 7).

75. Keating, A., Piomelli, U., Balaras, E., & Kaltenbach, H. J. (2004). A priori and a posteriori tests of inflow conditions for large-eddy simulation. *Physics of fluids*, *16*(12), 4696-4712. https://doi.org/10.1063/1.1811672.

76. Kaple, S., Hanmaiahgari, P. R., Gaudio, R., & Dey, S. (2017). Interference of an Upstream Pier on Downstream Pier Scour. *ACTA GEOPHYSICA*, *65*(1), 29-46. https://doi.org/10.1007/s11600-017-0004-2.

77. Khaple, S., Hanmaiahgari, P. R., Gaudio, R., & Dey, S. (2017). Splitter plate as a flow-altering pier scour countermeasure. *Acta Geophysica*, *65*, 957-975. https://doi.org/10.1007/s11600-017-0084-z.

78. Khodashenas, S. R., Shariati, H., & Esmaeeli, K. (2018). Comparison between the circular and square collar in reduction of local scouring around bridge piers. In *E3S Web of Conferences* (Vol. 40, p. 03002). EDP Sciences. https://doi.org/10.1051/e3sconf/20184003002.

79. Khosronejad, A., Kang, S., & Sotiropoulos, F. (2012). Experimental and computational investigation of local scour around bridge piers. *Advances in Water Resources*, *37*, 73-85. https://doi.org/10.1016/j.advwatres.2011.09.013.

80. Kim, I., Fard, M. Y., & Chattopadhyay, A. (2015). Investigation of a bridge pier scour prediction model for safe design and inspection. *Journal of bridge engineering*, *20*(6), 04014088. https://doi.org/10.1061/(ASCE)BE.1943.

81. Kirkil, G., Constantinescu, G., & Ettema, R. (2009). Detached eddy simulation investigation of turbulence at a circular pier with scour hole. *Journal of Hydraulic Engineering*, *135*(11), 888-901. https://doi.org/10.1061/(asce)hy.1943-7900.0000101.

82. Koken, M., & Constantinescu, G. (2008). An investigation of the flow and scour mechanisms around isolated spur dikes in a shallow open channel: 1. Conditions corresponding to the initiation of the erosion and deposition process. *Water Resources Research*, *44*(8). https://doi.org/10.1029/2007WR006489.

83. Kothyari, U. C., Hager, W. H., & Oliveto, G. (2007). Generalized approach for clear-water scour at bridge foundation elements. *Journal of hydraulic Engineering*, *133*(11), 1229-1240. https://doi.org/10.1061/(asce)0733-9429(2007)133:11(1229).

84. Kothyari, U. C., & Kumar, A. (2012). Temporal variation of scour around circular compound piers. *Journal of Hydraulic Engineering*, *138*(11), 945-957. https://doi.org/10.1061/(asce)hy.1943-7900.0000593.

85. Kreyenschulte, M., Schürenkamp, D., Bratz, B., Schüttrumpf, H., & Goseberg, N. (2020). Wave run-up on mortar-grouted riprap revetments. *Water*, *12*(12), 3396. https://doi.org/10.3390/w12123396.

86. Kuhnle, R. A., Alonso, C. V., & Shields Jr, F. D. (2002). Local scour associated with angled spur dikes. *Journal of Hydraulic Engineering*, *128*(12), 1087-1093. https://doi.org/10.1061/(asce)0733-9429(2002)128:12(1087).

87. Kumar, A. (2017). Three-Dimensional Flow Measurements at Circular Pier. In *Development of Water Resources in India* (pp. 397-406). Springer International Publishing. https://doi.org/10.1007/978-3-319-55125-8_34.

88. Kumar, V., Raju, K. G. R., & Vittal, N. (1999). Reduction of local scour around bridge piers using slots and collars. *Journal of hydraulic engineering*, *125*(12), 1302-1305. https://doi.org/10.1061/(ASCE)0733-9429(1999)125:12(1302).

89. Lagasse, P. F., Clopper, P. E., & Arneson, L. A. (2008). Partially Grouted Riprap as a Pier Scour Countermeasure. In *World Environmental and Water Resources Congress 2008: Ahupua'A* (pp. 1-10). https://doi.org/10.1061/40976(316)348.

90. Lagasse, P. F., Clopper, P. E., Pagan-Ortiz, J. E., Zevenbergen, L. W., Arneson, L. A., Schall, J. D., & Girard, L. G. (2009). *Bridge scour and stream instability countermeasures: experience, selection, and design guidance: Volume 1* (No. FHWA-NHI-09-111). National Highway Institute (US). https://rosap.ntl.bts.gov/view/dot/856/dot_856_DS1.pdf.

91. Lai, Y. G., Liu, X., Bombardelli, F. A., & Song, Y. (2022). Three-dimensional numerical modeling of local scour: A state-of-the-art review and perspective. *Journal of Hydraulic Engineering*, *148*(11), 03122002. https://doi.org/10.1061/(asce)hy.1943-7900.0002019.

92. Lança, R. M., Fael, C. S., Maia, R. J., Pêgo, J. P., & Cardoso, A. H. (2013). Clear-water scour at comparatively large cylindrical piers. *Journal of Hydraulic Engineering*, *139*(11), 1117-1125. https://doi.org/10.1061/(asce)hy.1943-7900.0000788.

93. Laxmi Narayana, P., Timbadiya, P. V., & Patel, P. L. (2022). Bed level variations around submerged tandem bridge piers in sand beds. *ISH Journal of Hydraulic Engineering*, *28*(sup1), 149-157. https://doi.org/10.1080/09715010.2020.1723138.

94. Liang, B., Du, S., Pan, X., & Zhang, L. (2019). Local scour for vertical piles in steady currents: Review of mechanisms, influencing factors and empirical equations. *Journal of Marine Science and Engineering*, *8*(1), 4. https://doi.org/10.3390/JMSE8010004.

95. Man, C., Zhang, G., Hong, V., Zhou, S., & Feng, Y. (2019). Assessment of turbulence models on bridge-pier scour using Flow-3D. *World Journal of Engineering and Technology*, *7*(2), 241-255. https://doi.org/10.4236/wjet.2019.72016.

96. Manish Kumar, 2022. Bridge In Bihar, Built At ₹ 13 Crore, Snaps Into 2 Before Inauguration. New Delhi Telev. Ltd. https://www.ndtv.com/india-news/video-rs-13-crore-bridge-in-bihar-collapses-in-river-before-inauguration-3619976.

97. Melville, B. W., & Sutherland, A. J. (1988). Design method for local scour at bridge piers. *Journal of Hydraulic Engineering*, *114*(10), 1210-1226. https://doi.org/10.1061/(ASCE)0733-9429(1988)114:10(1210).

98. Melville, B., Van Ballegooy, R., & Van Ballegooy, S. (2006). Flow-induced failure of cable-tied blocks. *Journal of Hydraulic Engineering*, *132*(3), 324-327. https://doi.org/10.1061/(ASCE)0733-9429(2006)132:3(324).

99. Melville, B., Van Ballegooy, S., Coleman, S., & Barkdoll, B. (2006). Countermeasure toe protection at spill-through abutments. *Journal of Hydraulic Engineering*, *132*(3), 235-245. https://doi.org/10.1061/(ASCE)0733-9429(2006)132:3(235).

100. Melville, B. W. (1997). Pier and abutment scour: integrated approach. *Journal of hydraulic Engineering*, *123*(2), 125-136. https://doi.org/10.1061/(asce)0733-9429(1997)123:2(125).

101. Melville, B. W., & Chiew, Y. M. (1999). Time scale for local scour at bridge piers. *Journal of Hydraulic Engineering*, *125*(1), 59-65. https://doi.org/10.1061/(ASCE)0733-9429(1999)125:1(59).

102. Melville, B. W., & Raudkivi, A. J. (1996). Effects of foundation geometry on bridge pier scour. *Journal of Hydraulic Engineering*, *122*(4), 203-209. https://doi.org/10.1061/(asce)0733-9429(1996)122:4(203).

103. Melville, B. W., & Raudkivi, A. J. (1977). Flow characteristics in local scour at bridge piers. *Journal of Hydraulic Research*, *15*(4), 373-380. https://doi.org/10.1080/00221687709499641.

104. Melville, B. W., & Hadfield, A. C. (1999). Use of sacrificial piles as pier scour countermeasures. *Journal of Hydraulic Engineering*, *125*(11), 1221-1224. https://doi.org/10.1061/(ASCE)0733-9429(1999)125:11(1221).

105. Memar, S., Zounemat-Kermani, M., Beheshti, A., Rahimpour, M., De Cesare, G., & Schleiss, A. J. (2020). Influence of collars on reduction in scour depth at two piers in a tandem configuration. *Acta Geophysica*, *68*, 229-242. https://doi.org/10.1007/s11600-019-00393-0.

106. Moghanloo, M., Vaghefi, M., & Ghodsian, M. (2020). Experimental study on the effect of thickness and level of the collar on the scour pattern in 180° sharp bend with bridge

pier. *Iranian Journal of Science and Technology, Transactions of Civil Engineering*, 1-19. https://doi.org/10.1007/s40996-020-00511-9.

107. Molinas, A., & Hosni, M. M. (1999). *Effects of gradation and cohesion on bridge scour: Volume 4: Experimental study of scour around circular piers in cohesive soils* (No. FHWA-RD-99-186, NCP 3D3C1-582). Turner-Fairbank Highway Research Center. https://rosap.ntl.bts.gov/view/dot/35817/dot_35817_DS1.pdf.

108. Moncada-M, A. T., Aguirre-Pe, J., Bolivar, J. C., & Flores, E. J. (2009). Scour protection of circular bridge piers with collars and slots. *Journal of Hydraulic Research*, *47*(1), 119-126. https://doi.org/10.3826/jhr.2009.3244.

109. Muhawenimana, V., Foad, N., Ouro, P., & Wilson, C. A. (2022). Local scour patterns around a bridge pier with cable-wrapping. *Fluids*, *8*(1), 3. https://doi.org/10.3390/fluids8010003.

110. Muhawenimana, V., Foad, N., Ouro, P., & Wilson, C. A. (2022). Local scour patterns around a bridge pier with cable-wrapping. *Fluids*, *8*(1), 3. https://doi.org/10.3390/fluids8010003.

111. Najafzadeh, M., & Barani, G. (2014). Experimental Study of Local Scour around a Vertical Pier in Cohesive Soils. *Scientia Iranica*, *21*(2), 241-250. https://scientiairanica.sharif.edu/article_1628.html.

112. Negm, A. M., Moustafa, G. M., Abdalla, Y. M., & Fathy, A. A. (2009). Optimal shape of collar to minimize local scour around bridge piers. *Proc. of IWTC13*, 12-15. https://citeseerx.ist.psu.edu/document?repid=rep1&type=pdf&doi=01893754bdb96f7a8301dccf5d1d0fdd637d1338.

113. Ningyu, L., Xiyun, L., Shanwu, W., & Lixian, Z. (1997). Large-eddy simulation of stratified channel flow. *Acta Mechanica Sinica*, *13*(4), 331-338. https://doi.org/10.1007/BF02487192.

114. Oliveto, G., & Hager, W. H. (2002). Temporal evolution of clear-water pier and abutment scour. *Journal of Hydraulic Engineering*, *128*(9), 811-820. https://doi.org/10.1061/(asce)0733-9429(2002)128:9(811).

115. Omara, H., Ookawara, S., Nassar, K. A., Masria, A., & Tawfik, A. (2022). Assessing local scour at rectangular bridge piers. *Ocean Engineering*, *266*, 112912. https://doi.org/10.1016/j.oceaneng.2022.112912.

116. Our Foreign Staff, 2017. Desperate search to find survivors as train crash in India kills 23 and injures 156. Telegr. https://www.telegraph.co.uk/news/2017/08/20/emergency-teams-desperately-search-find-survivors-train-crash.

117. Pandey, A. K., & Mohapatra, P. K. (2023). Flow Dynamics and Pollutant Transport at an Artificial Right-Angled Open-Channel Junction with a Deformed Bed. *Journal of Hydraulic Engineering*, *149*(4), 04023006. https://doi.org/10.1061/JHEND8.HYENG-13424.

118. Pandey, M., Azamathulla, H. M., Chaudhuri, S., Pu, J. H., & Pourshahbaz, H. (2020). Reduction of time-dependent scour around piers using collars. *Ocean Engineering*, *213*, 107692. https://doi.org/10.1016/j.oceaneng.2020.107692.

119. Pandey, M., Oliveto, G., Pu, J. H., Sharma, P. K., & Ojha, C. S. P. (2020). Pier scour prediction in non-uniform gravel beds. *Water*, *12*(6), 1696. https://doi.org/10.3390/W12061696.

120. Pandey, M., Pu, J. H., Pourshahbaz, H., & Khan, M. A. (2022). Reduction of scour around circular piers using collars. *Journal of Flood Risk Management*, *15*(3), e12812. https://doi.org/10.1111/jfr3.12812.

121. Park, S. K., Julien, P. Y., Ji, U., & Ruff, J. F. (2008). Case study: retrofitting large bridge piers on the Nakdong River, South Korea. *Journal of Hydraulic Engineering*, *134*(11), 1639-1650. https://doi.org/10.1061/(ASCE)0733-9429(2008)134.

122. Patel, P. L., & Ranga Raju, K. G. (1999). Critical tractive stress of nonuniform sediments. *Journal of Hydraulic Research*, *37*(1), 39-58. https://doi.org/10.1080/00221689909498531.

123. Pizarro, A., Manfreda, S., & Tubaldi, E. (2020). The science behind scour at bridge foundations: A review. *Water*, *12*(2), 374. https://doi.org/10.3390/w12020374.

124. Pourshahbaz, H., Abbasi, S., Pandey, M., Pu, J. H., Taghvaei, P., & Tofangdar, N. (2022). Morphology and hydrodynamics numerical simulation around groynes. *ISH Journal of Hydraulic Engineering*, *28*(1), 53-61. https://doi.org/10.1080/09715010.2020.1830000.

125. Prendergast, L. J., & Gavin, K. (2014). A review of bridge scour monitoring techniques. *Journal of Rock Mechanics and Geotechnical Engineering*, *6*(2), 138-149. https://doi.org/10.1016/j.jrmge.2014.01.007.

126. Qi, H., Tian, W., & Zhang, H. (2021). Modeling Local Scour around a Cylindrical Pier with Circular Collar with Tilt Angles (Counterclockwise around the Direction of the Channel Cross-Section) in Clear-Water. *Water*, *13*(22), 3281. https://doi.org/10.3390/w13223281.

127. Qi, H., Yuan, T., Zhao, F., Chen, G., Tian, W., & Li, J. (2023). Local Scour Reduction around Cylindrical Piers Using Permeable Collars in Clear Water. *Water*, *15*(5), 897. https://doi.org/10.3390/w15050897

128. Rahman, M., & Muramoto, Y. (1999). Prediction of maximum scour depth around spur-dike-like structures. *PROCEEDINGS OF HYDRAULIC ENGINEERING*, *43*, 623-628. https://doi.org/10.2208/prohe.43.623.

129. Raudkivi, A. J., & Ettema, R. (1983). Clear-water scour at cylindrical piers. *Journal of hydraulic engineering*, *109*(3), 338-350. https://doi.org/10.1061/(ASCE)0733-9429(1983)109:3(338).

130. Mariano, C., Edgar, C., Carlos, G., Gerardo, H., Gonzalo, P., Silvio, A., ... & Rodolfo, M. (2003). Análisis hidromorfológico y solución ingenieril para el cruce del poliducto Repsol-YPF sobre un tramo del Río Cuarto (Córdoba, Argentina). http://irh-fce.unse.edu.ar/Rios2003/TC/TC_1_5.pdf.

131. Van Rijn, L. C. (1989). Mathematical modelling of morphological processes in the case of suspended sediment transport.

132. Van Rijn, L. C. (1984). Sediment transport, part I: bed load transport. *Journal of hydraulic engineering*, *110*(10), 1431-1456. https://doi.org/10.1061/(ASCE)0733-9429(1984)110:10(1431).

133. Rijn, L. C. V. (1984). Sediment transport, part II: suspended load transport. *Journal of hydraulic engineering*, *110*(11), 1613-1641. https://doi.org/10.1061/(ASCE)0733-9429(1984)110:11(1613).

134. Van Rijn, L. C. (1984). Sediment transport, part III: bed forms and alluvial roughness. *Journal of hydraulic engineering*, *110*(12), 1733-1754. https://doi.org/10.1061/(ASCE)0733-9429(1984)110:12(1733).

135. Schindler, R., Whitehouse, R., & Harris, J. (2022). Sticky stuff: biological cohesion for scour and erosion prevention. *Environmental Technology*, 1-15. https://doi.org/10.1080/09593330.2022.2052362.

136. Shahriar, A. R., Ortiz, A. C., Montoya, B. M., & Gabr, M. A. (2021). Bridge Pier Scour: An overview of factors affecting the phenomenon and comparative evaluation of selected models. *Transportation Geotechnics*, *28*, 100549. https://doi.org/10.1016/j.trgeo.2021.100549.

137. Singh, R. K., Pandey, M., Pu, J. H., Pasupuleti, S., & Villuri, V. G. K. (2020). Experimental study of clear-water contraction scour. *Water Supply*, *20*(3), 943-952. https://doi.org/10.2166/ws.2020.014.

138. Tafarojnoruz, A., Gaudio, R., & Dey, S. (2010). Flow-altering countermeasures against scour at bridge piers: a review. *Journal of hydraulic research*, *48*(4), 441-452. https://doi.org/10.1080/00221686.2010.491645

139. Tang, Z. H., Melville, B., Singhal, N., Shamseldin, A., Zheng, J. H., Guan, D. W., & Cheng, L. (2022). Countermeasures for local scour at offshore wind turbine monopile foundations: A review. *Water Science and Engineering*, *15*(1), 15-28. https://doi.org/10.1016/j.wse.2021.12.010

140. Tiffany Ap and Sugam Pokharel, 2016. India bridge collapse: 14 bodies found after buses, cars plunge into river. Cable News Netw. https://edition.cnn.com/2016/08/05/asia/india-bridge-collapse/index.html

141. Tison, L. J. (1961). Local scour in rivers. *Journal of Geophysical Research*, *66*(12), 4227-4232. https://doi.org/10.1029/jz066i012p04227.

142. Vahdati, V. J., Yaghoubi, S., Torabipour, A., Correia, J. A., Fazeres-Ferradosa, T., & Taveira-Pinto, F. (2020). Combined solutions to reduce scour around complex foundations: An experimental study. *Marine Systems & Ocean Technology*, *15*, 81-93. https://doi.org/10.1007/s40868-019-00068-x.

143. Valela, C., Nistor, I., Rennie, C. D., Lara, J. L., & Maza, M. (2021). Hybrid modeling for design of a novel bridge pier collar for reducing scour. *Journal of Hydraulic Engineering*, *147*(5), 04021012. https://doi.org/10.1061/(asce)hy.1943-7900.0001875.

144. Valela, C., Nistor, I., Rennie, C. D., Lara, J. L., & Maza, M. (2021). Hybrid modeling for design of a novel bridge pier collar for reducing scour. *Journal of Hydraulic Engineering*, *147*(5), 04021012. https://doi.org/10.1061/(asce)hy.1943-7900.0001875.

145. Valela, C., Rennie, C. D., & Nistor, I. (2022). Improved bridge pier collar for reducing scour. *International Journal of Sediment Research*, *37*(1), 37-46. https://doi.org/10.1016/j.ijsrc.2021.04.004.

146. Valela, C., Sirianni, D. A., Nistor, I., Rennie, C. D., & Almansour, H. (2021). Bridge pier scour under ice cover. *Water*, *13*(4), 536. https://doi.org/10.3390/w13040536.

147. Vasquez, J. A., & Walsh, B. W. (2009, August). CFD simulation of local scour in complex piers under tidal flow. In *33rd IAHR Congress: Water Engineering for a Sustainable*

Environment (pp. 913-920). International Association of Hydraulic Engineering & Research (IAHR).

148. Vijayasree, B. A., Eldho, T. I., & Mazumder, B. S. (2020). Turbulence statistics of flow causing scour around circular and oblong piers. *Journal of Hydraulic Research*, *58*(4), 673-686. https://doi.org/10.1080/00221686.2019.1661292.

149. Vijayasree, B. A., Eldho, T. I., Mazumder, B. S., & Ahmad, N. (2019). Influence of bridge pier shape on flow field and scour geometry. *International Journal of River Basin Management*, *17*(1), 109-129. https://doi.org/10.1080/15715124.2017.1394315.

150. Wang, S., Wei, K., Shen, Z., & Xiang, Q. (2019). Experimental investigation of local scour protection for cylindrical bridge piers using anti-scour collars. *Water*, *11*(7), 1515. https://doi.org/10.3390/w11071515.

151. Wardhana, K., & Hadipriono, F. C. (2003). Analysis of recent bridge failures in the United States. *Journal of performance of constructed facilities*, *17*(3), 144-150. https://doi.org/10.1061/(asce)0887-3828(2003)17:3(144).

152. Wei, G., Brethour, J., Grünzner, M., & Burnham, J. (2014). The sedimentation scour model in FLOW-3D®. *Flow Sci Rep*, *3*, 1-29. https://flow3d.co.kr/wp-content/uploads/FSR-03-14_sedimentation-scour-model.pdf.

153. Wörman, A. (1989). Riprap protection without filter layers. *Journal of Hydraulic engineering*, *115*(12), 1615-1630. https://doi.org/10.1061/(ASCE)0733-9429(1989)115:12(1615).

154. Yoon, T. H., & Kim, D. H. (2001). Bridge pier scour protection by sack gabions. In *Bridging the Gap: Meeting the World's Water and Environmental Resources Challenges* (pp. 1-8). https://doi.org/10.1061/40569(2001)256.

155. Zarrati, A. R., Gholami, H., & Mashahir, M. B. (2004). Application of collar to control scouring around rectangular bridge piers. *Journal of hydraulic research*, *42*(1), 97-103. https://doi.org/10.1080/00221686.2004.9641188.

156. Zarrati, A. R., Nazariha, M., & Mashahir, M. B. (2006). Reduction of local scour in the vicinity of bridge pier groups using collars and riprap. Journal of Hydraulic Engineering, 132(2), 154-162. https://doi.org/10.1061/(ASCE)0733-9429(2006)132.

157. Zhang, H., & Nakagawa, H. (2008). Scour around spur dyke: recent advances and future researches. Annu. Disas. Prev. Res.., Kyoto Univ., Inst 633–652. (*京都大学防災研究所年報. B*, *51*(B), 633-652). http://hdl.handle.net/2433/73369.

158. Zhang, H., Nakagawa, H., & Mizutani, H. (2012). Bed morphology and grain size characteristics around a spur dyke. *International Journal of Sediment Research*, *27*(2), 141-157. https://doi.org/10.1016/S1001-6279(12)60023-7.

Publications

Journals publications

(i) **Gupta, L. K.**, Pandey, M., & Raj, P. A. (2023). Impact of airfoil collar on scour reduction around the bridge pier. *Ocean Engineering*, *290*, 116271. https://doi.org/10.1016/j.oceaneng.2023.116271

(ii) **Gupta, L. K.**, Pandey, M., & Anand Raj, P. (2023). Numerical simulation of local scour around the pier with and without airfoil collar (AFC) using FLOW-3D. *Environmental Fluid Mechanics*, 1-19. https://doi.org/10.1007/s10652-023-09932-2.

(iii) **Gupta, L. K.,** Pandey, M., Raj, P. A., & Pu, J. H. (2023). Scour Reduction around Bridge Pier Using the Airfoil-Shaped Collar. Hydrology, 10(4), 77. http://dx.doi.org/10.3390/hydrology10040077.

(iv) **Gupta, L. K.**, Pandey, M., Raj, P. A., & Shukla, A. K. (2023). Fine Sediment Intrusion and its Consequences for River Ecosystems: A Review. *Journal of Hazardous, Toxic, and Radioactive Waste*, 27(1), 04022036. https://doi.org/10.1061/(ASCE)HZ.2153-5515.0000729

(v) **Gupta, L. K.**, Pandey, M., & Raj, P. A. (2023). Numerical modeling of scour and erosion processes around spur dike. *CLEAN – Soil, Air, Water*, 2300136. https://doi.org/10.1002/clen.20230013

Under review

i. Bharadwaj, R., **Gupta, LK.**, Pandey, M., & Manousos Valyrakis. Countermeasures for local scour around the bridge pier: A review, Submitted to *Acta Geophysica*. **Under review**.

ii. **Gupta, L. K.,** Bharadwaj, R., & Pandey, M. Impact of airfoil collar on scour reduction around the bridge pier. *Ocean Engineering*. **Under review.**

iii. **Gupta, L. K.**, Pandey, M., & Raj, P. A. Numerical investigation of scour around pier using collars and sacrificial piles in non-uniform sediment. **Under drafting**

Patent

The accompanying design in, Class: 25-00-Building units and construction elements, Subclass: 25-99- MISCELLANEOUS and article name: AIRFOIL COLLAR. In the name of **Lav Kumar Gupta**, Dr. Manish Pandey & Prof. P. Anand Raj all having addressed as

National Institute of Technology Warangal, Warangal-506004, Telangana, India. **Second stage.**

Conferences proceedings

i. **Gupta, LK**., Pandey, M. and Anand Raj, P. (2021, June 18-20). *The Effects of Emergent Vegetation in Hydrodynamic Free-Surface Flow: A Research Review.* The International e-Conference on "WATER SOURCE SUSTAINABILITY" jointly organized by Indian Water Resources Society (IWRS) and Department of Water Resources Development and Management, IIT Roorkee, Roorkee, Uttarakhand, India.

ii. **Gupta, LK**., Pandey, M. and Anand Raj, P. (2022, October 13-14). *Interference between twin piers and its effect on local scour. "*FLOW-3D India Users Conference 2022" Taj, MG Road, Bangalore, India.

iii. **Gupta, LK**., Pandey, M. and Anand Raj, P. (2022, 28 November- 02 December). *Scour reduction around bridge pier using the airfoil-shaped collar.* 3rd IAHR Young Professionals Congress, Beijing, China.

iv. **Gupta, LK**., Pandey, M. and Anand Raj, P. (2022, 22-24 December). *Numerical Simulation of Twin Piers in Staggered Configuration Using FLOW-3D.* HYDRO 2022: 27th International Conference On Hydraulics, Water Resources, Environmental And Coastal Engineering, Punjab Engineering College, Chandigarh, India.

v. Bharadwaj, R., **Gupta, LK**. and Pandey, M. (2022, 22-24 December). *Structural countermeasures for local scour around the bridge pier: A Review.* HYDRO 2022: 27th International Conference On Hydraulics, Water Resources, Environmental And Coastal Engineering, Punjab Engineering College, Chandigarh, India.

vi. **Gupta, L. K.,** Pandey, M., & Bharadwaj, R. Impact of an octagonal collar on scour reduction around the bridge pier. **submitted** to HYDRO23.

vii. **Gupta, LK**., Pandey, M. Bharadwaj, R., and Rahil Ahmad. *Comparative Study Between Experimental and Numerical Simulation for Reduction Of Local Scour Using Circular Collar In Non-Uniform Sediment* **submitted** to10th International Symposium on Hydraulic Structures Zurich, Switzerland 17-19 June 2024.

Acknowledgement

"This thesis owes its existence to the invaluable assistance and unwavering support of many. I am profoundly grateful for their guidance, mentorship, and encouragement."

The research work during my PhD years at NITW has been the most fulfilling of my life. I would like to thank my supervisor, **Prof. P. Anand Raj** & co-supervisor, **Dr. Manish Pandey** with deepest gratitude for providing me with an opportunity to work in their lab. I had the luxury of unlimited freedom to explore new ideas and directions. This thesis would not have been materialized without their constant guidance.

I would like to thank Prof. N V Umamahesh, Prof. P. Rathish Kumar, and Prof. Debashis Dutta for their insights, encouragement and guidance during the progress review each semester throughout my PhD. I also want to thank all the Water and Environment Division faculty, students and staff members for building a synergistic environment to work in.

My deepest thanks to **Gude Padmaja** (Room owner) for her hospitality during my PhD made me feel at home, and I'm immensely grateful for her kindness and support. Thank you for creating a welcoming environment that was instrumental in my academic journey.

My deepest thanks to **Mr. Rahul Bharadwaj Mangu (M. Tech, WRE, NITW), Miss Mantasha Fatima (MSc, Mathematics Department, NITW), and Malasani Gopichand (IIT Madras)** for their excellent guidance, enthusiastic discussion, good company and active involvement in all phases of this work. I was lucky to be around a sincere group of people as my lab mates; each one of them was very helpful and understanding. I thank all my lab members Satyaki Sen Gupta, Gaurav Pathak, Vooke Sirivennela, Bhavesh, Patabi Ramana, Swagat Patra, Pradeep Gopal, Eqbal Husain, Swati Kumari, K. Shrikant and Sai Guguloth.

I wouldn't have been able to complete this thesis without the support of my parents **Mr. Parmatma Nand Gupta** and **Mrs. Munni Devi**; my sisters, **Mrs. Pratibha Gupta** and **Khushabu Gupta**, and my younger brothers, **Piyush Gupta, Swaraj Gupta and Darshil**

Gupta. In addition, my deepest thanks to **Mr. Dinesh Gupta** (maternal uncle), **Mrs. Sandhya Gupta** (maternal aunt), **Mrs. Devrati Devi** (maternal grandmother), **Mrs. Humaira Parveen** (mother figure), and **Hira Fatima** (sister). They ensured that I did not worry about anything and could focus entirely on my research. I am fortunate to have a loving extended family where my grandma, uncles, aunts, cousins, and entire family take pride in the smallest of my achievements.

I want to thank all the lab assistants from Fluid Mechanics & Water Resources Lab, especially **Mr. K Purushottam, Mr. K. Malikarjun, Mr. Suresh Guguloth and Mr. Manohar** for their constant help in the lab, which made me work very smoothly considering all the hindrance.

It is my privilege to thank the authority of National Institute of Technology (Department of Civil Engineering) for providing the necessary facilities for education and research. I am also thankful to the office and technical staff for their co-operation.

Thank you very much.

Lav Kumar Gupta

Date: / /202

Responds to Examiners' reports

Thank you for taking time to review my thesis and providing me with such valuable feedback. I really appreciate your efforts to provide me with constructive comments that will help improve the quality of my work. I hope the revised thesis addresses your comments and provides a better understanding of my work.

Chapter 1

(i) Please add the bridge collapse figures, if possible.

Reply: Thank you for the comment.

Figure 1.1: Railway bridge collapses amid heavy rains in Himachal's Kangra

(ii) These piers often resist loads coming on them with the help of the friction between themselves and the surrounding soil. The frictional force depends on the contact area between the pier and the soil. For a given pier, the contact area depends on the grip length of the pier below the river bed (Zhang & Sun, 2003). In the case of alluvial rivers, the grip length is to be

reckoned not from the original bed of the river but from the scoured bed around the pier." These sentences are not clear. There are several types of frictional forces. For instance, the friction between the fluid and the pier surface, depending on the shape of the pier. Or, in the presence of debris accumulation, the friction force due to the debris. Overall, it is not clear what authors want to mean by that. Please revise and clarify.

Reply: Thank you for the comment. Revised version as shown below is replaced in the thesis.

“These piers counteract incoming loads by relying on the skin friction generated between them and the adjacent soil (Zhang & Sun, 2003). Scour around the pier leads to a reduction in the magnitude of skin friction, diminishing the load-bearing capacity of the pier.”

Chapter 2

i. "This phenomenon of bed erosion continues until the equilibrium condition, which is the balance between the rate of deposition and erosion." Apparently, the described mechanism does not reflect what happens under clear-water condition. Please clarify.

Reply: Thank you for the comment. Scour definition, in general considers all types of scour. Clear-water and live-bed conditions occur only during local scour or contraction scour.

ii. Eqs. (2) and (3): these are velocity components. Therefore, I would change "radial and tangential velocities" to "radial and tangential velocity components". Also, please clarify that the sign depends on the reference system.

Reply: Thank you for the comment. "radial and tangential velocities" is changed to "radial and tangential velocity components" in line 107. Equations of radial and tangential velocity components i.e., Eqs. (2) and (3) are of polar coordinate system. Sign convention is with respect to the Fig 3 i.e., in the flow direction which is clockwise direction, radial angle is positive.

iii. Table 2 equations of other authors from recent articles to be added.

Reply: Thank you for the comment. equations of other authors from recent articles are added.

Authors	Expression	Remarks
Choi and Choi (2016)	$\frac{d_t}{d_{se}} = e^{0.065\left(\frac{V}{V_{cr}}\right)^{0.35}\left(\frac{y}{b}\right)^{0.19} ln\left(\frac{t}{t_e}\right)}$	$t_e = \begin{cases} 18.94\left(\frac{V^2}{V_{cr}b}\right)^{-1}\left(\frac{y}{b}\right)\left(\frac{b}{d}\right)^{2.6} & \text{for } \frac{y}{b} > 6 \\ 0.36\left(\frac{V^2}{V_{cr}b}\right)^{-1}\left(\frac{y}{b}\right)^{0.52}\left(\frac{b}{d}\right)^{2.6} & \text{for } \frac{y}{b} \le 6 \end{cases}$ used for the cylindrical pier in uniform sediment
Franzetti et al., (2022)	$\frac{d_t}{b} = 0.257F_1\left(\frac{y}{b}\right)F_2\left(\frac{b}{d_{50}}\right)F_3(\sigma_g)F_4\left(\frac{V}{V_{cr}}\right)F_5\left(\frac{tV}{\sqrt{(S-1)b}}\right)$	$F_1\left(\frac{y}{b}\right) = 1 - 0.675e^{-1.451\left(\frac{y}{b}\right)}$ $F_2\left(\frac{b}{d_{50}}\right) = 0.849\left(\left(\frac{b}{d_{50}}\right)^{1.815} e^{-2.99\left(\frac{b}{d_{50}}\right)^{0.235}} + 0.511\right)$ $F_3(\sigma_g) = 0.74\left(e^{-0.066\sigma_g^{3.923}} + 0.416\right)$ $F_4\left(\frac{V}{V_{cr}}\right) = \begin{cases} 1 - 0.217(1-V)^3 & \text{for } V \le 1 \\ 1 & \text{for } V > 1 \end{cases}$

		$F_5\left(\frac{tV}{\sqrt{(S-1)b}}\right) = 1 - e^{-0.083\left(\frac{tV}{\sqrt{(S-1)b}}\right)^{0.231}}$ used for the cylindrical pier in clear water conditions
Nandi and Das (2023)	$\frac{d_t}{b} = 2.86F_1\left(\frac{V}{V_{cr}}\right)F_2\left(\frac{y}{b}\right)F_3(\sigma_g)$ $F_4\left(\frac{b}{d_{50}}\right)F_5\left(\frac{tV}{\sqrt{(S-1)b}}\right)F_6(\beta)$	$F_1\left(\frac{V}{V_{cr}}\right) = \begin{cases} 1.1791\left(1-\frac{V}{V_{cr}}\right) & \text{for } \frac{V}{V_{cr}} \le 1 \\ 1 \text{ for } \frac{V}{V_{cr}} > 1 \end{cases}$ $F_2\left(\frac{y}{b}\right) = \begin{cases} 0.7786\left(\frac{y}{b}\right)^{0.1759} & \text{for } \frac{y}{b} \le 4 \\ 1 \text{ for } \frac{y}{b} > 4 \end{cases}$ $F_3(\sigma_g) = 0.3538 + \frac{0.6854}{1+e^{6.9924ln\left(\frac{\sigma_g}{1.7196}\right)}}$ $F_4\left(\frac{b}{d_{50}}\right) = 0.8491\left(\left(\frac{b}{d_{50}}\right)^{1.8158} e^{-2.9905\left(\frac{b}{d_{50}}\right)^{0.235}} + 0.5112\right)$ $F_5\left(\frac{tV}{\sqrt{(S-1)b}}\right) = 1 - e^{-0.1\left(\frac{tV}{\sqrt{(S-1)b}}\right)^{0.2}}$ used for the cylindrical pier in clear water conditions

iv. What is lenticular type of collar? Is it similar to elliptical collar?

Reply: Thank you for the comment. Lenticular and elliptical collars are distinct in terms of their shapes, with lenticular collars having a lens-like appearance and elliptical collars having an elliptical shape which is a geometric shape resembling a flattened circle.

v. Please add collar countermeasures or combinations countermeasure .. just recently published paper: Afaridegan, E., Heidarpour, M., Fallahi, B., Amanian, N., & Talebi, A. (2023). Laboratory Investigation of the Effect of Air Injection and Trapezoidal Collar on Reducing Local Scouring around Bridge Pier. *Journal of Hydraulic Engineering*, *149*(11), 04023043.

Reply: Thank you for the comment. It has beed cited to combination of scour countermeasures.

Chapter 3

(i) How the author chooses turbulence model?

Reply: Thank you for the comment. Choosing the correct turbulence model to provide the necessary near-wall details and the wide range of eddies around the pier consisted of a trial-and-error procedure. After performing a series of tests, it was found that the Large Eddy Simulation (LES) turbulence model could accurately predict the flow circulation of the horseshoe vortex.

(ii) What are "θ and θ_{cr} (local and critical Shields parameters) respectively through scouring modeling??

Reply: Thank you for the comment. Critical Shield numbers which is a ratio between the shear stress by the submerged weight of the sediment particles at incipient condition but local Shields parameter is ratio of shear stress to submerged weight of sediment particle at any conditions.

(iii) Why choose LES method as turbulence model? Why not other turbulence models?

Reply: Thank you for the comment. For simulating the turbulent flow, LES is considered as the most popular technique. This feature allows one to explicitly solve for the large eddies in calculation and implicitly account for the small eddies by using a Sub Grid-Scale (SGS) model. The LES model resolves transient character of vortices which RANS-type turbulence models are unable to tackle. The k-ε model is one of the most common turbulence models, although it just doesn't perform well in cases of large adverse pressure gradients. The k-ω model improves upon the k-ε model in that the damping functions are no longer employed and the Dirichlet boundary conditions allow for better numerical stability. The k-ω turbulence closure significantly improves the modeling of flows with adverse pressure gradient, although it is sensitive to the value chosen for the free-stream variable. the k-ε model, the k-ω model under predicts the flow separation. The Shear Stress Transport (SST) model improves upon the standard k-ω model and assumes that the turbulence shear-stress is proportional to the turbulence kinetic energy in the logarithmic and wake regions of the boundary layer, and the eddy viscosity is limited by taking the maximum term in the denominator of the eddy viscosity equation.

(iv)The establishment process and verification part of the numerical model are supplemented.

Reply: Thank you for the comment. Simulation results have underestimated the observed results by 11%. The value of coefficient of correlation between numerical model and observed is 0.92.

(v) The reason for the difference between experimental results and simulation results should be further studied.

Reply: Thank you for the comment. Numerical model does not measure the velocity of turbulent pulsation. Also, the smallest mesh cell size is not capable of capturing the actual scour hole location. The second reason might be that it does not consider the sliding, rolling and jumping of sediment particles as in real-world scenarios.

(vi) How is the equilibrium scour depth defined?

Reply: Thank you for the comment. If the change in scour depth is less than 0.05b in 24 hours then it is defined as equilibrium scour depth. (Melville, B. W., & Chiew, Y. M. (1999). Time scale for local scour at bridge piers. Journal of Hydraulic Engineering, 125(1), 59-65.)

(vii)According to the manuscript, i = 1, 2 and 3. Which are the values of index j?

Reply: Thank you for the comment. $\bar{u}_i$ is the ith component of filtered velocities, x_j is cartesian coordinates, where j = 1, 2 and 3. [Page number 10 and line number 257-258]

(viii)What do "filtered velocities" and "filtered pressure" mean?

Reply: Thank you for the comment. The decomposition of instantaneous variables (velocity, pressure) into filtered (resolved) and sub-filter (unresolved or residual) variables. Here, velocity is used as an example.

$$u_i = \bar{u}_i + u'_i$$

$\bar{u}_i$ is the filtered (resolved) and u'_i sub-filter (unresolved or residual) variables.

(ix) How is τij defined?

Reply: Thank you for the comment. These equations govern the evolution of the large, energy-carrying, scales of motion. The effect of the small scales appears through a subgrid-scale (SGS) stress term.

Subgrid-scale stress (τ_{ij}) is defined by

$$\tau_{ij} = \bar{u}_i\bar{u}_j - \overline{u_i u_j}$$

(x) Figure 10(a): What does the right scale express?

Reply: Thank you for the comment. The right scale express packed sediment: elevation net change contours (in meter).

(xi) Figure 10(b): What do the negative values of the upper scale mean?

Reply: Thank you for the comment. The negative values of the upper scale mean scour depth.

Chapter 4

(i) The flow structures are uniform in the vertical direction (contour line). I would like to know the reason.

Reply: Thank you for the comment. The flow structures are uniform in the vertical direction. It means that the flow patterns are consistent throughout the vertical extent of the fluid. The flow is steady and is not accelerating in the vertical direction. This is important because it simplifies the modeling and analysis of fluid flows, allowing researchers to make assumptions about the flow based on measurements at a single height or depth. This concept is known as homogeneity in the vertical direction and is relevant in fields such as fluid mechanics, atmospheric science, and oceanography.

(ii) Does this means the spanwise averaged sediment transport rate? In that situation, how the local scour profile is calculated as shown in Fig.9?

Reply: Thank you for the comment. Equation represents the van Rijn equation which provides an estimate of the sediment transport rate over the entire flow depth and does not explicitly account for variations in sediment transport near the bed. Therefore, it does not represent the spanwise averaged sediment transport rate, but rather the total sediment transport rate in the channel. It is based on the concept of an equilibrium boundary layer where the sediment transport rate is balanced by the settling velocity of sediment particles and the turbulent diffusion of particles in the water column.

In FLOW-3D, the scour hole profile is typically calculated using the sediment transport model. This model simulates the movement of sediment particles in the water and predicts how they will interact with the bed of the river or channel. This involves solving the Navier-Stokes equations for the fluid flow, as well as the equations of motion for the sediment particles (morphological equation). As sediment is transported downstream, it can cause erosion and deposition of sediment on the bed. The scour hole profile is the final result of this process. Overall, the method used to calculate local scour profile depends on the specific situation and available data, and may require a combination of empirical relationships and numerical modelling.

(iii)What is the meaning of the constant term in the temporal variation of scour depth around the pier with airfoil collar?

Reply: Thank you for the comment. The meaning of the constant term in the temporal variation of scour depth around the pier with airfoil collar is as follows:

(iv) It Improves the model fit.

(v) Constant term removes the unbias from the analyzed data is why it is known as bias term.

(vi) It represents the value of dependent variable when all dependent variables are zero.

(vii)Without a constant term, model would be force to pass through origin which may not be appropriate for real-world scenarios.

(viii)Including a constant term allows the model to capture additional complexity beyond just the linear effect of the independent variables.

(ix) Constant term ensure that the model will be unbiased; otherwise, the mean of residual will be zero.

(iii) In Statistical analysis, what are the ranges for different indices for better accuracy and reliability?

Reply: Thank you for the comment.

Correlation Coefficient (r): The range for the correlation coefficient is -1 to +1. Values closer to +1 or -1 indicate a stronger relationship between variables, while values closer to 0 indicate a weaker relationship.

Coefficient of Determination (R-squared): R-squared values range from 0 to 1. Higher values (closer to 1) indicate that the model explains a larger proportion of the variability in the data.

Root Mean Square Error (RMSE) or Mean Absolute Error (MAE): These are used in predictive modeling. Lower values of RMSE or MAE indicate better model accuracy.

(iv) What is the ideal value and ranges for R^2, RMSE, MAE, MAPE, etc.??

Reply: Thank you for the comment. R-squared values range from 0 to 1. Lower values of RMSE or MAE indicate better model accuracy.

(v) In statistical analysis, it is important to indicate the experiment's uncertainties, because the movable bed experiment's repeatability is generally low.

Reply: Thank you for the comment.

Uncertinites carries from various sources such as measurement error, experimental setup, instrumentation error, variability of system, environmental factors and human error.

Indicating and accounting for uncertainties in statistical analyses of movable bed experiments is indeed crucial, especially due to the inherent low repeatability of such experiments. Here's a more focused explanation of how to handle experimental uncertainties in your statistical analysis:

(i) Uncertainty Assessment: It includes identify sources of uncertainty, quantify uncertainties and systematic vs. random uncertainties.

(ii) Repeatability and Reproducibility: Assess the repeatability of the experiments by conducting multiple trials or replicates under identical conditions. If possible, consider performing experiments in different setups or by different researchers to assess reproducibility.

(iii) Statistical Analysis: The various statistical indices, such as the coefficient of determination (R^2) indicates the proportion of the variance in the dependent variable that can be explained by the independent variable(s) in a regression model. It is a common tool for assessing the goodness of fit of a regression model. Root Mean Square Error ($RMSE$) measures the performance of derived equations. Mean Absolute Error (MAE) measures the average magnitude of errors between computed and observed values. It provides a measure of how far,

Part-II

(i) Comment on the salient features of the work reported in the Thesis and the basis of the recommendations (use additional sheets, if necessary) The work is done in a excellent way. The countermeasures tested can be of improvement for real world applications.

Reply: Thank you for the comment.

This paper investigates the effectiveness of four different airfoil collars (b_{c1}, b_{c2}, b_{c3}, and b_{c4}) in reducing scour around the bridge pier. This study investigates the scour hole profiles and their depth, effect of flow intensity, collar diameter, and location on scour depth, and computes the protection efficiencies. The results show that the collar effectively reduces the scour depth. When the collar is located at bed level (i.e., $y = 0$, where y is water depth from the bed), $y/4$, $y/2$, and $3y/4$ above the bed level, the protection efficacies are found to be ranging between the percentages 65-100%, 40-53%, 23-38%, and 8-29% for b_{c1}, b_{c2}, b_{c3}, and b_{c4}, respectively. Empirical relationships are proposed for maximum scour depth and variation in scour depth with time. Statistical sensitivity analyses are performed and found that the most and least sensitive parameters are h/y and T_c, where h and T_c are the collar's location from the water surface and dimensionless time, respectively.

The experimental results are also validated with the numerically simulated results using FLOW-3D. The circular pier of diameter (b) of 0.05 m is considered in the simulation and is kept at the center in the longitudinal and transverse directions of the working section. The turbulence model used in this study is Large Eddy Simulation and the bed-load transport model utilized is the van Rijn model. A nested mesh configuration is used with 12.234 million mesh cells. A nested mesh configuration in which coarse mesh cells cover the entire geometry and finer meshing is used near the pier with airfoil collar. The error between the experimental and simulated results is 7%, indicating a good correlation between them. Temporal variation of scour depth and the percentage reduction of scour depth using the AFC are explored. The percentage reduction of scour depth (E) for various case studies and different orientations of the collar ranges between 11% to 100%. Scour depth contours, longitudinal scour hole profiles, transverse scour hole profiles, and streamlines are developed and analyzed for salient features.

Part-III

(i) What happens to the countermeasures adopted in case of wood debris in the flow?

Reply: Thank you for the comment.

The collars are often designed to create flow patterns that reduce the erosive forces acting on the riverbed. They work by altering the flow dynamics, dispersing energy, and minimizing the potential for scour caused by wood debris. Additionally, regular maintenance may be required to ensure the effectiveness of these countermeasures over time. Collars used as scour countermeasures for wood debris typically help stabilize the riverbed and protect structures from erosion. These collars can trap or redirect debris, preventing it from causing scour or damage downstream. It's essential to design and place them strategically to effectively mitigate the impact of wood debris on the flow and surrounding structures. The use of collars as scour countermeasures is intended to reduce scour. By strategically placing these collars to influence flow patterns, disperse energy, and trap debris, the goal is to minimize erosive forces on the riverbed. Effectively implemented, these countermeasures should help mitigate the potential for scour caused by wood debris in the flow.

(ii) Which are the case in which the proposed countermeasures doesn't work properly?

Reply: Thank you for the comment.

The effectiveness of an airfoil-shaped collar as a scour countermeasure may be compromised in certain situations, such as:

1. Incorrect installation or placement of the airfoil-shaped collar can lead to suboptimal performance, allowing scour to occur.

2. If collar pier system is placed at the centre of meandering channel (U shaped and sinusoidal channel).

3. In case of sand mining on river bed which leads to degradation of entire sediment bed.

4. Poorly designed collars may not effectively alter flow patterns or disperse energy, reducing their ability to prevent scour.

5. If the waterway experiences an exceptionally high concentration of debris, especially large

or irregularly shaped objects, the collar may struggle to effectively manage such conditions.

6. Fluctuations in water flow rates, such as sudden increases during heavy rainfall or snowmelt, could pose challenges for the collar's ability to maintain optimal scour prevention.

7. Unusually high-water velocities, extreme weather events, or other environmental factors beyond the design specifications may challenge the effectiveness of the scour countermeasure.